



Titre: Design of Small Structural Titanium Aeronautic Parts Made by Laser
Title: Powder Bed Fusion

Auteur: Jean-Philippe Carmona
Author:

Date: 2016

Type: Mémoire ou thèse / Dissertation or Thesis

Référence: Carmona, J.-P. (2016). Design of Small Structural Titanium Aeronautic Parts Made
Citation: by Laser Powder Bed Fusion [Mémoire de maîtrise, École Polytechnique de
Montréal]. PolyPublie. <https://publications.polymtl.ca/2286/>

 **Document en libre accès dans PolyPublie**
Open Access document in PolyPublie

URL de PolyPublie: <https://publications.polymtl.ca/2286/>
PolyPublie URL:

**Directeurs de
recherche:** Lionel Birglen
Advisors:

Programme: Génie mécanique
Program:

UNIVERSITÉ DE MONTRÉAL

DESIGN OF SMALL STRUCTURAL TITANIUM AERONAUTIC PARTS MADE BY
LASER POWDER BED FUSION

JEAN-PHILIPPE CARMONA
DÉPARTEMENT DE GÉNIE MÉCANIQUE
ÉCOLE POLYTECHNIQUE DE MONTRÉAL

MÉMOIRE PRÉSENTÉ EN VUE DE L'OBTENTION
DU DIPLÔME DE MAÎTRISE ÈS SCIENCES APPLIQUÉES
(GÉNIE MÉCANIQUE)

JUILLET 2016

© Jean-Philippe Carmona, 2016.

UNIVERSITÉ DE MONTRÉAL

ÉCOLE POLYTECHNIQUE DE MONTRÉAL

Ce mémoire intitulé :

DESIGN OF SMALL STRUCTURAL TITANIUM AERONAUTIC PARTS MADE BY
LASER POWDER BED FUSION

présenté par : CARMONA Jean-Philippe

en vue de l'obtention du diplôme de : Maîtrise ès sciences appliquées

a été dûment accepté par le jury d'examen constitué de :

M. TURENNE Sylvain, Ph. D., président

M. BIRGLEN Lionel, Ph. D. membre et directeur de recherche

Mme BROCHU Myriam, Ph. D., membre

DEDICATION

À Kim,

ACKNOWLEDGEMENTS

I first wish to thank the CRSNG, FRQNT and Bombardier Aerospace for giving me the financial support through the Industrial Research Scholarship Program. My thanks go as well to my professor Lionel Birglen for his great advises and the use of his whip at sound moments.

My work at Bombardier was under the direct supervision of Julien Chaussée, Engineering Professional at Bombardier. One of the most creative person I ever met, his support was a huge contribution to this work. He originally acted as a focal for additive manufacturing and he patiently transferred me his knowledge and experiences on the technology. I want to thank him for the countless hours spent on discussing innovation and other philosophical things. He thought me how to communicate in a complex environment and how to go from “guts feeling” to “proven facts”. His geekiness is contagious.

Nothing of all this would have been possible without Martin Deshaies, Technologist at Bombardier Aerospace. Despite his young age, Martin is a living library of aircraft design. If he had received 1\$ every time I went to see him for help, today he could fly his own Challenger 350. Driven by the quality of his work, Martin was a great mentor. He showed me how to manage pressure in difficult times and how to search for answers when I was outside my comfort zone.

All this work was initiated by Franck Dervault my manager at Bombardier. Franck pulled the strings at crucial moments. Whether I needed some signatures or phone calls from unreachable people he was always there to help. I want to thank him for the intense but yet friendly conversations we had about my career and other philosophical things. I have to apologize to him for thinking he was 10 years older than he actually is but that is, I guess, the side effect of climbing in the hierarchy.

I also have to thank the skillful Edmond Boileau from Bombardier Aerospace for his time spent on the CATIA interpretation of the track fitting. Special thanks to Bruce Thomas as well from Bombardier Aerospace for his contribution on the materials and processes aspect of this project.

RÉSUMÉ

Ce mémoire explore à l'aide d'études de cas l'utilisation et l'intégration de la fabrication additive dans l'industrie aéronautique. La fabrication additive est définie comme étant tous les « procédés de mise en forme d'une pièce par ajout de matière, par empilement de couches successives, en opposition aux procédés par retrait de matière, tel que l'usinage » [1]. Un survol du monde de la fabrication additive est présenté dans ce travail ainsi qu'un état de l'art concernant l'optimisation topologique, un outil mathématique qui « consiste à trouver la répartition de matière idéale dans un volume donné soumis à des contraintes » [2].

La fabrication de structures aéronautiques étant majoritairement dominée par les procédés soustractifs comme l'usinage ou de mise en forme comme le forgeage, les méthodes de conception sont peu adaptées aux procédés additifs. En effet, les contraintes des procédés de fabrication conventionnels limitent les géométries innovantes. Une nouvelle méthode de conception est proposée ici qui intègre l'usage de l'optimisation topologique afin de réduire le poids des pièces d'avion. Une revue des solveurs commerciaux disponibles sur le marché est aussi faite avec une évaluation de leur niveau de maturité ainsi que leur potentiel pour à des développements futurs.

La configuration des modèles d'optimisation topologiques est explorée et des lignes directrices sont extraites. Subséquemment vient l'interprétation des résultats d'optimisation qui a toujours été un grand défi, spécialement avec la méthode d'optimisation topologique SIMP, utilisée dans ce mémoire. Ici, une approche innovante est présentée qui permet de déterminer le degré d'exactitude d'un résultat d'optimisation topologique et donc éviter l'interprétation de résultats aux performances insatisfaisantes. De plus, comme l'interprétation avec des outils de modélisation avec éléments paramétrés comme CATIA est une étape très longue, une étape d'interprétation partielle a été ajoutée à la méthodologie. À l'aide d'un outil de conception basé sur la déformation du maillage, on est alors capable d'adoucir et de corriger les erreurs numériques d'un résultat d'optimisation. Ceci permet de réduire l'étape d'interprétation de plusieurs heures à quelques minutes.

La qualification et la certification des pièces et du procédé est un élément majeur de l'intégration de la fabrication additive en aéronautique. C'est pourquoi une des études de cas sera amenée jusqu'à la qualification dans ce projet. Une petite pièce de la structure primaire faite en titane et se trouvant à l'arrière d'un avion d'affaire a été conçue pour la fusion laser sur lit de poudre. Sa

résistance mécanique a été analysée numériquement et une campagne de test comprenant 88 coupons et 18 répliques grandeur nature a été lancée. Les résultats expérimentaux ne seront pas présentés dans ce travail dû à des contraintes d'échéancier.

ABSTRACT

This paper explores through case studies the use and integration of additive manufacturing in the aerospace industry. Additive manufacturing is the “process of joining materials to make objects from 3D model data, usually layer upon layer, as opposed to subtractive manufacturing methodologies such as machining” [3]. A brief overview of the additive manufacturing industry is presented along with a literature review of a design simulation technology called topology optimization. “Topology optimization is a mathematical approach that optimizes material layout within a given design space, for a given set of loads and boundary conditions such that the resulting layout meets a prescribed set of performance targets” [4].

Manufacturing of aeronautics structures is mostly dominated by subtractive processes such as machining or by forming processes such as forging. Thus, design methodologies are not well adapted to additive methods. Therefore, a new design methodology is proposed with the use of topology optimization as a design tool to potentially minimize weight of the parts. Review of available commercial solvers is done with comprehensive insights from their maturity level and their potential.

Configurations of optimization models is explored and general guidelines are extracted. Interpretation of optimization results always represented a great challenge, especially with SIMP method. An innovative approach is presented here that helps to determine if an optimization result is worth being interpreted. As well, interpreting with feature-based tools being a lengthy process, a partial interpretation step has been added in the methodology. With help of mesh-based tool from the video game industry we are now able to smooth surfaces and correct numerical discrepancies from optimization results. This helped reducing interpretation stage from hours to minutes.

Qualification and certification of the parts and processes is also a major milestone in the integration of additive manufacturing in aerospace. That’s why one of the design case studies will be pushed into qualification in this project. A small titanium part of the primary structure in the aft of a business aircraft was designed for laser powder-based fusion. Its strength was numerically analyzed and a test campaign with 88 coupons and 18 full size parts replica was launched. Experimental results won’t be presented in this report due to schedule problem.

TABLE OF CONTENTS

DEDICATION.....	iii
ACKNOWLEDGEMENTS.....	iv
RÉSUMÉ	v
ABSTRACT	vii
TABLE OF CONTENTS.....	viii
LIST OF TABLES	x
LIST OF FIGURES	xiii
LIST OF SYMBOLS AND ABBREVIATIONS.....	xvii
LIST OF APPENDICES	xix
CHAPTER 1 INTRODUCTION.....	1
CHAPTER 2 LITERATURE REVIEW.....	5
2.1 Design and qualification in aerospace.....	5
2.2 Additive manufacturing.....	6
2.2.1 Growth and recent development	11
2.2.2 Selective laser melting process	16
2.3 Topology optimization	16
2.3.1 Solid Isotropic Material Penalization (SIMP) Method	17
2.3.2 Level Set.....	23
CHAPTER 3 DESIGN METHODOLOGY FOR ADDITIVE MANUFACTURING	26
3.1 Topology optimization	27
3.1.1 Configuration	29
3.1.2 Meshing.....	32
3.1.3 Loads and boundary conditions.....	35

3.1.4	Optimization setup	39
3.2	Interpretation	41
3.2.1	Result analysis	41
3.2.2	Partial interpretation of result.....	50
3.3	Model validation	54
3.3.1	Size optimization and final analysis.....	55
3.3.2	Final design and analysis.....	57
3.4	Topology optimization with level set method.....	66
CHAPTER 4 CERTIFICATION OF ADDITIVE MANUFACTURING IN AEROSPACE..		73
4.1	Qualification.....	74
4.1.1	Tensile coupons.....	74
4.1.2	Bearing, shear and compression coupons	75
4.1.3	Fatigue coupons.....	75
4.1.4	Non-destructive inspection of hinges.....	76
4.1.5	Static hinge testing	76
4.1.6	Fatigue testing of hinges	77
4.1.7	Chemical composition test	78
CHAPTER 5 CONCLUSION AND RECOMMENDATIONS.....		80
BIBLIOGRAPHY		84
APPENDICES.....		89

LIST OF TABLES

Table 2.1 – Categories of additive manufacturing technologies with their benefits and limitations	6
Table 2.2 – Most important AM machine manufacturers in the world and their accumulated sales and revenues in 2014 [6].	11
Table 2.3 – Publicly released AM aerospace applications.....	15
Table 3.1 – Performance and volume of an in-solver optimization result and its interpreted model. Volume of the latest is significantly lower than in-solver which leads to higher stress level and displacement. The iso-density filter was 0.75.	42
Table 3.2 – Example 1. Performance and volume difference between in-solver and interpreted models with iso-density filter at 0.5065.	44
Table 3.3 – Example 2. Performance and volume difference between in-solver and interpreted models.	46
Table 3.4 – Example 3. Performance and volume difference between in-solver and interpreted models.	48
Table 3.5 – Comparison between geometry from optimization result, mesh-based modeling and feature-based modeling. Interpretation time is significantly shorter when interpreted with mesh-based software. The red arrow shows where one bolt has not been considered during partial interpretation with mesh-based software.	53
Table 3.6 – Performance of optimization results and its interpretations.....	54
Table 3.7 – Loads applied on forward hinge.....	58
Table 3.8 – Loads applied on aft hinge	59
Table 3.9 – Material allowable at 200F for FE analyses.....	60
Table 3.10 – Margins of safety of the forward hinge.....	63

Table 3.11 – Margins of safety of the aft hinge	64
Table 3.12 – Lug margins of safety of the forward hinge	64
Table 3.13 – Lug margins of safety of the aft hinge	64
Table 3.14 – Margins of safety of bolts on forward hinge	65
Table 3.15 – Margins of safety of bolts on aft hinge	65
Table 3.16 – Partial interpretation methodology with SIMP and LSM	69
Table 3.17 – Comparison between two similar models optimized with SIMP (left) and LSM (right) on different computers	70
Table 3.18 – Comparison between original design and LSM optimizations done with volume target and stress target	71
Table 4.1 – Original (left) and optimized (right) demonstration models made in aluminum by additive manufacturing.....	73
Table 4.2 – Ti-6Al-4V AMS4928 element content tolerance	78
Table 5.1 – Summary of the results and their interests for the industrial partner and for professional development of the author.....	80
Table A.1 – Mechanical properties of wrought annealed Ti-6Al-4V titanium [36]	89
Table A.2 – Lugs parameters	92
Table A.3 – allowable on each lug.....	97
Table A.4 – Axial and transverse components of the forward hinge loads	98
Table A.5 – Axial and transverse components of the aft hinge loads	98
Table A.6 – Margins of safety of the forward hinge	100
Table A.7 – Margins of safety of the aft hinge	100
Table A.8 – CBUSH stiffness properties	101
Table A.9 – Bolts strength analyses from finite element model results.....	102
<i>Table C.1 – Optimization parameters matrix.....</i>	<i>109</i>

<i>Table C.2 – Margin of safety of original part</i>	<i>110</i>
<i>Table C.3 – Optimization results are compared to simplified model of the original part (see Figure C.2).</i>	<i>111</i>
<i>Table C.4 – Results of static finite element analysis on original part, smoothing interpretation, CAD interpretation and results from setup 2. Original model results are from the complete model (see Figure 2).</i>	<i>113</i>

LIST OF FIGURES

Figure 2.1 – Proportion of units sold above 5000\$USD in 2014 by each machine manufacturers	12
Figure 2.2 – Growth and overall revenues of the additive manufacturing industry of the last 20 years	13
Figure 2.3 – Proportion of typical usage of additive manufacturing	14
Figure 2.4 – Industrial sectors in which AM is mostly used according to machine manufacturers and service provides	14
Figure 2.5 – Topology optimizations of 2D beam using material density approach. The optimal topology lies within its design space [16]	17
Figure 2.6 – Influence of penalization factor on relative stiffness. Adapted from [18]......	19
Figure 2.7 – Topology optimization of a 2D L-shape beam with stress constraints [24]. The stress concentration is not avoided with global method in Optistruct (left) whereas a radius is created at the corner with clustered method in TRINITAS (right)......	23
Figure 2.8 – 2D example with boundary represented by all the points on the level set surface at time (t) equals k [29].	24
Figure 2.9 – Level set optimization of the two-bar example with a perforated initial design [26]	25
Figure 3.1 – Design methodology with topology optimization	26
Figure 3.2 – Case study 1: flap track fitting in the trailing edge of a business aircraft.....	27
Figure 3.3 – Case study 2: APU door hinge of the CSeries commercial aircraft.....	28
Figure 3.4 – Case study 3: APU door hinge in the Global 7000/8000 business aircraft. Lugs are pointed by the red arrow.....	28
Figure 3.5 – Original assembly of the flap with the outboard fitting with all the surrounding components.....	29
Figure 3.6 – Design space for optimization of the outboard fitting with pockets for surrounding elements and fasteners. Design space is in green, non-design space in yellow.	30

Figure 3.7 – Design space used for CSeries APU door hinge.....	30
Figure 3.8 – Result from optimization with an iso-density filter that keeps only elements with density above 0.07. It is clear that density of elements is too low to be relevant.	31
Figure 3.9 – Design space (left) and result from topology optimization (right) of Global APU hinge. The iso-density filter is at 0.6.....	32
Figure 3.10 – Results from same optimization configuration done with fine elements (left) and coarse elements (right)	32
Figure 3.11 – Extracted from [16]. Mesh refinement and dependency of results.....	33
Figure 3.12 – CSeries hinge with load components inducing bending (pink arrow) and torsion (blue arrow) in the part	33
Figure 3.13 – Two models with different number of elements. The model on the left with fewer elements is not accurately transferring torsion in the structure thus leading to an underestimated displacement value compared to the model on the right with finer mesh. ...	34
Figure 3.14 – Results from topology optimization with poor torsion stiffness due to large average size of elements not accurately transferring moments in the structure	35
Figure 3.15 – On the left: design space with the ultimate load in pink. On the right: optimization result with a bending node exactly where bending efforts vanish, i.e. aligned with the load.	36
Figure 3.16 – Load has been rotated downward so it is not aligned with the design space.....	37
Figure 3.17 – Boundary conditions too stiff can lead to unrealistic optimization results.....	37
Figure 3.18 – Design space of the track fitting with boundary conditions modeled as non-design space with RBE3 and CBUSH to give a relative stiffness to the model	38
Figure 3.19 – Cseries hinge optimization with two models (left column). Upper model has a contact condition at its base and the lower one does not. Both optimization gave similar results (right column).....	39
Figure 3.20 – Elements to avoid in an optimization result: checkerboard pattern (left) and unconnected elements (right)	40

Figure 3.21 – Two optimization results with same configuration but the model on the right has a symmetry constraint which led to a result with a lot of intermediate density elements	41
Figure 3.22 – Example 1. Difference between in-solver and interpreted volume with theoretical zero volume difference at iso-density filter = 0.5065.	43
Figure 3.23 – Proportion of elements in each density bracket of the optimization result from example 1	45
Figure 3.24 – Proportion of elements in each density bracket of optimization result from example 2.....	46
Figure 3.25 – Example 2. Difference between in-solver and interpreted volume. One can note that the volume difference is within 5% from iso-density filter between 0.1 and 0.7	47
Figure 3.26 – Example 3. Difference between in-solver and interpreted volume	49
Figure 3.27 – Example 3. Proportion of elements in each density bracket of optimization result	49
Figure 3.28 – Examples of bad geometry following the filtering by iso-density.....	50
Figure 3.29 – Validation and interpretation cycle of a topology optimization result	51
Figure 3.30 – Design space of the flap track fitting and its optimization result	51
Figure 3.31 – Element density distribution of the flap track fitting topology optimization result.	52
Figure 3.32 – Influence of final interpreted volume vs the chosen iso-density filter	52
Figure 3.33 – Optimization of the Global APU door hinge from the design space to the interpretation	55
Figure 3.34 – Free-shape optimization of a section at the foot of the part. Nodes in the red (top left) area are moved to minimize the stress (top right).	56
Figure 3.35 – Free-shape optimization of stress peak to lower the stress below the 100ksi limit .	56
Figure 3.36 – Load coordinate system of forward hinge	57
Figure 3.37 – True stress vs true plastic strain for Ti-6Al-4V at 200F.....	60
Figure 3.38 – Assembly of the hinge with stiffeners underneath (left) and FEA model with equivalent SPCs (right)	61

Figure 3.39 – Finite element models of the forward (left) and aft (right) optimized hinges	61
Figure 3.40 – C1B (ult.) maximum stress zone on forward hinge	62
Figure 3.41 – C11B' Maximum stress zone on aft hinge.....	63
Figure 3.42 – Results of the track support optimizations with different single point constraints configurations giving unrealistic stress distributions	67
Figure 3.43 – Optimization results with SIMP method where iso-density filtering produces irrelevant features	68
Figure 3.44 – Results from optimization with SIMP (left) and LSM (right).	68
Figure 4.1 – S-N curve of AMS4928 titanium coupons with surface finish of 100-125 Ra and 40-63 Ra	75
Figure 4.2 – Forward hinge with its fixture to ensure the test machine applies the loads in the desired orientation	76
Figure 4.3 – Numerical render with a testing fixture (blue) with virtual mating surface (yellow) with the hinge (green)	77
Figure 4.4 – Signed Von Mises stress of the hinge with a 1,952 lbf load magnitude.....	78
Figure A.1 – Ramberg-Osgood curve and complete engineering stress-strain curve of Ti-6Al-4V [36]	90
Figure A.2 – Material data points at room temperature and at 200F	91
Figure A.3 – True stress vs true plastic strain for Ti-6al-4v @200F	91
Figure A.4 – Dimensions of the forward (left) and aft (right) hinges	92
Figure A.5 – diagram of lug section.....	92
Figure A.6 – Lug axial loading failures	93
Figure A.7 – Axial tensile failure factor of Ti-6Al-4V	94
Figure A.8 – Axial shear-bearing failure factor	95
Figure A.9 – Axial yield factor	95
Figure A.10 – Transverse Failure Factor of Ti-6Al-4V	96

Figure A.11 – Load diagram of the loads in the elements of the lug assembly	99
Figure A.12 – Fasteners between hinges and base plate are represented by RBE2 and CBUSH	101
Figure C.1 – Model view of flap assembly	108
<i>Figure C.2 – complete (right) finite element model will be used to validate the final designs only and the simplified (left) model will be used to perform the topology optimization study. ...</i>	<i>109</i>
<i>Figure C.3 – Design space of the outboard fitting in the flap assembly (left) and isolated view (right).</i>	<i>109</i>
<i>Figure C.4 – Finite element model (first on the left) and Von Mises stress contour of load case 1 (second) and load case 2 (third) of the outboard fitting. The part was first analyzed with the simplified model.</i>	<i>110</i>
<i>Figure C.5 – Results from optimization 7 and 8 with thin features and checkerboard effect.....</i>	<i>111</i>
<i>Figure C.6 – Optimization 2 gave the most satisfactory results and is used for interpretation ..</i>	<i>111</i>
<i>Figure C.7 – Comparison between results out of the optimization solver (left) and after smoothing in Blender (right).....</i>	<i>112</i>
<i>Figure C.8 – Damaged elements around bolts due to sculpting in Blender</i>	<i>112</i>
<i>Figure C.9 – Interpretation of optimization setup 2 in Catia V5</i>	<i>112</i>
<i>Figure C.10 – Von Mises stress distribution from finite element analyses of the original and the optimized models for load case 1, the most severe. Ultimate tensile strength of Ph13-8Mo steel is 208,000psi.....</i>	<i>113</i>

LIST OF SYMBOLS AND ABBREVIATIONS

AM	Additive Manufacturing
LPBF	Laser powder-based fusion
MMPDS	Metallic Material Properties Development and Standardization
TO	Topology optimization
SIMP	Solid Isotropic Material Penalization
CRSNG	Conseil National de Recherche en Sciences Naturelles et Génie du Canada
FRQNT	Fond de Recherche du Québec – Natures et Technologies

LIST OF APPENDICES

Appendix A – Global APU hinge analyses calculations.....	89
Appendix B – Test Matrix of qualifications coupons	106
Appendix C – Article 1: Paper of partial interpretation submitted to the Canadian Aeronautic and space Journal	107

CHAPTER 1 INTRODUCTION

This master's thesis gathers 30 months of work conducted jointly with Bombardier Aerospace and Polytechnique Montréal. Thanks to the Industrial Innovation Scholarship Program from NSERC and FRQNT, the author worked on the integration of additive manufacturing (AM) technologies on productions parts at Bombardier Aerospace.

Additive manufacturing processes are defined, as the name suggests, by the fact that they build parts by adding material without mold or tooling. It is opposed to subtractive methods such as machining or other methods that require molds, e.g. casting or forging. AM methods therefore have a great geometrical freedom which allows to produce complex parts that wouldn't be possible or very expensive otherwise.

In fact, now, in the aerospace industry, manufacturability dominates the design process. Thus, conservative compromises are made when considering efficient load bearing. In other words, manufacturing constraints of conventional methods limit the complexity of the structure which leads to heavier parts.

Therefore, designing parts solely in order to accomplish certain functions, such as bearing loads, instead of ensuring manufacturability, could help taking a lot of weight off an aircraft. With AM, this would be feasible but design methods and tools need to be revised.

Simulation tools such as finite element analysis (FEA) help predicting the performance of a part. With the increasing computing power available in the industry, FEA becomes standard and widely accepted as a stress validation method. Recent technologies can now even help predicting mathematically the optimal shape or topology of a part at the very beginning of the design life cycle. This is referred to as topology optimization.

Nevertheless, aerospace industry showed little interest in topology optimization since it creates parts with "organic" features that are hard if not impossible to manufacture. With AM, those parts could finally be manufactured with ease and yield the associated weight saving.

First AM processes were invented more than 30 years ago but the recent interest of Bombardier aerospace for producing parts with these technologies is motivated by several indicators.

Among other things, penetration of AM is significantly growing in the manufacturing sector for many consecutive years which partly testifies the capacities of the processes. More specifically, sales of AM machines rose significantly among other aerospace companies. Publicly released case studies demonstrate the intense investment in AM of the aerospace sectors, whether in military, civil or space.

Numerous elements also indicated that properties of metallic AM parts were sufficient to produce them steadily with great mechanical properties. Anterior research project showed that mechanical properties of titanium made in AM are close to these of regular wrought titanium. Moreover, several industrial suppliers were identified and some had relevant aeronautic experience which increases the level of confidence of their quality controls. Machine manufacturers improved the quality control of the machines themselves, helping to monitor defects *in situ*.

Stability of the supply chain also improved drastically during the last 3 to 5 years. In aerospace, large production requires stable and various suppliers. For instance, powder manufacturers specialized in raw powder for AM machines appeared recently. In addition, actual aerospace suppliers started to buy and use AM machines. Having suppliers with solid knowledge of the standard and quality requirements of the aerospace industry is a key aspect identified by Bombardier to invest in this area.

Furthermore, normalization organizations recently started to produce standards for processes, powders and mechanical testing which will ease qualification and certification of AM parts.

However, at Bombardier, several challenges needed to be tackled in order to integrate additive manufacturing processes with the associated positive effects. In fact, very limited experience with numerical tools such as topology optimization previously existed. Design with simulation had been used only to optimize machined or forged parts. Moreover, full-size components were never produced using AM. Scalability risks and qualification needed to be addressed.

Ultimately, being able to scale the benefits of AM at Bombardier aerospace implies to have experts, called knowledge owners, able to identify areas where the technology could be integrated successfully. This requires to build practical experience and establish identification mechanisms among a focus group.

The present project was led by the Core Engineering - Structure department and partly financed by the Strategic Technology department. The role of the latter is to explore new technologies and

assess Technology Readiness Level (TRL) [5] of technologies that can potentially improve their products in different ways. On the other hand, the role of the Core Engineering – Structure department focuses specifically on improving the design and fabrication methods of the structures and their components. Depending on the TRL gate in which a certain technology is situated and the interest for Bombardier Aerospace, the scope of the projects will vary from technological surveillance to integration into production.

In the case of additive manufacturing, the readiness level was judged as sufficiently high to explore process qualification, a prerequisite to integration into production. However, all supporting areas of this manufacturing process such as design methodologies needed to be addressed. Therefore, a project was launched with several stakeholders from different engineering areas to cover: part selection, cost evaluation, supply chain, quality, design and stress. Those last two are the subject of this work. The presence of graduate students is favorable in this context since it allows to have a theoretical approach and explore with complete freedom the possibilities of the technologies.

The first hypothesis that led the project was that additive manufacturing and use of numerical design tools such as topology optimization can lead to lighter products and therefore, more competitive aircrafts. The second hypothesis was that it is possible to qualify AM parts with short schedule and low resources. Indeed, integration of new manufacturing processes are historically resource and time extensive but with a new approach this could be reduced significantly.

Therefore, the first objective was to develop a methodology to design for additive manufacturing with the help of topology optimization. The second objective was to explore the qualification of additively manufactured parts in the aerospace industry with the associated qualification challenges with limited testing.

Although recent research has increased its 3 dimensional capacities, topology optimization was always used as a tool to benchmark concepts. Yet several challenges needed to be addressed in order to use this numerical technique to produce detailed designs. Exploration of topology optimization limitations and capabilities was done on 3 case studies of conventionally manufactured aeronautic parts. General guidelines are extracted at the different steps of the design lifecycle with topology optimization for additive manufacturing.

Few studies cover the complex venture of interpreting an optimization result. In this work, new approaches are proposed at the interpretation stage of the design to increase the level of confidence

of an optimization result and reduce the interpretation time. Moreover, a quick overview of the next generation of topology optimization solvers is introduced including novel algorithms such as the level-set method. This allows to assess the potential of the near-coming technologies in that field.

Moreover, no publicly available document covers the qualification of an AM part in aerospace. Design lifecycle in civil aviation includes material and process qualification. In this work, an affordable and rapid method to integrate a specific AM part on a civil aircraft is proposed. That's why, in this study, to validate numerical analyses done on one of the aforementioned optimization case studies, a complete campaign of qualification tests was led. Qualifying a simple part requires low amount of resources and putting it into production then allows to accumulate statistical data over time which contributes to raising the confidence level of the whole process.

The following study is snapshot in time of two technologies in one industry at a specific point in time. It is foreseen that these findings will need to be updated in a few years when the technologies will get more mature.

CHAPTER 2 LITERATURE REVIEW

2.1 Design and qualification in aerospace

The design of aircrafts in the civil aerospace industry is regulated by national agencies. In Canada, Transport Canada “*establishes and regulates standards for aeronautical products designed and operated in Canada*” [1].

For detailed metallic components, specific rules exist related to their function, location or flight criticality in the aircraft. On the other hand, some general rules apply to all load bearing components. One of the most critical rule for certification is the stress criterion, stating that all components should not reach failure of the material at ultimate load and should not exceed plastic deformation at limit load.

The stress requirements are critical when designing parts for additive manufacturing because the properties of the material are not yet thoroughly established. On the other hand, for metallic parts machined out of wrought billets for example, material databases are complete enough to list statistical scatter of properties and subsequently extract material allowable. Those allowable are then used when analyzing the parts to ensure the stress level is below what's permissible. In aerospace, the most common material database referred to is the *Metallic Material Properties Development and Standardization* [2] (MMPDS), which is approved by Transport Canada and the Federal Aviation Administration as well as the NASA in the US. However, no allowable is yet available in the MMPDS for additive manufactured materials, therefore, requiring other avenues for certification.

Since the development of an aircraft is driven by safety requirements, adding new components or technologies requires extensive testing. It is therefore often faster and more economical to copy already approved designs instead of finding new ways of improving parts.

Moreover, since the most predominant manufacturing technique nowadays is still machining, several constraints need to be taken into consideration during the design phase. Complex geometries that the machining tools cannot easily produce become expensive to produce if not downright impossible. This significantly limits the design freedom and instead of creating a part optimized for its functions such as bearing loads, it is designed to ease manufacturing.

As it is exposed in the following sections, additive manufacturing allows a great geometrical freedom that allows to align the design on the functions.

2.2 Additive manufacturing

Additive manufacturing, or 3D printing, is a family of manufacturing techniques characterized by the fact that material is bound together. The ASTM F42 committee in charge of normalizing additive manufacturing defines the latter as a “process of joining materials to make objects from 3D model data, usually layer upon layer, as opposed to subtractive manufacturing methodologies” [3] such as carving, drilling, machining, etc. Although a distinction is made between AM and 3D printing by the F42 committee, in general, both terms are used as synonyms.

As of 2015, ASTM F2792 divides all the AM technologies into 7 categories, detailed at Table 2.1 [3] [4].

Table 2.1 – Categories of additive manufacturing technologies with their benefits and limitations

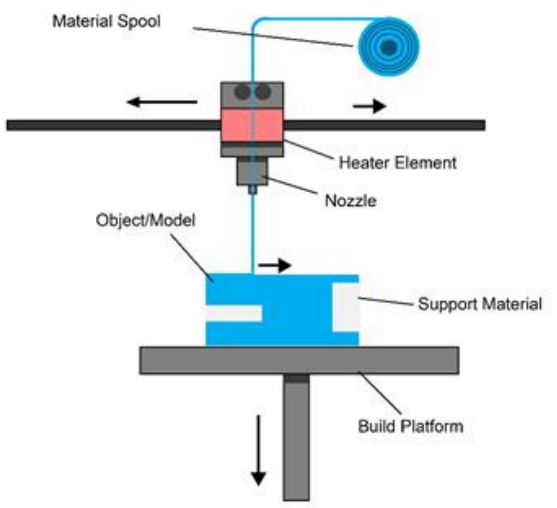
Definitions and typical usage	Applications
<p><u>Material extrusion (ME)</u>: material is selectively dispensed through a nozzle or orifice. Raw materials are generally wires of thermoplastics or metal. Most low-cost printers use ME because it is simple, safe, and works in typical office environments. Industrial ME machines are typically fast compared to powder-based processes. While typical plastic are relatively weak, certain patented materials such as Ultem® (Polyether ether ketone) produced by ME can be quite strong. Precision of the features</p>	<div data-bbox="743 1066 1414 1627">  <p>The diagram illustrates the Material Extrusion (ME) process. A material spool (blue) feeds a filament (blue) into a nozzle assembly. The assembly includes a heater element (red) and a nozzle (black). The filament is extruded through the nozzle to form an object/model (blue) on a build platform (grey). Support material (white) is also extruded to support the object. Arrows indicate the flow of material and the direction of the build platform movement.</p> </div> <p>Source: Loughborough University</p>

Table 2.1 – Categories of additive manufacturing technologies with their benefits and limitations (continued)

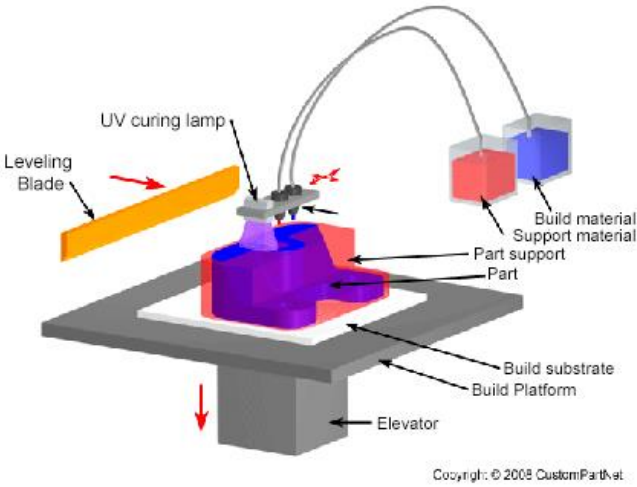
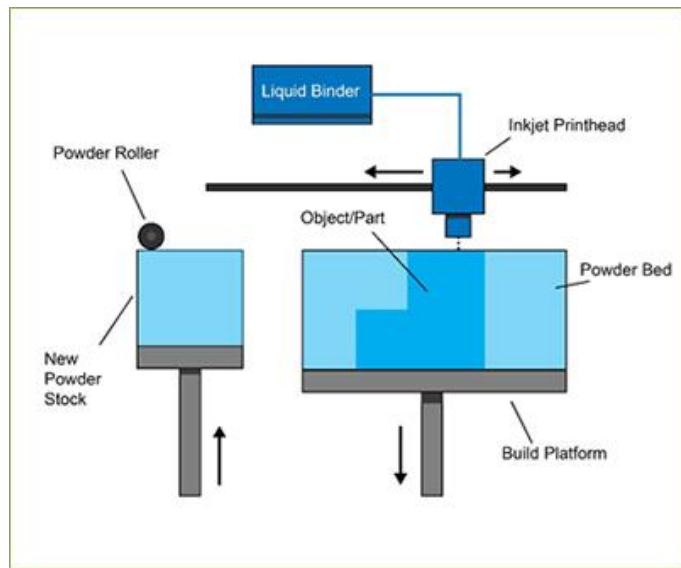
<p>made in ME depends on the wire and is therefore rougher than other processes. Additionally, delamination between layer is frequent. Used for affordable prototyping, larger machines are popular for building tools and molds.</p>	
<p><u>Material jetting (MJ)</u>: droplets of material are selectively deposited and cured by an energy source, generally UV lights. This is one of the most precise process with moderate build speed. The ability to produce multi-material is a notable advantage of this technology. Mechanical properties are lower than other processes and often degrades after time due to light sensitivity. It is used mostly for prototyping.</p>	 <p>Source: Loughborough University</p>

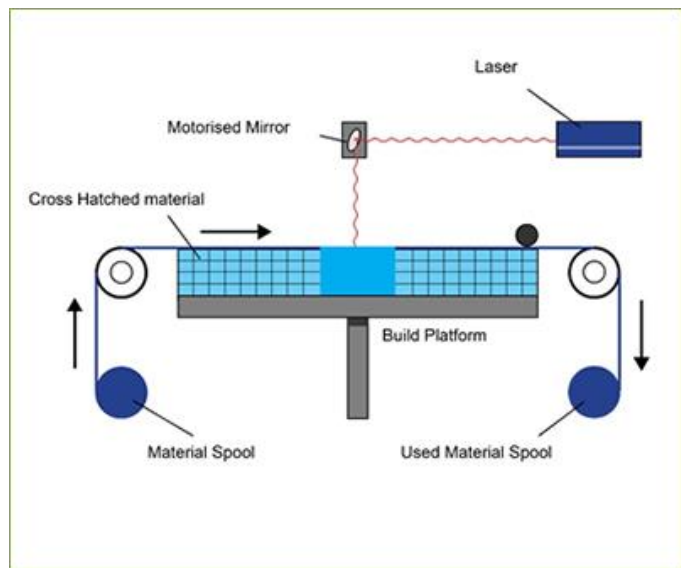
Table 2.1 – Categories of additive manufacturing technologies with their benefits and limitations (continued)

Binder jetting (BJ): liquid bonding agent is selectively deposited to join powder materials. All kind of powders can be used (plastics and metals). Bonding agent can be replaced in a post-processing operation by low viscosity metals such as gold, brass, etc. Only sintering of material is achievable with this technology and thus, low mechanical properties must be expected. Typical applications are plugs for casting, filters and jewelry.



Source: Loughborough University

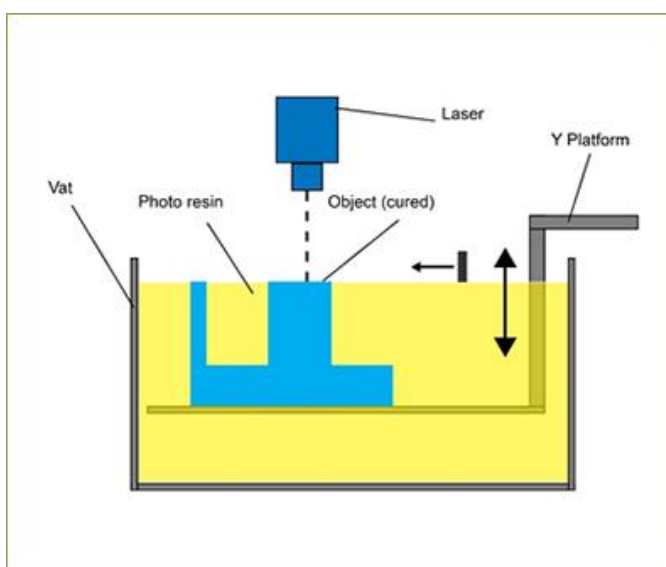
Sheet lamination (SL): a laser or a robotized knife cuts a layout in multiple sheets of paper. The sheets are then bonded together to form an object. Colors can be printed on the paper prior to cut of the layout. This process is affordable and allows to make model with a complete palette of colors. However, it is slow and parts made by SL have very low mechanical properties.



Source: Loughborough University

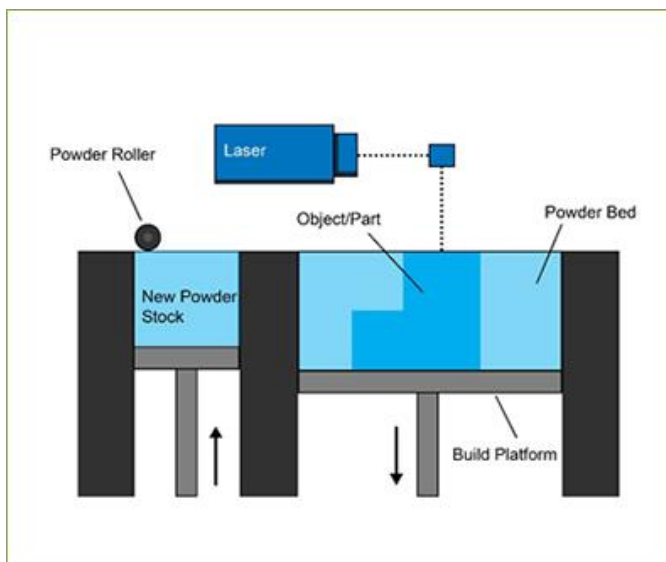
Table 2.1 – Categories of additive manufacturing technologies with their benefits and limitations (continued)

Vat photopolymerization (VP): liquid photopolymer in a vat is selectively cured by light-activated polymerization. This was the first 3D printing process to be invented. It remains the most precise technique and offers acceptable mechanical properties. Many types of resins can be used while many sizes of machines at different prices exist. However, the process is expensive to run since uncured resin is often wasted. Typical applications are functional prototypes, custom medical devices (tooth braces, hearing aids, etc.) and investment casting plugs.



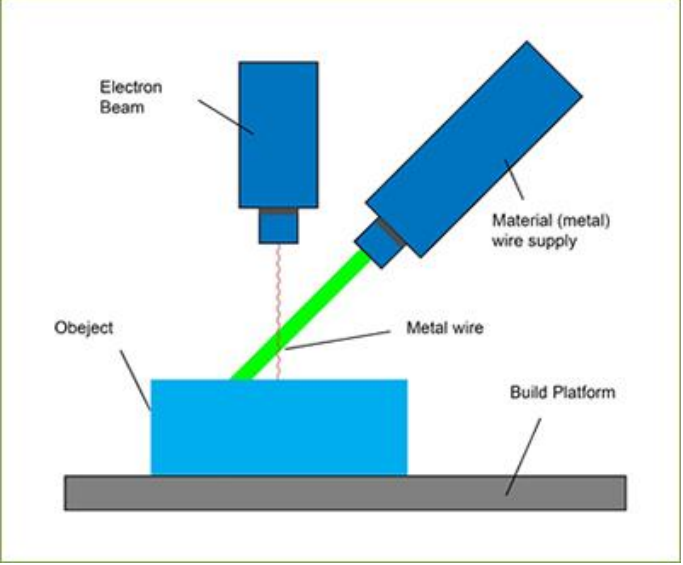
Source: Loughborough University

Powder bed fusion (PBF): thermal energy selectively fuses regions of a powder layer. Once the powder is consolidated, the build platform goes down, another layer of powder is dropped on top of the previous one by a powder roller and the process starts over. Thermoplastics and metals with good weldability can be manufactured. This technique offers a good precision on dimensions but this is variable



Source: Loughborough University

Table 2.1 – Categories of additive manufacturing technologies with their benefits and limitations (continued)

<p>depending on the material. Mechanical properties are comparable to other processes. It is probably the most economical technology. Metallic parts made in PBF are generally used in medical, aerospace and oil & gas industries.</p>	
<p><u>Directed energy deposition (DED)</u>: focused thermal energy is used to fuse materials by melting as the material is deposited. Feed material can be a projected powder or metallic wire. This process has a better build volume rate compared to PBF. The geometry definition is approximate and surface finish is often rough. Post-processing such as machining is often required. DED is used for the repair on existing structure or to create stock for machining. It has great scalability and good potential for aerospace since larger components could be produce faster and at lower cost in the near future.</p>	 <p>The diagram illustrates the Directed Energy Deposition (DED) process. It shows a blue rectangular block labeled 'Object' being built on a grey 'Build Platform'. A green 'Electron Beam' is directed at the top surface of the object. A blue 'Material (metal) wire supply' is shown feeding a 'Metal wire' into the point where the electron beam strikes the object. The wire is shown melting and fusing with the existing material to form a new layer.</p> <p>Source: Loughborough University</p>

According to Wohlers Associates [5], the AM technologies market can be divided in 2 sectors: industrial grade machines and consumer “desktop” machines selling for less than 5000\$USD. This last category is mostly constituted of material extrusion machines and won’t be discussed in this work.

2.2.1 Growth and recent development

As of 2015, the largest industrial AM machines manufacturers in terms of units sold are Stratasys from Israel, 3D Systems from the USA and Envisiotech from Germany. EOS from Germany could be added to this group as it is the leading powder-bed fusion machine manufacturer and whose notable growth illustrates the interest for this technology. Figure 2.1 and Table 2.2 below picture the financial results and the importance of the larger machine manufacturers.

Table 2.2 – Most important AM machine manufacturers in the world and their accumulated sales and revenues in 2014 [6].

Companies	Technologies	Units sold since 1990	Revenues in 2014 (USD\$)
Stratasys	Material extrusion	41869	750M
	Material Jetting		
3D Systems	Vat photopolymerization	17792	654M
	Polymer powder-bed fusion		
	Metal powder-bed fusion		
	Binder jetting		
	Material jetting		
	Material extrusion		
EnvisioTech	Vat photopolymerization	5878	Undisclosed (around 100M)
	(bio) Material extrusion		
EOS	Polymer powder-bed fusion	1762	195M
	Metal powder-bed fusion		

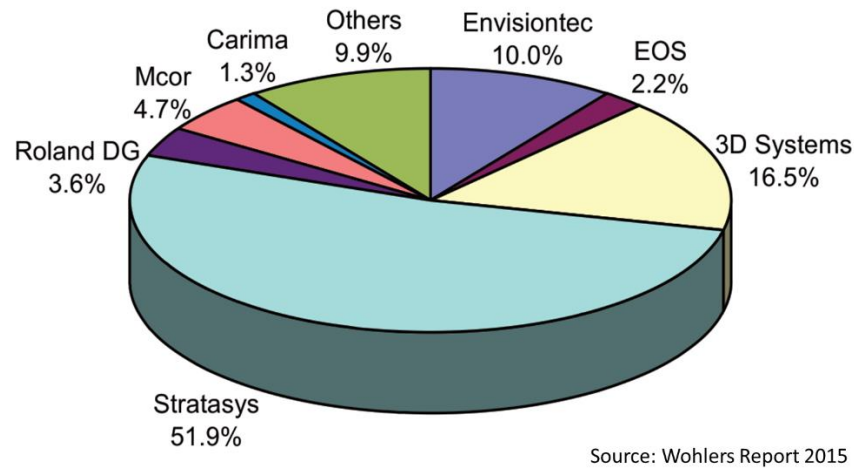


Figure 2.1 – Proportion of units sold above 5000\$USD in 2014 by each machine manufacturers

Additive manufacturing industry including revenues of products (sales of machines, materials, software, etc.) and services (production of parts by service providers, maintenance, training, etc.) trade around the world has been increasing rapidly for the last 20 years. According to Wohlers Associates [5], the most renowned AM consulting firm in the world, since 2010, compound annual growth rate (CAGR) of AM industry is above 20%, with a record of 35.2% in 2014.

Figure 2.2 shows the overview of the revenues and CAGR of this industry for the past 20 years. Numbers exclude the sales relative to the desktop 3D printed machines.



Figure 2.2 – Growth and overall revenues of the additive manufacturing industry of the last 20 years

Historically, AM was mostly used for prototyping purposes. The fast turnovers allow to iterate rapidly on a design without having to invest in tooling just for prototypes. The cost of AM production was previously too high to be cost-effective in actual production. Moreover, the limited materials available 10 to 20 years ago made it hard to get the desired results. However, the technologies have now matured and the most popular applications for AM have shifted from prototyping towards functional parts, although prototyping still remains the most frequent application, as depicted in Figure 2.3.

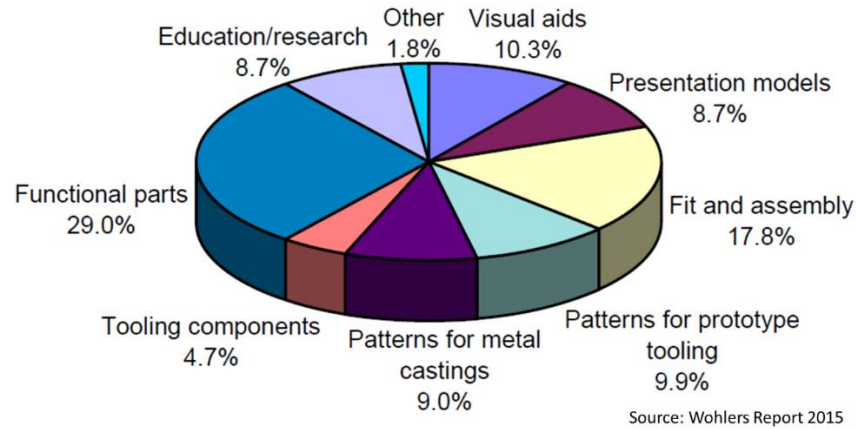


Figure 2.3 – Proportion of typical usage of additive manufacturing

Almost all manufacturing industries and many services industries are now using AM somewhere in their business model. Figure 2.4 illustrates the distribution of customers per industry according to 127 of the largest AM machine manufacturers and AM service providers across the world.

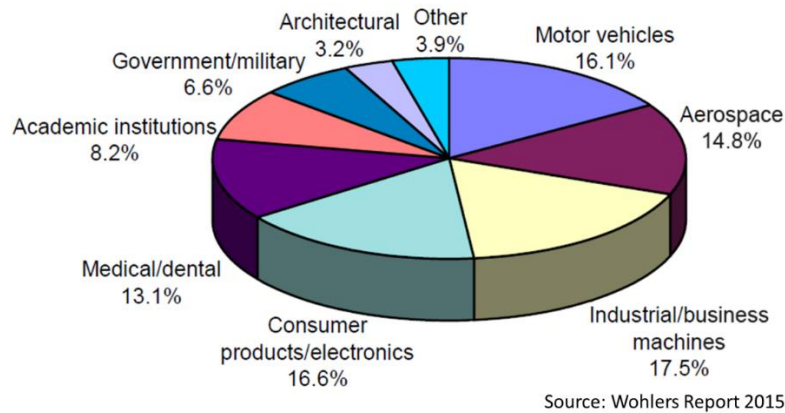


Figure 2.4 – Industrial sectors in which AM is mostly used according to machine manufacturers and service providers

Among all industries, aerospace is probably the most interested in AM and its potential applications. Indeed, high-value components and low production volume constitutes an ideal scenario for AM. Boeing engineers stated that they already installed around 100,000 AM parts on 16 of their commercial and military aircrafts. Although most of those parts were in polymers, the interest for metal parts made by powder-bed fusion is increasing. Table 2.3 gathers some examples of metal parts for aerospace applications that were publicly demonstrated from 2013 to 2015.

Table 2.3 – Publicly released AM aerospace applications




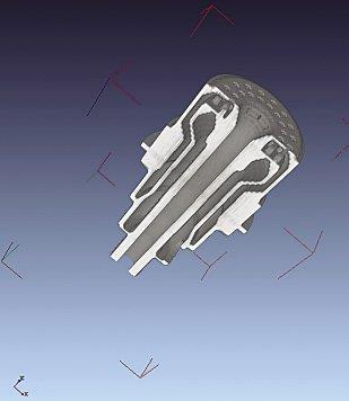

General Electric	Fuel nozzle for LEAP engine, combining 18 parts into 1 while being 25% lighter and lasting 5 times longer. In 2015 only, 30,000 units will be produced [7].	
Airbus	Cabin bracket, optimized by topology optimization. It flew on Airbus' new A350 in June 2014. The part is reported as 30% lighter than its machined counterpart [8].	
SpaceX	Falcon 9 Rocket main oxidizer valve. It was originally casted but powder-bed fusion allowed to have greater material properties and a manufacturing lead time of 2 days instead of months [9].	
Aerojet Rocketdyne	Bantam demonstration motor entirely produced with 3 powder-bed fusion parts assembled together allowed to consolidate dozens of parts together. The cost of the motor was reduced by 65% [10].	

Table 2.3 – Publicly released AM aerospace applications (continued)

GKN Aerospace	Leading edge concept component optimized by topology optimization and built by powder-bed fusion. Several sub-components were combined in the final part [11].	
---------------	--	--

2.2.2 Selective laser melting process

Powder-bed fusion process, as explained before, melts powder to consolidate a part. The energy required to this aim can be provided by a laser (laser powder-bed fusion, LPBF) or an electron beam (electron beam powder-bed fusion). Although the electron beam technology has its advantages and is promising, the present work focuses on LPBF. Particularly, the material that is of interest in this work is the titanium Ti-6Al-4V (60% of titanium production in USA and EU). Due to its raw price 10 times higher than aluminum for instance [12], titanium is often avoided in civil aviation, despite its interesting mechanical and thermal properties [2].

As an exotic and new manufacturing process, AM can be quite expensive and has a narrow window for good business cases. However, considering the potential weight saving of an optimized design and the high cost of machining titanium, producing parts in titanium by AM can be competitive.

2.3 Topology optimization

One of the greatest interest of aerospace for AM is the ability to design products with few manufacturing constraints on the geometry. Thus, it allows to get designs optimized to meet certain

performance targets such as weight or aerodynamic properties instead of optimizing manufacturability.

In order to do so, numerical tools exist that help predicting what is the best material distribution within a volume to optimize certain criteria while respecting defined constraints. The most popular algorithm for this is called topology optimization (TO). Based on finite element models, TO solvers can be well integrated into the design methodology in aerospace. Several TO algorithms exist but focus is placed on the more mature which are already used commercially. In this study, for its applicability to the aerospace industry, only TO software able to optimize 3D parts (volume) will be considered and the one prominently used is Optistruct by Altair.

2.3.1 Solid Isotropic Material Penalization (SIMP) Method

Rozvany [13] classifies the different topology optimization approaches in the following categories: Isotropic Solid/Empty (ISE), Anisotropic Solid/Empty (ASE) and Isotropic Solid/Empty/Porous (ASEP). More specifically, the ISE approach includes the Solid Isotropic Material Penalization method (SIMP) which is in 2015, the most commonly used in commercially available software.

2.3.1.1 Homogenization of density

One can argue that topology optimization started at the end of the 1980s with the paper of Bendsoe and Kikuchi [14]. Before that, most of the research efforts in numerical structures optimization were concentrated on shape optimization. In two papers published in 1988 and 1989 [15], Bendsoe proposed a method, later coined as Solid Isotropic Material Penalization (SIMP). This numerical method is based on the idea that the optimal material distribution of a structure can be comprised within a bigger volume called the design space. By discretizing the design space in elements, some elements can be turned on or off so they contribute or not to the overall stiffness of the structure. Therefore, in finite element modeling, every element is a design variable that can be either solid (turned on) or a void (turned off), see Figure 2.5 below.

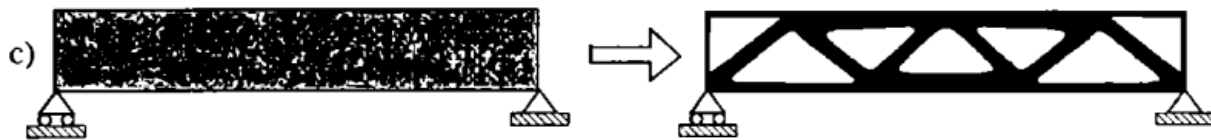


Figure 2.5 – Topology optimizations of 2D beam using material density approach. The optimal topology lies within its design space [16]

However, in practice, the discrete nature of the solid/void concept is numerically hard to handle. Thus, Bendsoe [15] proposed the material density approach which works with continuous variables that are easier to compute. The stiffness equation, where f is the external forces vector applied on the structure, K the stiffness matrix and u the displacement vector is:

$$f = K \cdot u \quad (1)$$

The stiffness matrix can be written as:

$$K = K(\rho(x)) = (\rho_e(x))^p K_e \quad (2)$$

Where $\rho_e(x)$ is a density function varying between 0 and 1 for all design variables (elements) denoted as x . Thus, the stiffness K can vary continuously between 0 and K_e , the actual stiffness of the material.

An ideal solution would have all the densities at either 0 or 1 since intermediate stiffness don't have any physical meaning with homogenous materials. Thus, the exponent p over the density function is introduced to penalize intermediate density values. It is repeated in the literature that $p = 3$ works well [17].

Figure 2.6 illustrates the influence of the penalization factor on the relative stiffness of the element. As p increases, intermediate values of density are closer to either 0 or 1.

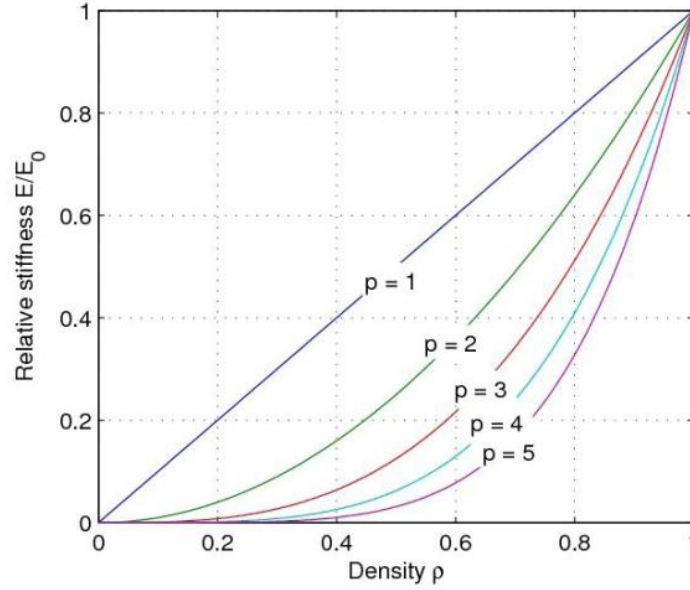


Figure 2.6 – Influence of penalization factor on relative stiffness. Adapted from [18].

2.3.1.2 Sensitivity analysis

The SIMP method is gradient-based, meaning it evaluates sensitivity of the responses to changes of the design variables. For example, if a design variable, in this case an element of the model, contributes in increasing the stiffness of the model, its density is raised. Otherwise, density of the element decreases until it eventually vanishes. This is important since most mathematical numerical algorithms are based on sensitivity analyses. Thus, optimizations can be formulated with different objectives and constraints (minimize compliance, reduce displacement, reduce weight, etc.) and sensitivity of all these parameters with the design variables shall be established. The general mathematical formulation of an optimization problem being of the following form:

$$\min h(x) \quad (3)$$

$$g_i(x) \leq G ; i = 1, \dots, m \quad (4)$$

Where $h(x)$ is the objective function, i.e.: the response to be optimized, and $g_i(x)$ are the m constraints to be respected. In numerical optimization, the responses are all the monitored output such as compliance, stress, displacement, etc. Most of the possible responses are related to displacement $u(x)$ (see stiffness equation above). Therefore, sensitivity analysis of all responses are often derived from sensitivity between displacement and design variables:

$$\frac{\partial h(x, u(x))}{\partial x_j} \text{ for } j = 1, \dots, n$$

Where x_j is a design variable and n the total number of design variables (i.e. number of elements). In problems with large amounts of design variables such as most topology optimization problems, the response function sensitivity is found by the adjoint variable method [16]. Instead of calculating the displacement sensitivity for all variables and for each response, the adjoint method allow to compute sensitivity for all variables once for each response, significantly reducing the calculation time.

2.3.1.3 Formulations

Several optimization methods can be used to solve topology optimization problems but the details will not be explained in this work. Here's a short list of the most commonly used optimization methods:

- Optimality criteria (OC), reviewed and explained in details in the book of Bense [16].
- Method of moving asymptotes (MMA) or convex linearization (CONLIN) which are both similar. The former, proposed by Svanberg in 1987 [19] is based on the later by Fleury and Braibant in 1985 and 1989 [20]. The idea is to divide the domain into smaller sections where the optimization function will be convex and where a linearization is possible. This is probably the most widely used method in numerical topology optimization.
- Method of feasible directions (MFD), initially proposed by Vanderplaats in 1983 [21].

2.3.1.4 Responses

The standard optimization formulation is the following:

$$\min h(x) = \frac{1}{2} f^T u(x) \quad (5)$$

with

$$\sum_{e=1}^N \rho_e(x) v_e \leq V \text{ with } e = 1, \dots, N \quad (6)$$

where v_e is the volume of an element and the function $h(x)$ is the compliance. The variable f is the external load vector and $u(x)$ is the displacement vector. Compliance is inversely proportional to stiffness thus measuring the flexibility of a structure. Therefore, the objective is to reduce the compliance (increasing stiffness) with a limited amount of volume V . Compliance is an interesting response to work with since it is closely related to displacement and its sensitivity is greatly simplified by the adjoint method.

2.3.1.5 Stress driven optimization

When topology optimization is used as a design tool, several factors need to be considered such as stress distribution in the structure. Indeed, in an industrial context, the design of parts is often driven by the acceptable stress level. Thus, depending on the material used, a maximum stress level is to be respected.

$$\sigma_e < \overline{\sigma_{VM}}; e = 1, \dots, N \quad (7)$$

Where σ_e is the stress measured in element e and $\overline{\sigma_{VM}}$ is, for example, the maximum Von Mises stress allowable by the material. Adding this constraint in the formulation of the optimization results in adding one stress constraint for each element, or design variable in the model. This is in practice totally impossible to use as it would be too time-consuming to compute sensitivity for each constraint.

Another problem with stress constraint is the singularity problem. For example, with a bar in tension, as the diameter of the bar decreases, its stress level increases. In an optimization problem, this would prevent the bar (or element) to vanish.

The stress penalization method has been studied by several authors to avoid the singularity problem [22]. The idea is to penalize the stress the same way the stiffness is penalized.

$$\sigma_e = \rho_e(x)^q \widehat{\sigma}_e; e = 1, \dots, N \quad (8)$$

Thus, the calculated stress level of an element σ_e decreases if the density of the element vanishes, even if the actual stress level $\widehat{\sigma}_e$ increases. Exponent q helps again enforcing intermediate value elements toward 0 or 1.

To reduce the number of design variables when optimizing a problem with local stress constraints, several techniques can be used but few have been successfully implemented in a commercial solver.

A popular technique is to use a global constraint, where only the elements with the highest stress level are considered in the optimization. Initially proposed by Werme in 2008 [23], this technique is not efficient in avoiding stress concentrations.

A recent clustering technique developed by Holmberg [24] proposes a promising compromise between global and local constraints that is worth being mentioned. The idea is to group all the elements with similar stress level in clusters where only one stress constraint will be computed for each cluster. To do this, all the measured stress points are placed in descending order.

$$\underbrace{\sigma_1 \geq \sigma_2 \geq \sigma_3 \geq \dots \geq \sigma_{\frac{n_a}{n_i}}}_{cluster\ 1} \geq \underbrace{\dots \geq \sigma_{\frac{2n_a}{n_i}}}_{cluster\ 2} \geq \dots \geq \underbrace{\sigma_{\frac{Xn_a}{n_i}}}_{cluster\ X} \geq \dots \geq \underbrace{\sigma_{\frac{(n_i-1)n_a}{n_i}} \geq \sigma_{n_i}}_{cluster\ n_i} \quad (9)$$

Where n_a is the number of stress measured points and n_i the number of clusters. Then, a constraint is extracted from the cluster with a P-norm averaging.

$$\sigma_i(x) = \left(\frac{1}{n_i} \sum_{a \in \Omega_i} (\sigma_a(x))^p \right)^{\frac{1}{p}} \quad (10)$$

Where σ_i is the stress constraint for cluster i (Ω_i), σ_a the stress measured at points contained in Ω_i and p , a predetermined factor. As factor p increases, the value of σ_i gets closer to the maximum stress measure point of the cluster ($\max_{a \in \Omega_i} \sigma_a(x)$). Holmberg reports using values for p between 8 and 12.

A comparison between the clustered and the global techniques is illustrated in Figure 2.7 where an L-shape beam is optimized with two different stress constraint techniques: global and clustered. The global stress constraint being too rough, it cannot get rid of the stress concentration in the corner as opposed to the clustered stress constraint where a radius is created to smooth the concentration. The latter has been implemented in the TRINITAS solver.

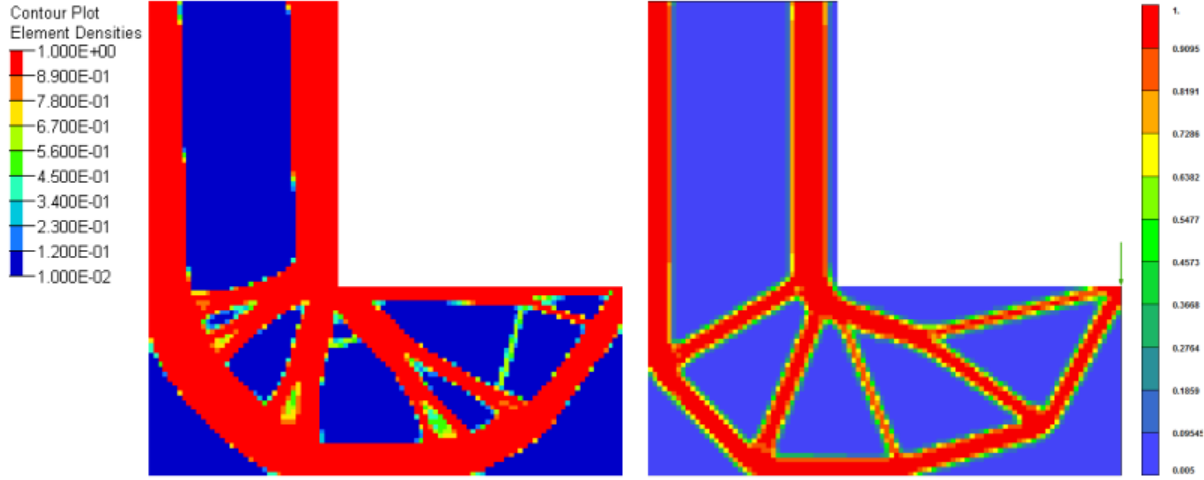


Figure 2.7 – Topology optimization of a 2D L-shape beam with stress constraints [24]. The stress concentration is not avoided with global method in Optistruct (left) whereas a radius is created at the corner with clustered method in TRINITAS (right).

However, Holmberg shows that the clustered approach can be much more time-consuming than the global approach.

2.3.2 Level Set

The level set method (LSM) was first introduced by Osher and Sethian [25] to study front propagation under a speed vector, such as lava dripping down along the contour of a volcano. Its adaptation to topology optimization was initially proposed by Wang [26] and Allaire [27]. The fundamental principle of the level set method for topology optimization are briefly described here but for further information, the reader is referred to the review by Van Dijk et al. [28].

The level-set method can be exemplified with a 2D contour moving along a surface. The idea is to implicitly represent the boundary S with a higher dimension model $\varphi(x, t)$, where x is the coordinate vector, t is the virtual time, representing boundary variations. Therefore, as illustrated in Figure 2.8, the 2D space hatched in red is represented as the contour of a 3D surface at a certain value of $t = k$. Points x that belong on the boundary are defined by the iso-contour S that intersect the level set model at height k .

$$S = \{x: \varphi(x, t) = k\} \quad (11)$$

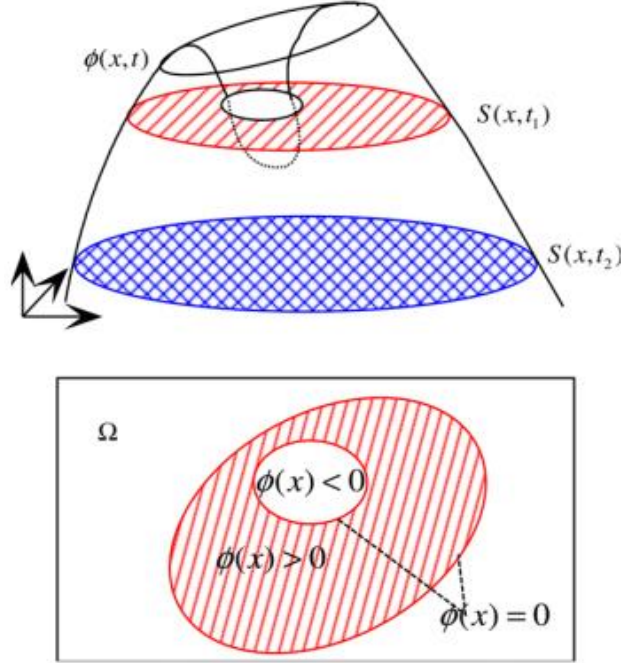


Figure 2.8 – 2D example with boundary represented by all the points on the level set surface at time (t) equals k [29].

The boundary is defined with the following relation:

$$\varphi(x) \begin{cases} > 0 & \text{if inside boundary} \\ = 0 & \text{if on boundary} \\ < 0 & \text{if outside boundary} \end{cases} \quad (12)$$

Using partial derivative of the surface, the level set can be modified to satisfy a certain objective under certain constraints (e.g. minimizing compliance with a maximum volume). As shown in Figure 2.9, during the optimization, holes in the level set can vanish or be combined with each other. However, new holes cannot be created. Therefore, the original solutions proposed by Wang [26] is to introduce holes in the design space.

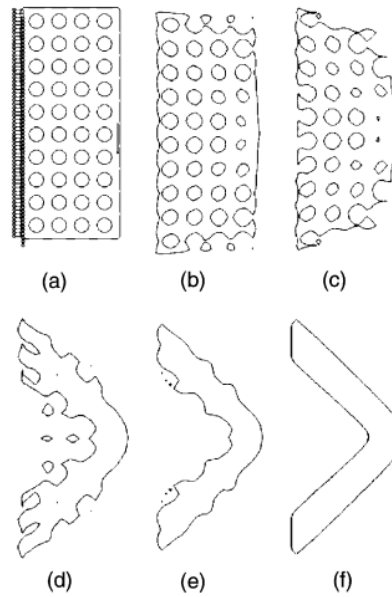


Figure 2.9 – Level set optimization of the two-bar example with a perforated initial design [26]

This method is design dependent and several authors have published methods to avoid the artificial introduction of holes in the design space with topological derivatives [30] [31] or with the evolutionary “hard-kill” method [29].

Complexity of the LSM is proportionate to the surface it describes rather than the volume it encapsulates, which makes it more efficient at dealing with problems with large number of degrees of freedom. Furthermore, the level set model does not homogenize the density of elements. Thus, stiffness of the resulting topologies is more accurate and, as it is exposed later, interpretation is easier.

Level set method is highly scalable and can be used for 3D models. As of 2016, several commercial software incorporate topology optimization with the level set method and some exploratory work with this method is exposed in Section 3.4.

CHAPTER 3 DESIGN METHODOLOGY FOR ADDITIVE MANUFACTURING

The rationale of this work focuses on part replacement. The approach is different than a clean sheet design and it is often a much harder task as well. Indeed, when a part is replaced, there is no flexibility on the surrounding space which limits the available choices. Complementary to this, when the boundary conditions are fixed there is less room for optimization of the load paths.

However, succeeding to design a proper replacement part is a clear proof that topology optimization make sense even in difficult scenarios. Moreover, as an earlier exploration of this technology, there are less risks to design new parts *a posteriori*, meaning it is outside of the engineering master schedule during the development of an aircraft.

Nonetheless, it is believed that the greatest usage of topology optimization with additive manufacturing parts in aerospace would be at the early stages of development where there is more flexibility on all components.

Figure 3.1 illustrates the different steps in order to design a part with topology optimization. In the following sections, those steps will be explored with their opportunities and limitations.

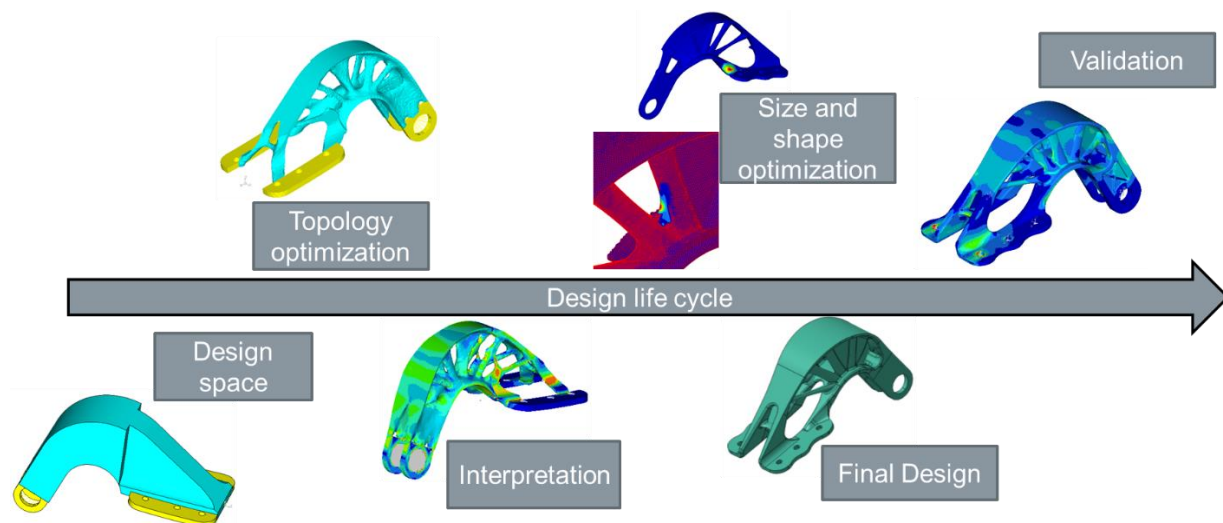


Figure 3.1 – Design methodology with topology optimization

3.1 Topology optimization

The results obtained with topology optimization are dependent on what is done at each of the steps. They are mostly independent but to certain extent, some choices at a particular step limit the others. There is no such thing as a unique recipe that will work every time in every situation. However, there are things to favor and to avoid when configuring a topology optimization. Failing to do so can lead to unsatisfactory optimization results. The first part of this chapter is dedicated to the description of good practices in configuring a topology optimization.

Furthermore, even when satisfactory results are obtained, it is a challenge to objectively select which result is best. Additionally, the following step, i.e. to interpret this finite element result into an aerospace part, is the subject of many research work in the optimization community. In the later portion of this chapter, a new approach will be detailed on how partial interpretation introduced in the actual methodology can help increasing the pace of the design lifecycle.

Throughout this thesis, 3 case studies will be exposed to illustrate the findings. They are presented in no particular order. The last case study on the auxiliary power unit (APU) door hinge of the Global aircraft will also be the sole subject of Chapter 4.

The first case deals with a fitting that supports the flap track in the trailing edge of a business aircraft, see Figure 3.2. This part is made in corrosion resistant steel and is riveted to the wing and bolted to track of the flap. Therefore, it is a highly critical part bearing large stress levels. Moreover, the part is large (14in x 6in x 12in) compared with the other two. This case study remains theoretical and never intended to be produced by ALM since it is too large for all the commercial PBFL machines currently available.

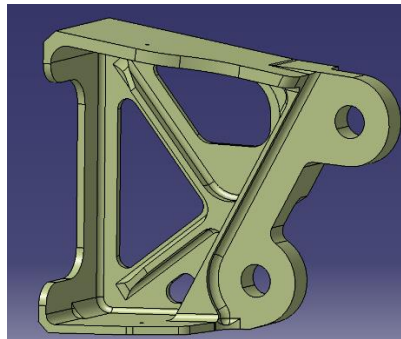


Figure 3.2 – Case study 1: flap track fitting in the trailing edge of a business aircraft

The second part studied here is illustrated in Figure 3.3. It is the hinge attaching the door of the auxiliary power unit (APU) in the CSeries, a commercial airplane. Built out of titanium for its strength at 200°F and 400°F, the CSeries' hinge has an arched geometry to allow a clearance when opening the door. The arch connects to a single lug. The loading scenarios involve in severe conditions such as 200F temperature with some surrounding components that have failed. Moreover, the part is bolted to a composite door which is less tolerant to impacts than a metallic one. Therefore, although they are normally small during regular operating conditions, the design loads are pretty high.

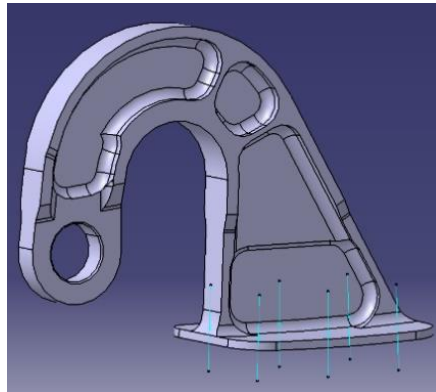


Figure 3.3 – Case study 2: APU door hinge of the CSeries commercial aircraft

The third case study focuses on a part with the same functions than the previous one but in a different aircraft. In the Global 7000 and 8000 aircrafts, although smaller than the CSeries, the APU door hinge is larger with dual lugs, see Figure 3.4. This part is an older design and therefore much heavier and bulkier than the CSeries' one. Design loading scenarios are similar to the second case.

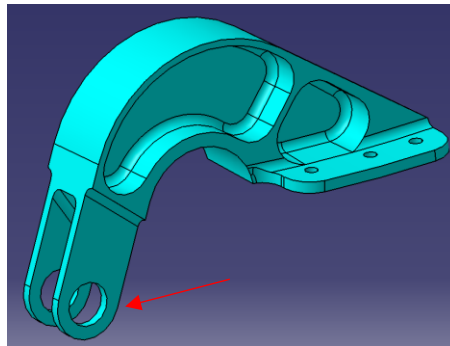


Figure 3.4 – Case study 3: APU door hinge in the Global 7000/8000 business aircraft. Lugs are pointed by the red arrow

3.1.1 Configuration

In a part replacement approach, modeling the design space can be more complex compared to a situation where no component is yet fixed in the environment of the part. Thus, as the example in Figure 3.5 shows, the design space of the flap track fitting has to nest between several other components. Moreover, fixation of the fasteners has to be considered, including their installation.

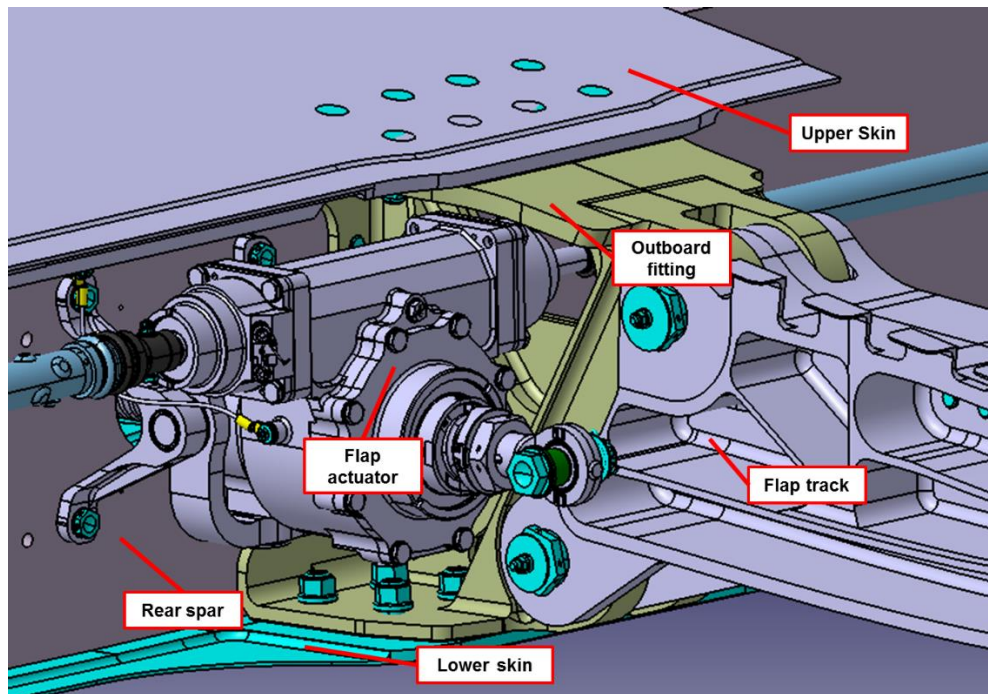


Figure 3.5 – Original assembly of the flap with the outboard fitting with all the surrounding components

In the numerical model, a non-design space has also to be set. This is the area that needs to be kept fully dense and therefore cannot be modified. Critical features of the part are often important to put as non-design space since their integrity is not calculated by FEA. For example, lugs and areas around bolts which are designed according to empirical equations must be preserved. Figure 3.6 shows design space in green and non-design spaces in yellow for the optimization model of the flap track fitting.

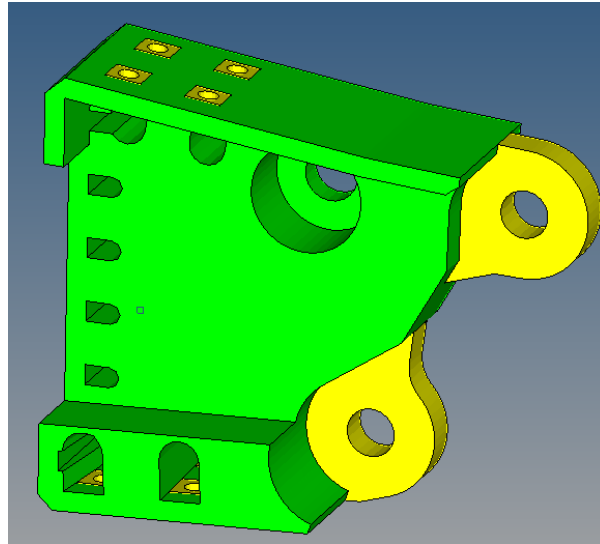


Figure 3.6 – Design space for optimization of the outboard fitting with pockets for surrounding elements and fasteners. Design space is in green, non-design space in yellow.

One can think that the larger the design space, the better are the chances to capture the right topology. However, in practice, it is often the opposite. Too large design spaces can lead to results with very low density elements. In Figure 3.7, the illustrated design space used for the CSeries APU hinge is much bigger than the original part: 32.8in^3 vs. 2.4in^3 respectively.

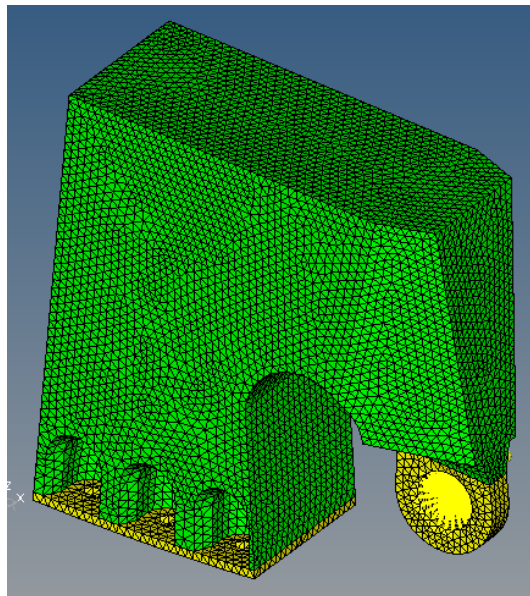


Figure 3.7 – Design space used for CSeries APU door hinge.

In order to obtain a weight reduction, in this example, more than 93% of the elements must have a density of 0. However, in practice, convergence of low density elements is never perfect and a lot of elements with medium density value appear, like it is exposed in Figure 3.8. Those elements bias the results by increasing artificially the stiffness according to Equation (2).

Later, when the geometry is interpreted and low density elements deleted, the stiffness will be much different. This dichotomy between in-solver results and interpreted results is addressed later.

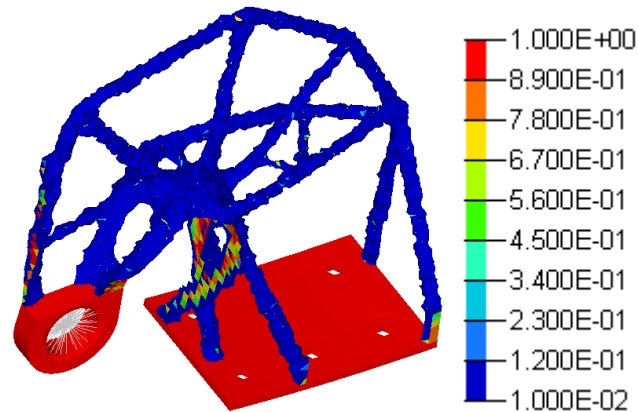


Figure 3.8 – Result from optimization with an iso-density filter that keeps only elements with density above 0.07. It is clear that density of elements is too low to be relevant.

Thus, targeting low volume fraction (below 15%) implies that most of the elements should be around 0. Therefore, the design space has to be narrowed down around the most probable area so the targeted volume fraction is high enough.

The design space of the Global APU hinge illustrated in Figure 3.9 is a good example of all the elements mentioned above. The areas around fasteners are set as non-design spaces to prevent them to be altered. The design space has been reduced near the foot of the part to allow a clearance to install fasteners. Also, the design space is of reasonable size so there are fewer mid-density elements present in the result.

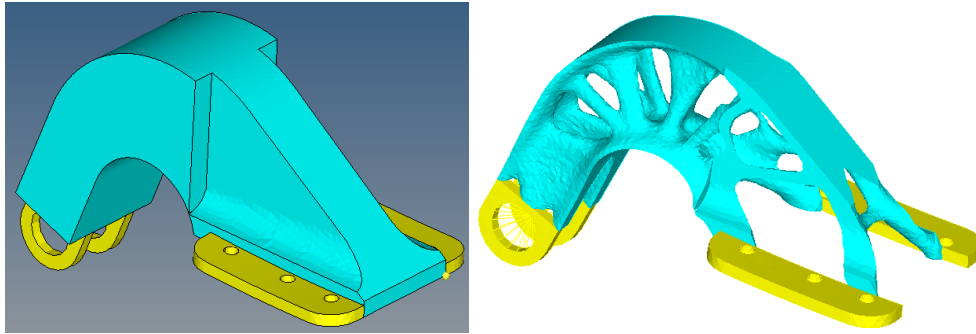


Figure 3.9 – Design space (left) and result from topology optimization (right) of Global APU hinge. The iso-density filter is at 0.6.

3.1.2 Meshing

Meshing of the model can have a significant influence on the results but the effect can be reduced if a handful of general rules are followed. The parameters to control when meshing a topology optimization model are the size and the type of elements.

The resulting topology from an optimization is directly influenced by the average size of elements in its model. Results from the same models but with different average elements sizes are illustrated in Figure 3.10. It can be seen that the model with smaller elements has finer features that could not be revealed when elements are larger.

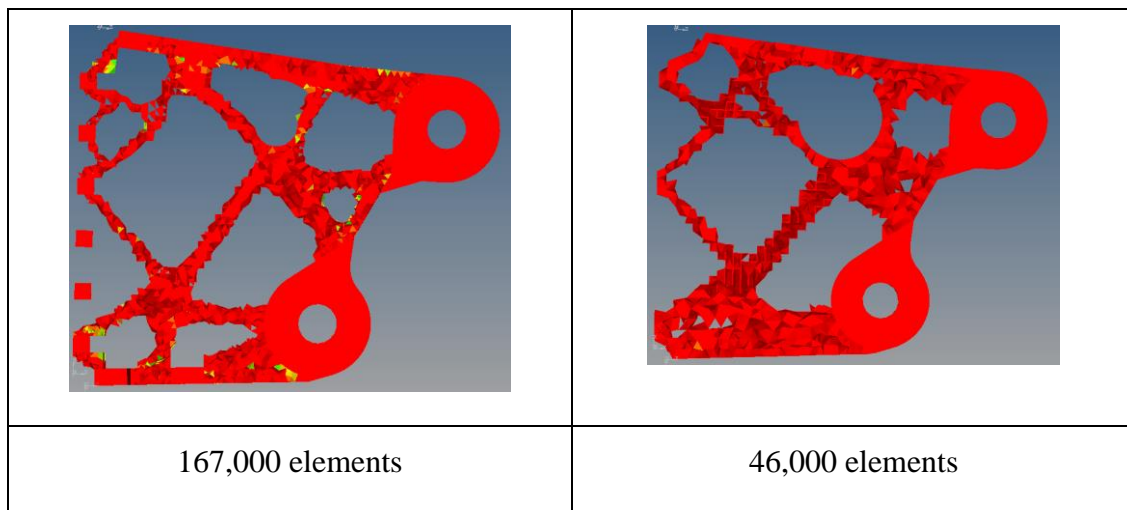


Figure 3.10 – Results from same optimization configuration done with fine elements (left) and coarse elements (right)

As mentioned by Bensoe [16], mesh dependency of results can lead to problems of microstructures and checkerboard patterns. A popular and robust method to avoid this mesh dependency is by using the minimum member size filter. That filter ensures that all features in the topology are of a minimum size by measuring the distance between important changes of density [32].

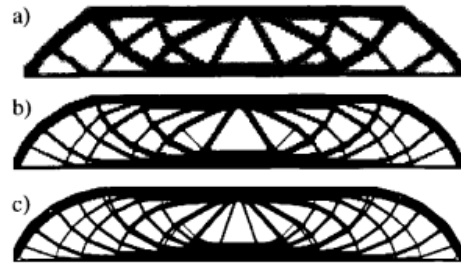


Figure 3.11 – Extracted from [16]. Mesh refinement and dependency of results

It could be tempting to choose a small minimum member size value since additive manufacturing can produce micro-features. Although that is true, in an aerospace context there is a ruggedness criterion that applies to prevent defects in cases of mishandlings and drops which cannot be taken into account during the optimization. Moreover, the filter becomes unstable when the minimum member size specified is below 3 times or above 12 times the average element size. Consequently, the user must be careful when meshing to make sure TO converges towards topology with appropriate feature sizes and that the meshing can accommodate the minimum member size value.

Moreover, meshing with smaller elements is also important to make sure stiffness is accurate enough. Indeed, in some cases with part solicited in bending, a coarse mesh will tend to give a high flexural stiffness to the model. The phenomenon can be exposed clearly with the analysis of the CSeries hinge.

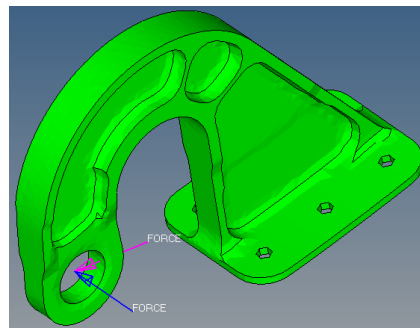


Figure 3.12 – CSeries hinge with load components inducing bending (pink arrow) and torsion (blue arrow) in the part

Figure 3.12 shows the orientation of the loads applied on the part: one component bending the part (pink) and the other inducing torsion (blue). In finite element analysis, one has to be careful to check convergence of the model; that is testing models with an increasing number of elements to make sure the results converge toward steady values (displacement, stress, etc.). The two models illustrated in Figure 3.13 were meshed with different elements size. In this example, the importance of torsion load on the overall load path is revealed as the number of elements increases. This greatly influences displacement of the node in the middle of the lug where it has more than doubled when mesh of model is refined to 1,8 million elements.

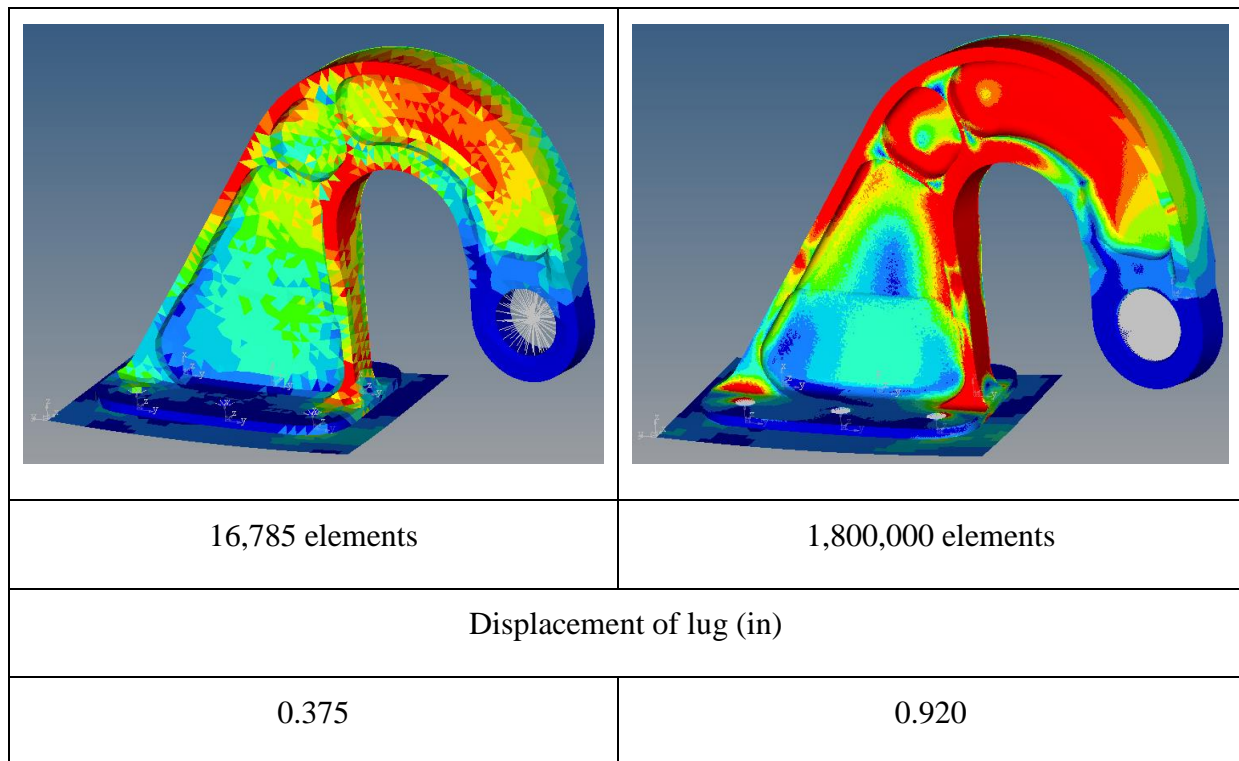


Figure 3.13 – Two models with different number of elements. The model on the left with fewer elements is not accurately transferring torsion in the structure thus leading to an underestimated displacement value compared to the model on the right with finer mesh.

As mentioned before, most sensitivities of the design output in topology optimization are related to displacement. Therefore, with a limited number of elements, optimizing the model with the actual loads will result in unsatisfactory results. Figure 3.14 illustrates one topology result for the CSeries hinge with low resistance to torsion although this mode governs the load path. Increasing the number of elements could of course help but computing capability quickly limits mesh

refinement, as it would take several weeks to optimize a model of 1.8 million elements, for example.

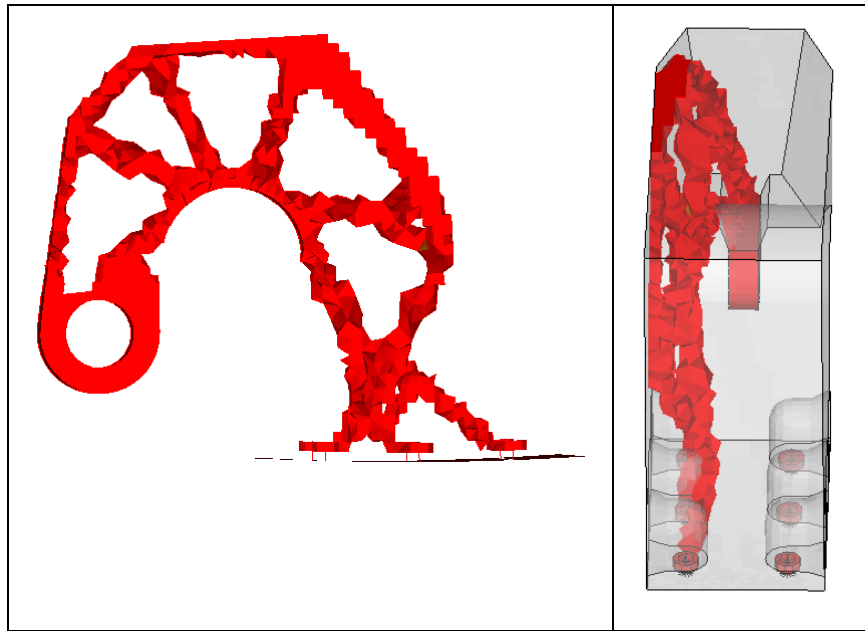


Figure 3.14 – Results from topology optimization with poor torsion stiffness due to large average size of elements not accurately transferring moments in the structure

Thus, it is paramount to accurately evaluate the load path and the convergence of a model before trying to optimize its topology. If such a mesh dependency occurs, the user can either increase number of elements or artificially increase the components of loads that are under-represented, as in the previous case with torsion.

It is assumed as well that changing the order of the elements can increase the accuracy of flexural stiffness. Indeed, quadratic elements (TET10) deal better with moments than linear elements (TET4) but raise computation time.

3.1.3 Loads and boundary conditions

It is important at this stage to mention that fatigue load cases have not been considered at the optimization stage throughout this research. The author focused mostly on static-loaded parts because, as of 2016, knowledge of the additive technologies at Bombardier Aerospace is not deep enough to develop highly critical parts that sustain fatigue loadings.

In a part replacement approach, defining loads and interfaces are simpler since most of the environment is determined at an earlier design stage. It is most likely that loads can be extracted from a load report and this prevents having to analyze the whole structure to derive forces at all interfaces.

Moreover, it is common in aerospace to design components with their maximum loads, namely the ultimate and limit load cases. These extreme loads are good to determine the maximum stress levels to sustain. However, ultimate and limit loads have specific orientations that may not be representative of the general loading conditions and not take into account the general ruggedness criterion.

For example, with the CSeries hinge, the ultimate load applied is aligned with the structure. Figure 3.15 exposes the optimization done on this part. Obviously the optimization converges towards a solution efficient at supporting bending since this load governs the part's behavior. However, something the author qualifies as a bending node appears in the topology, where efforts in bending tend to zero and only shear is present. The integrity of the structure is then compromised if the orientation of the load changes even slightly.

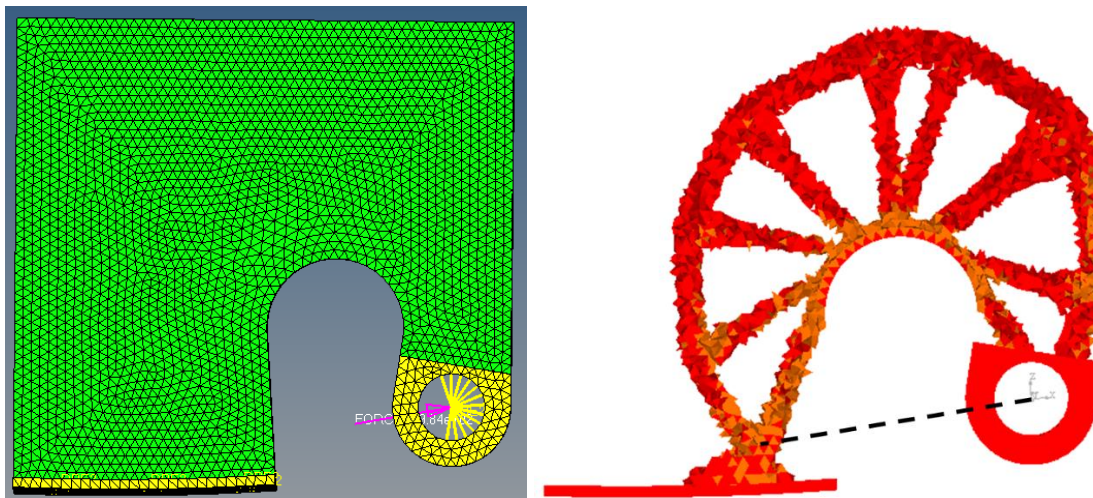


Figure 3.15 – On the left: design space with the ultimate load in pink. On the right: optimization result with a bending node exactly where bending efforts vanish, i.e. aligned with the load.

There are many solutions to overcome bending node problems such as: rotating the load until it is not aligned with the design space anymore (see Figure 3.16), combining multiple loads cases with different orientations, applying a moment instead of a force, etc.

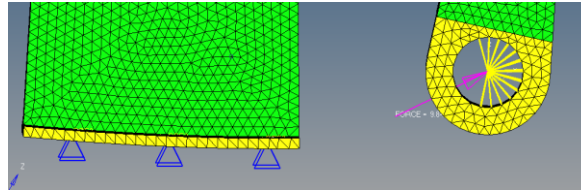


Figure 3.16 – Load has been rotated downward so it is not aligned with the design space

These modifications are in accordance with the general ruggedness criterion mentioned previously. In other words, ultimate and limit load cases can be used for optimization but changing them is possible as long as the loading modes are respected: tension, bending, torsion, etc. It can also be beneficial to separate the load components with adjusted magnitude to favor a loading mode. As illustrated in Figure 3.14, the torsion component of the load can be boosted to make sure it is taken into account during optimization.

Boundary conditions also play an important role in topology optimization since it is based on stiffness of the structure. It is very important to design boundary conditions that are as realistic to the actual structure as possible. A good example of bad boundary conditions is shown in Figure 3.17 where all nodes on the exterior of the design space have been fixed with single point constraints (SPC). Obviously, a really low amount of material is necessary to connect the design to the infinitely stiff SPC.

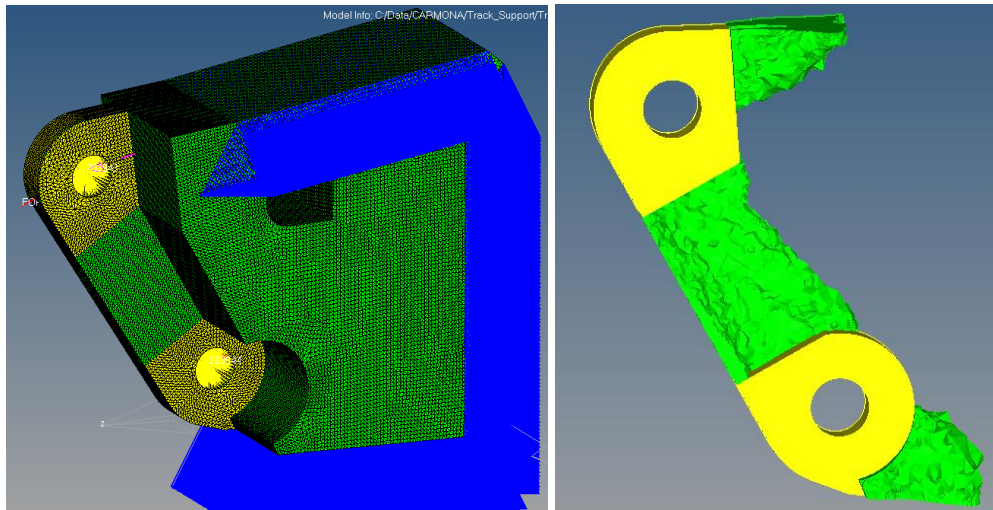


Figure 3.17 – Boundary conditions too stiff can lead to unrealistic optimization results

In reality, those attachments are flexible and can bear a limited amount of stress. The optimal boundary condition configuration tested with this part was to create non design spaces representing

the fasteners and connecting their elements to a SPC with a flexible 1D element (CBUSH) and a rigid body element (RBE3), shown in Figure 3.18. The realistic compliance of this assembly prevents the solver to converge towards a topology overloading one fastener.

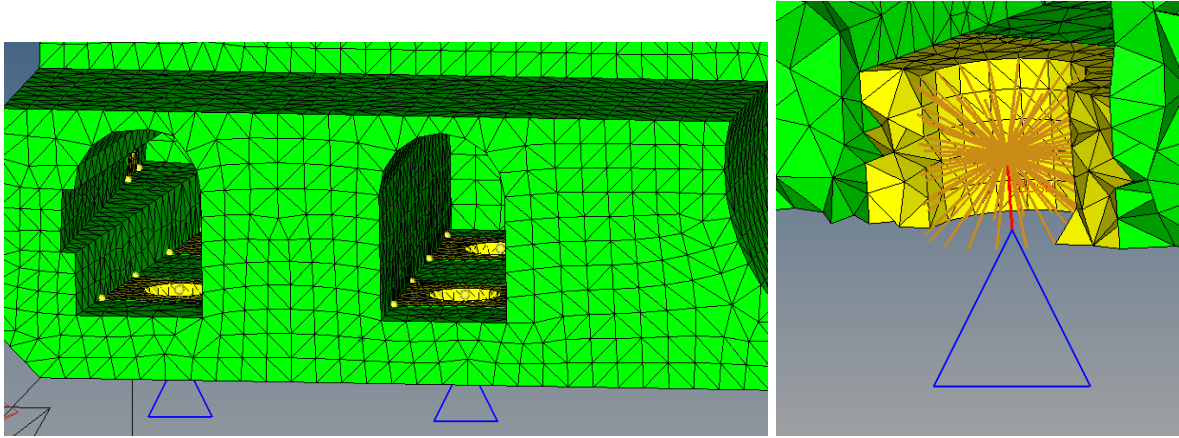


Figure 3.18 – Design space of the track fitting with boundary conditions modeled as non-design space with RBE3 and CBUSH to give a relative stiffness to the model

Most non-linearities such as plastic material behavior or large displacements are not taken into account for topology optimization in the Optistruct software. One exception is the contact condition which simulates interaction between two surfaces in a model that is supported by Optistruct. However, applying contact condition greatly increase computation time and several examples have proven that it doesn't affect the results significantly. Figure 3.19 shows that results from identical models but one with contact condition at its base (pink elements), both give similar topologies.

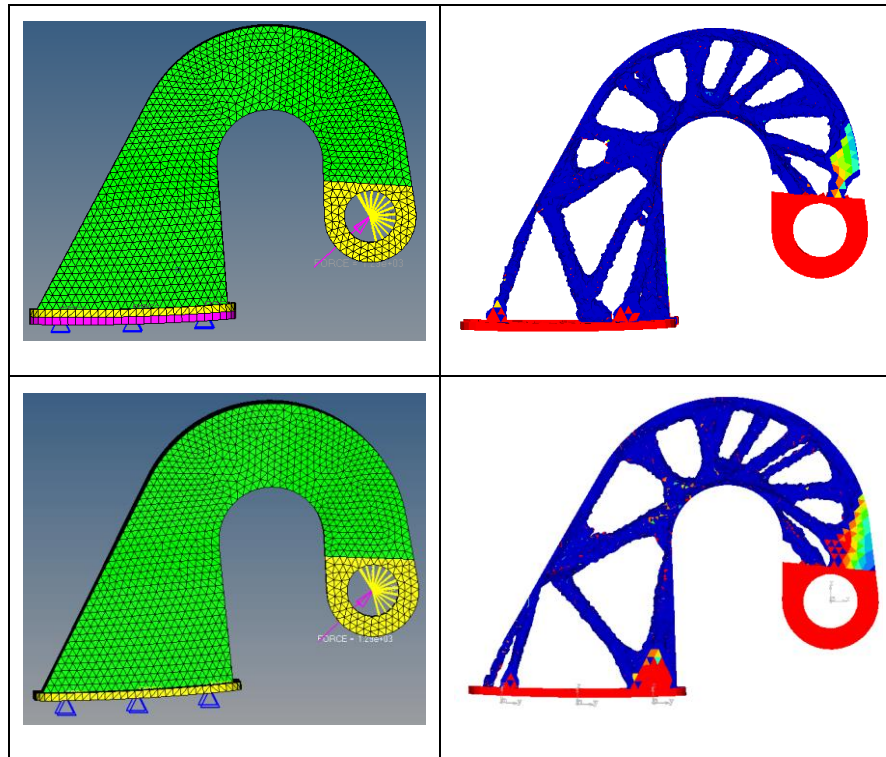


Figure 3.19 – Cseries hinge optimization with two models (left column). Upper model has a contact condition at its base and the lower one does not. Both optimization gave similar results (right column).

3.1.4 Optimization setup

As explained before, during an optimization, there is a balance between one or multiple constraints and the objective. In Optistruct, there are numerous optimization parameters that can be selected. Using different parameters can lead to different optimization results and some configurations might fail to optimize or converge toward unsatisfactory topologies. Therefore, it is desirable to test several different objectives and constraints combinations.

The quality of an optimization result is first measured by its density distribution. As will be detailed in section 3.2.1, the optimization results with many elements with a density between 0 and 1 have unreliable performance. Small details such as presence of checkerboard patterns and numerical artifacts must also be taken into consideration, as is presented in Figure 3.20.

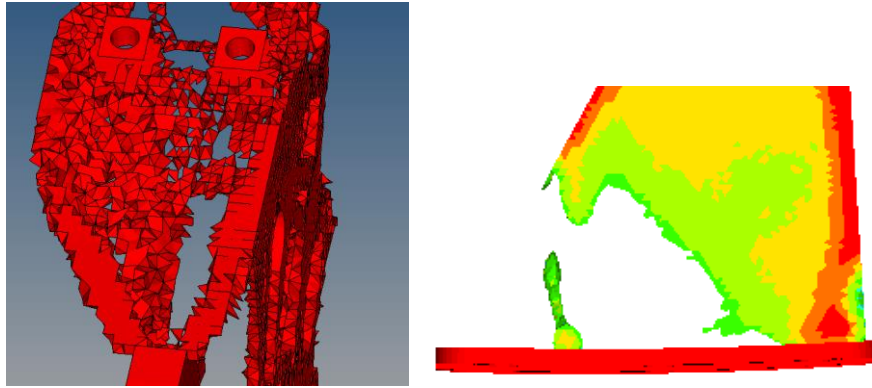


Figure 3.20 – Elements to avoid in an optimization result: checkerboard pattern (left) and unconnected elements (right)

The most common optimization formulation is to minimize the compliance with a target volume fraction. It is by far the most stable configuration and always converge toward satisfactory element density distribution. The compliance is estimated by:

$$C = \frac{1}{2} u^T K u = \frac{1}{2} \int \varepsilon^T \sigma dv \quad (13)$$

Where u is the vector of displacement, K is the stiffness matrix, ε and σ are the strain and stress vectors respectively. This compliance is associated with a load. When several loads need to be taken into account, a weighted compliance factor can be computed as the sum of all compliances from all loads;

$$C_W = \sum W_i C_i = \frac{1}{2} \sum W_i u_i^T f_i \quad (14)$$

Where W_i is the weight factor given to the compliance C_i associated with the considered load. Using this characteristic as an objective to minimize leads to stable results but in several occasions it also led to the predominance of intermediate density elements. When several loads in multiple orientations are applied to a part, it could be preferable to have a ruggedness optimization criterion such as maximizing eigenfrequencies of the model. However, proper care has to be taken when selecting a target frequency since sometimes it is not achievable.

Another possible configuration is to minimize the mass of the model with a target displacement. In fact, in engineering, it is common to limit the displacement of specific nodes since it is critical for

assembly or interference purposes. In this study, it was used several times and always yielded good element density distribution.

In Optistruct, manufacturing constraints exist to force the result to respect certain criteria. For example, the symmetry constraint that allows to determine a plane in the design space from which the result has to be symmetrical. Figure 3.21 shows two optimizations with the same model but one has a symmetry constraint applied to it. The result using this constraint had a lot of intermediate density elements.

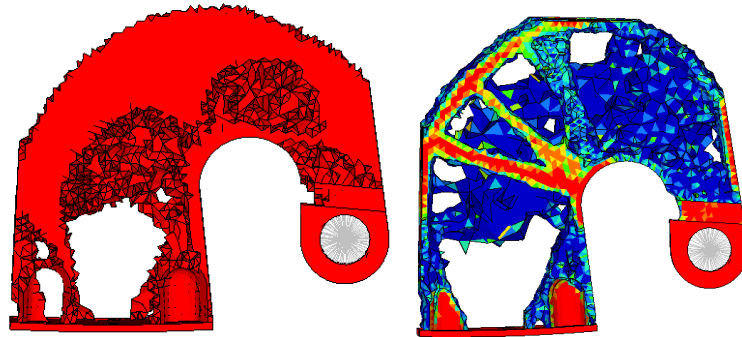


Figure 3.21 – Two optimization results with same configuration but the model on the right has a symmetry constraint which led to a result with a lot of intermediate density elements

3.2 Interpretation

As mentioned previously, our approach is different from what topology optimization was developed for. Used originally to compare between concepts with a great level of abstraction, the interest with additive manufacturing is to use topology optimization up to the detailed design stage. That is often governed by specific stress and stiffness requirements. The challenges in using topology optimization as a detailed design tool instead of a comparative one are emerging mostly in the interpretation phase as it is explored in the following section.

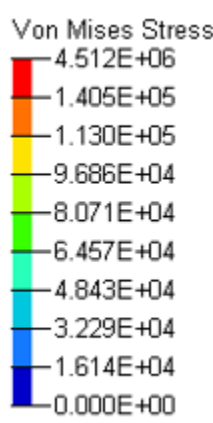
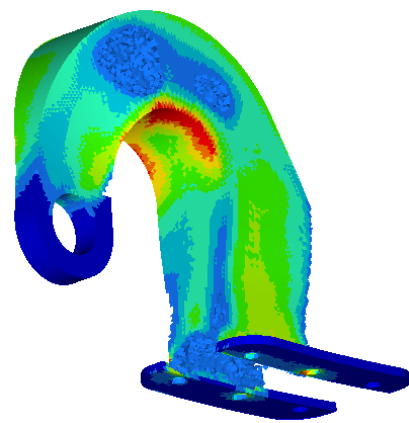
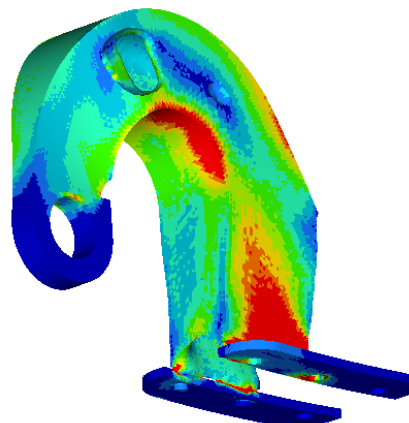
3.2.1 Result analysis

One of the two major obstacles faced when designing with topology optimization is to validate a result out of the solver. Because a topology optimization configuration converges towards a local optimum, launching several optimizations with different configurations is often used to reveal many local optima. However, although in-solver performance seems satisfactory, when interpreted,

volume, stiffness or stress level of the part can significantly vary. This can result in a design heavier than expected or lower performance.

Table 3.1 illustrates an example of an optimization result of the CSeries hinge and its associated interpretation. Stress level and displacement of the part are greater than forecasted by the optimization due to the lower volume of the part.

Table 3.1 – Performance and volume of an in-solver optimization result and its interpreted model. Volume of the latest is significantly lower than in-solver which leads to higher stress level and displacement. The iso-density filter was 0.75.

	In-solver model	Interpreted model	
			
Von Mises stress in reference area (psi)	127,000	152,000	+16.5%
Lug center disp (in)	0.0951	0.1436	+33.8%
Volume (in ³)	3.473	2.752	-20.8%

This difference between in-solver and interpreted results is explained by the interpretation process which consists in redistributing elements density according to an iso-density filter. Indeed, in an optimization result with SIMP method, all elements' densities are between 0.01 and 1.0. When this optimization result is filtered, all elements densities $\rho_e(x)$ of the model above the iso-density filter threshold F arbitrarily chosen by the user are raised to 1 to make it full solid and elements with

density below this value are brought to 0 and therefore vanish. With the volume of each element v_e , the volume of the part in-solver is:

$$\text{In - solver volume} = \sum_{e=1}^N \rho_e(x) v_e \quad (15)$$

Compared with the volume of the interpreted result:

$$\text{Interpreted volume} = \sum_{e=1}^N D_e v_e ; \text{ where } \begin{cases} D_e = 0 & \text{if } \rho_e(x) < F \\ D_e = 1 & \text{if } \rho_e(x) \geq F \end{cases} \quad (16)$$

The difference between the two values for the model in Table 3.1 is plotted against the value of the iso-density filter F in Figure 3.22.

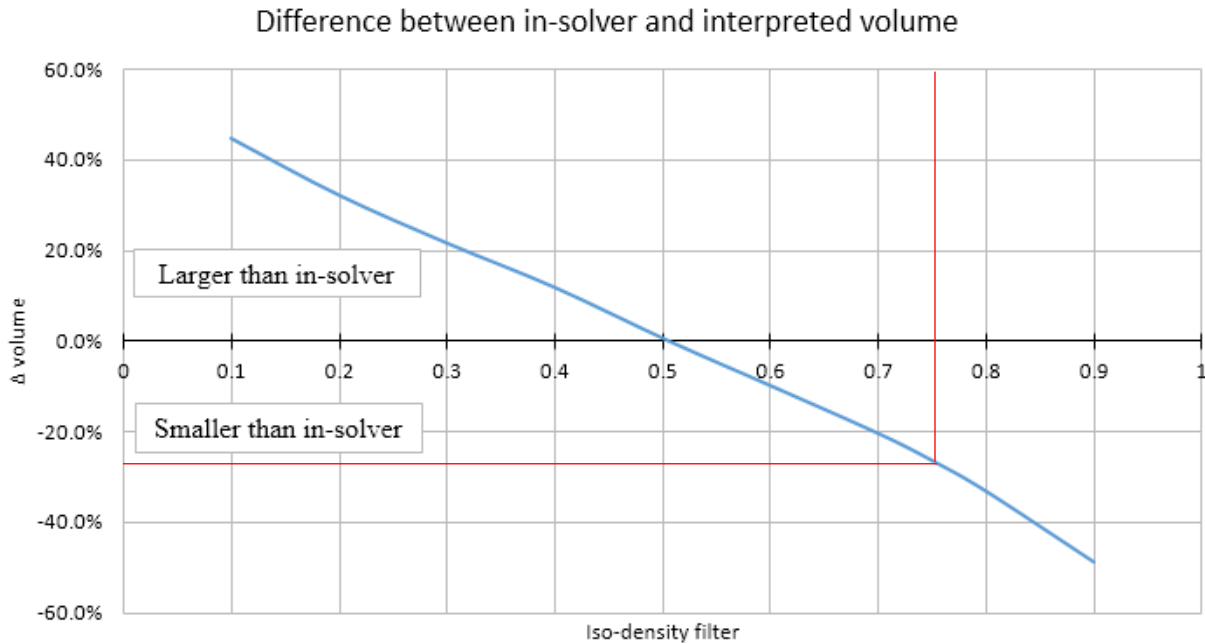
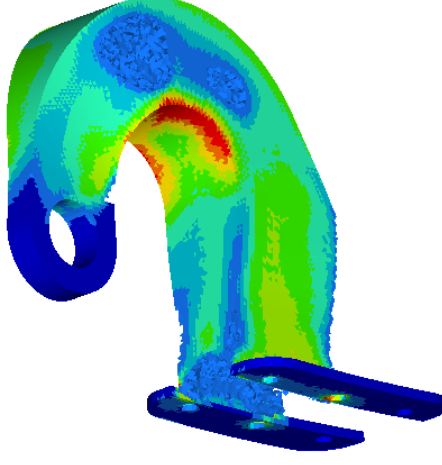
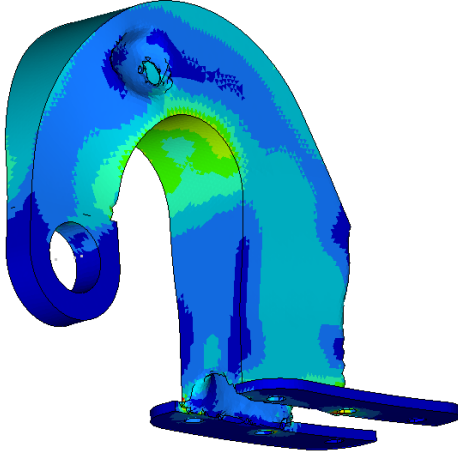


Figure 3.22 – Example 1. Difference between in-solver and interpreted volume with theoretical zero volume difference at iso-density filter = 0.5065.

The iso-density filter used to interpret the part being 0.75, the volume should be 26.3% lower than generated by the optimization. This actually corresponds to the -20.8% listed in Table 3.1. The difference resides in the partial interpretation step explained in Section 3.2.2 which modifies the geometry.

To get a 0% difference, the interpretation has been done with the filter at 0.5065 as suggested by the previous table. The results are shown in Table 3.2.

Table 3.2 – Example 1. Performance and volume difference between in-solver and interpreted models with iso-density filter at 0.5065.

	In-solver model	Interpreted model	
			
VM stress in reference area (psi)	127,000	92,000	-27.6%
Lug center disp (in)	0.0951	0.0635	-33.3%
Volume (in ³)	3.473	3.538	1.86%

The interpreted volume is kept but the stress level and displacement are lower than in-solver. This difference in performance is around 30% and it is explained by the stiffness distribution in the optimization model, namely:

$$In - solver\ stiffness = \rho_e^3(x) \cdot K_e \quad (17)$$

The stiffness matrix K_e is thus multiplied by values between 0.000001 and 1. Similarly to the previous volume calculations, when interpreted, the stiffness value of all elements above the iso-

density filter are brought to 1. If many of those elements have intermediate density values, the overall interpreted stiffness will significantly vary from the in-solver model. It is therefore useful to plot the elements density distribution to monitor the influence after interpretation. Figure 3.23 shows the density distribution for each elements' density brackets for the optimization result of the previous example.

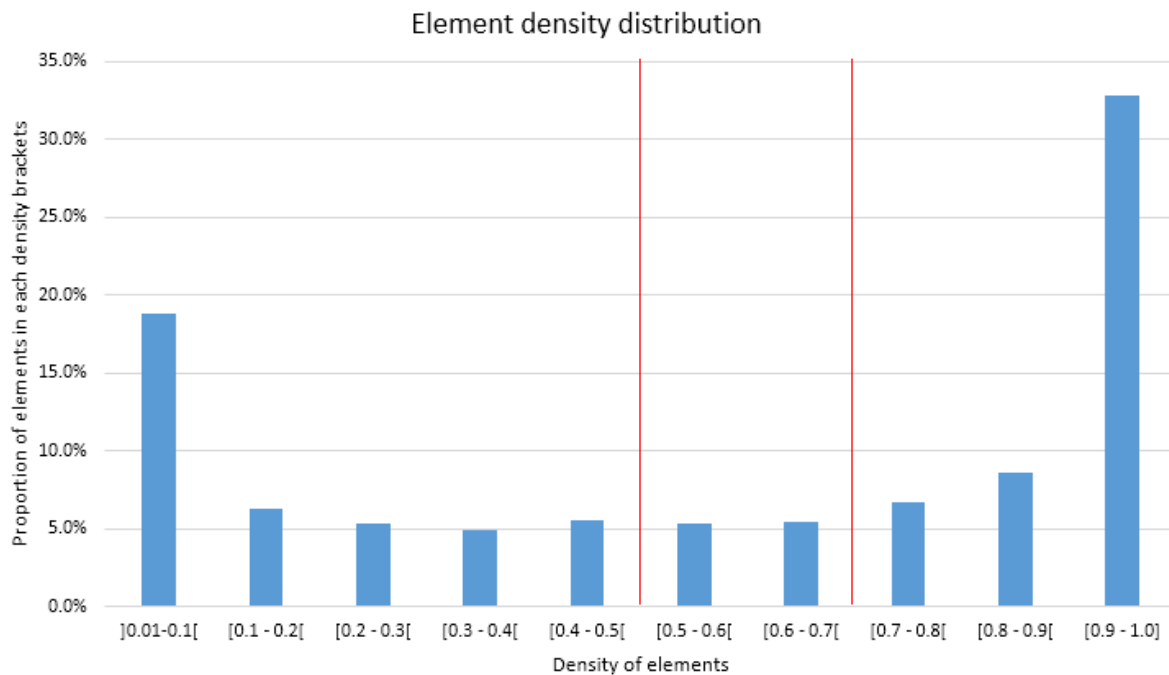


Figure 3.23 – Proportion of elements in each density bracket of the optimization result from example 1

Note that elements with density at the minimum 0.01 were not included in the graph because they have an insignificant impact on stiffness. Nonetheless, with an iso-density filter at 0.5065 or 0.75, many elements that did not contribute to the in-solver stiffness will have their density raised to 1 and take part in making the interpreted result stiffer than expected.

The next example is another optimization of the CSeries hinge but with a different configuration, namely the objective is to minimize mass while respecting maximum displacement to avoid clash during assembly. As opposed to the previous one, this result has an almost binary elements density distribution, i.e. closer to either 0.01 or 1.0, as it is shown in Figure 3.24.

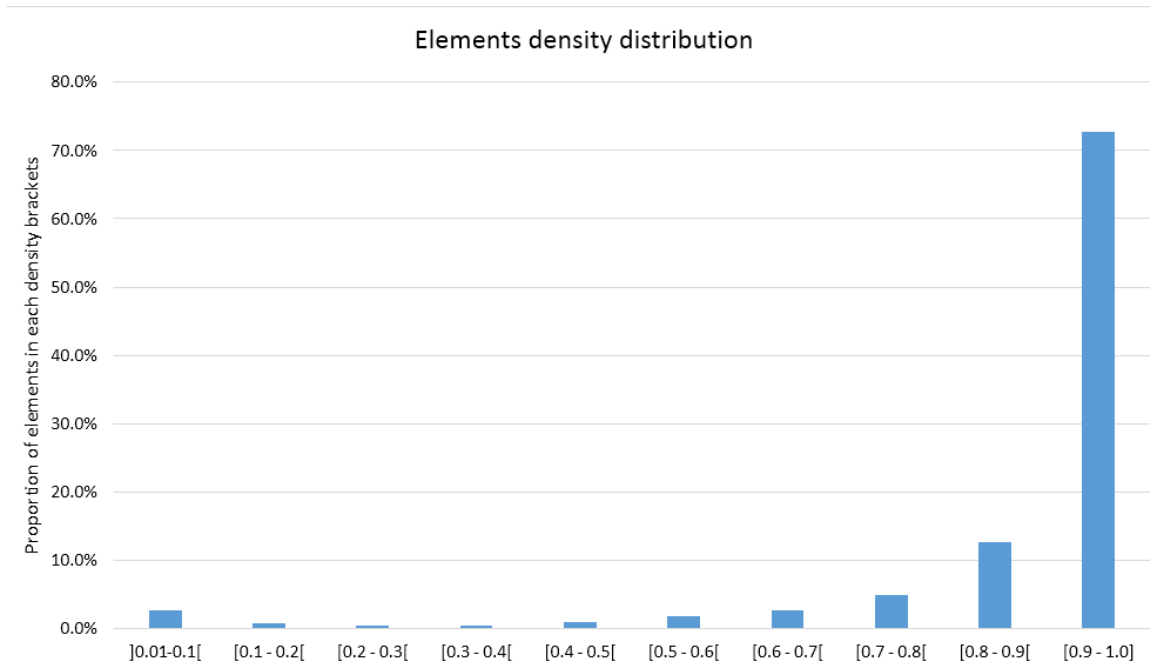
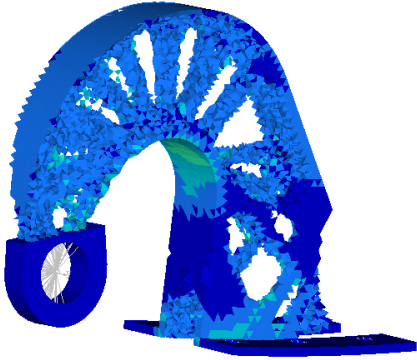
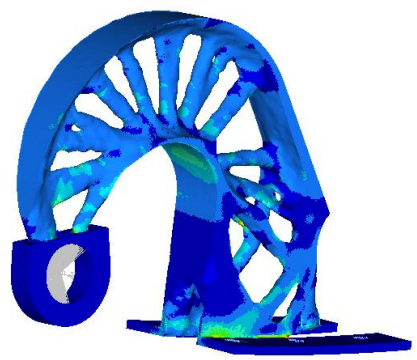


Figure 3.24 – Proportion of elements in each density bracket of optimization result from example 2

Table 3.3 – Example 2. Performance and volume difference between in-solver and interpreted models.

	In-solver model	Interpreted model	
			
VM stress in reference area (psi)	47,060	47,360	-0.6%
Lug center disp (in)	0.0349	0.0349	0.0%

Volume (in ³)	1.497	1.595	6.6%
---------------------------	-------	-------	------

The volume and performance of this optimization are reported in Table 3.3. The interpreted volume varies from about 7% and this is explained by the iso-density filter chosen at 0.43. Figure 3.25 shows the influence of the iso-density filter on the difference between volumes of the models. One will notice a theoretical difference within $\pm 5\%$ for a great range of iso-density filter.

However, for all practical purposes the performances of the interpreted model are equal to the in-solver result. This is explained by the really high proportion of elements in the 0.9-1.0 density bracket. Practically, over our research, this bracket has become an indicator of the accuracy of the performance. When 70% or more of all the model's elements (excluding density = 0.01) have density above 0.9, the results were found to be reliable up to interpretation.

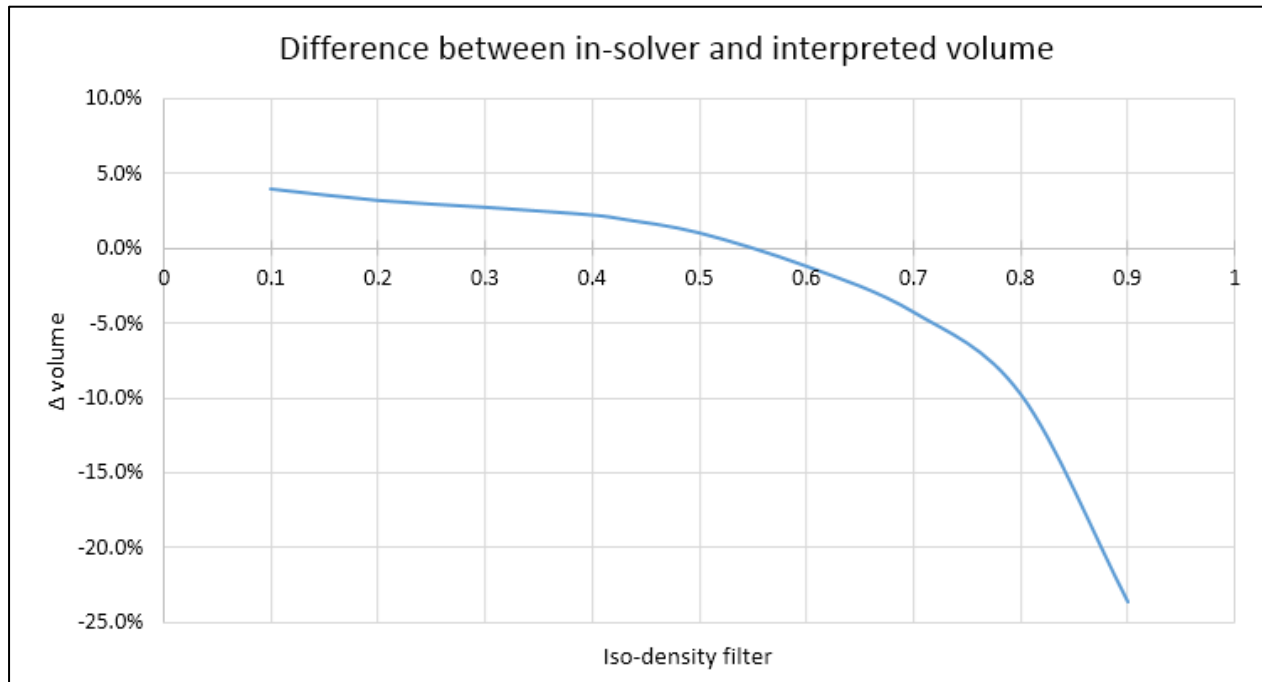
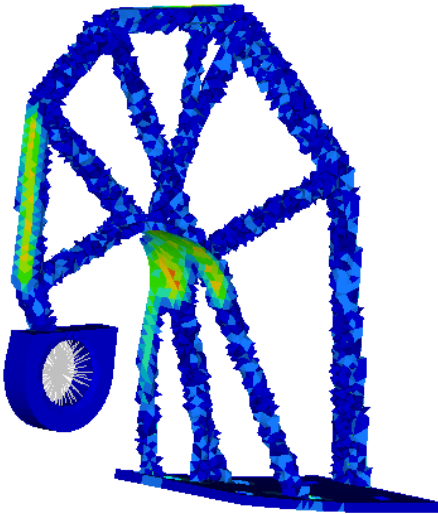
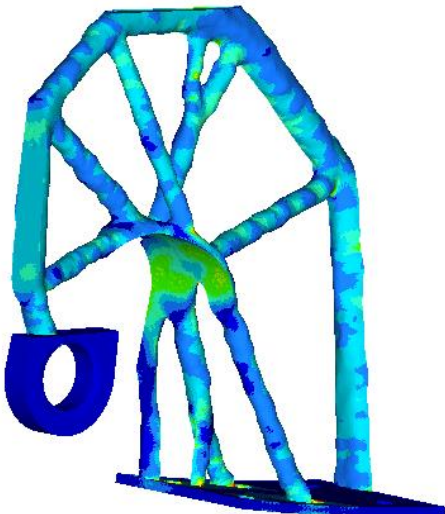


Figure 3.25 – Example 2. Difference between in-solver and interpreted volume. One can note that the volume difference is within 5% from iso-density filter between 0.1 and 0.7

This desirable binary distribution is however very seldom. In fact, optimization results often have scattered density distribution but can still lead to valid structural parts. The next optimization done as well on the CSeries hinge in Figure 2.7, Figure 3.26 and Figure 3.27 has an unusual density distribution but still yield interesting properties after interpretation.

Table 3.4 – Example 3. Performance and volume difference between in-solver and interpreted models.

	In-solver model	Interpreted model	
			
VM stress in reference area (psi)	55,930	40,900	-36.8%
Lug center disp (in)	0.0787	0.0293	-168.6%
Volume (in ³)	3.343	2.339	-42.92%

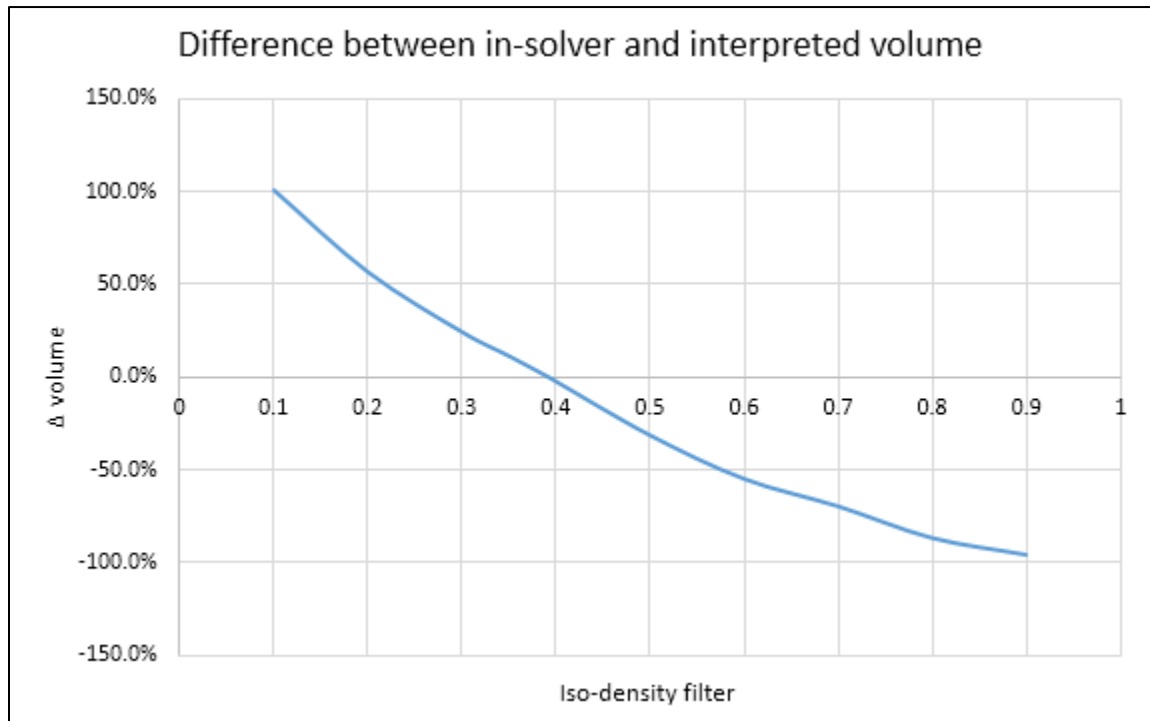


Figure 3.26 – Example 3. Difference between in-solver and interpreted volume

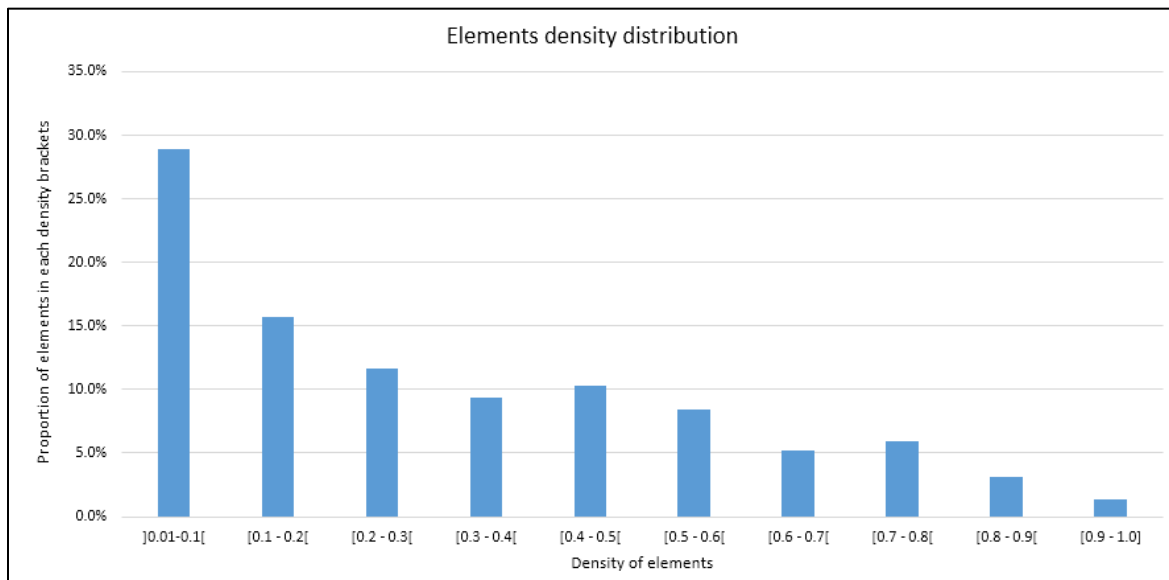


Figure 3.27 – Example 3. Proportion of elements in each density bracket of optimization result

The best way to completely overcome the difference between in-solver and interpreted performance of an optimization result is to use non-homogenization algorithm. The level-set method discussed later addresses this issue.

3.2.2 Partial interpretation of result

Filtering the optimization results by iso-density leads to only rough geometries. In fact, direct interpretation simply subtracts all elements below an iso-density filter which leaves sharp edges and surfaces depending on the type and density of elements in the part. Therefore, a secondary interpretation of the optimization is necessary.

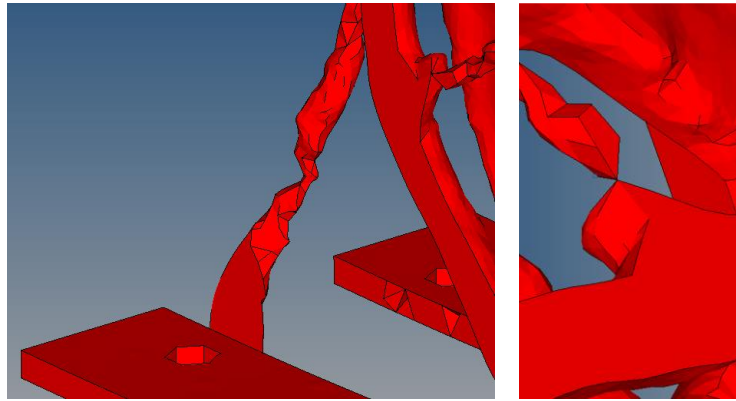


Figure 3.28 – Examples of bad geometry following the filtering by iso-density

However, interpretation with a feature-based parametric CAD software has some drawbacks: 1) it needs to restart modeling from the beginning which is time consuming and 2) fully controlled features used in feature-based tools don't allow to exactly reproduce the resulted geometries.

Moreover, because the performance of an optimization result is not entirely reliable, it is probable that the interpreted result doesn't lead to satisfactory properties. As seen previously, results with a 0.9-1.0 density bracket gathering above 70% of the contributory elements that give acceptable performance can be considered valid. Results that don't comply with this metric need to be validated. Sometimes, several optimizations are needed before getting the desired performance. The effort needed to interpret optimizations with feature-based tool is too heavy to be appropriate.

To avoid having to validate optimization results with a CAD software, an intermediate step which is a partial interpretation is introduced. This partial interpretation is done with a mesh-based software that modifies the optimization result instead of remodeling it from the beginning and only be inspired by the optimization. Figure 3.29 illustrates how partial interpretation is introduced in the topology optimization methodology.

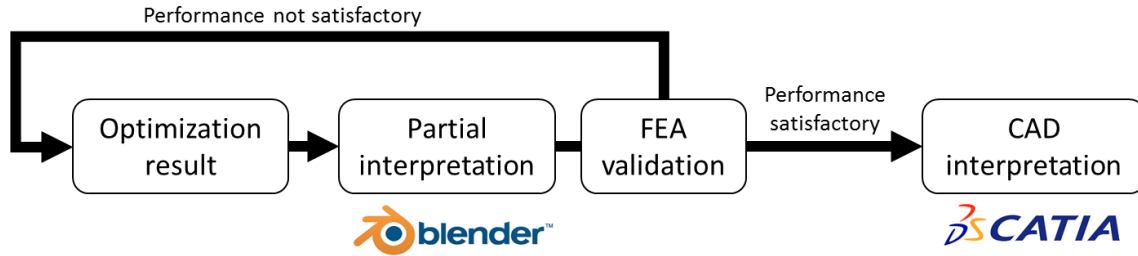


Figure 3.29 – Validation and interpretation cycle of a topology optimization result

This step greatly shortens the design lifecycle. Partial interpretation with a polygon modeler software (Blender) instead of a NURBS modeler software (Catia) allows to quickly correct results from the topology optimization.

In the following example, an optimization result has been interpreted in both a mesh-based and a feature-based software to compare the effort needed and the efficiency from both options. This case study has been submitted to the *Canadian Aerospace and Space Journal* and is under review at the time of publication of this thesis. The original article is in Appendix C.

The optimization was made on the flap track fitting. The design space used and the resulting geometry is presented in Figure 3.30. The optimization objective was to minimize the compliance with a target volume fraction of 15% with a minimum member size constraint of 12 times the average element size.

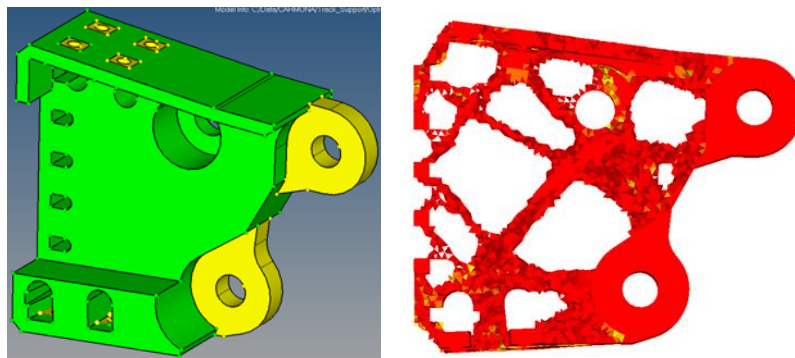


Figure 3.30 – Design space of the flap track fitting and its optimization result

The obtained element density from the optimization was well distributed with more than 70% of non-zero density elements between 0.9 and 1.0. This, as previously discussed, ensures the performances measured on the model will generally be accurate. The iso-density filter was chosen at 0.2 which didn't have significant impact on the final part's volume as seen in Figure 3.32.

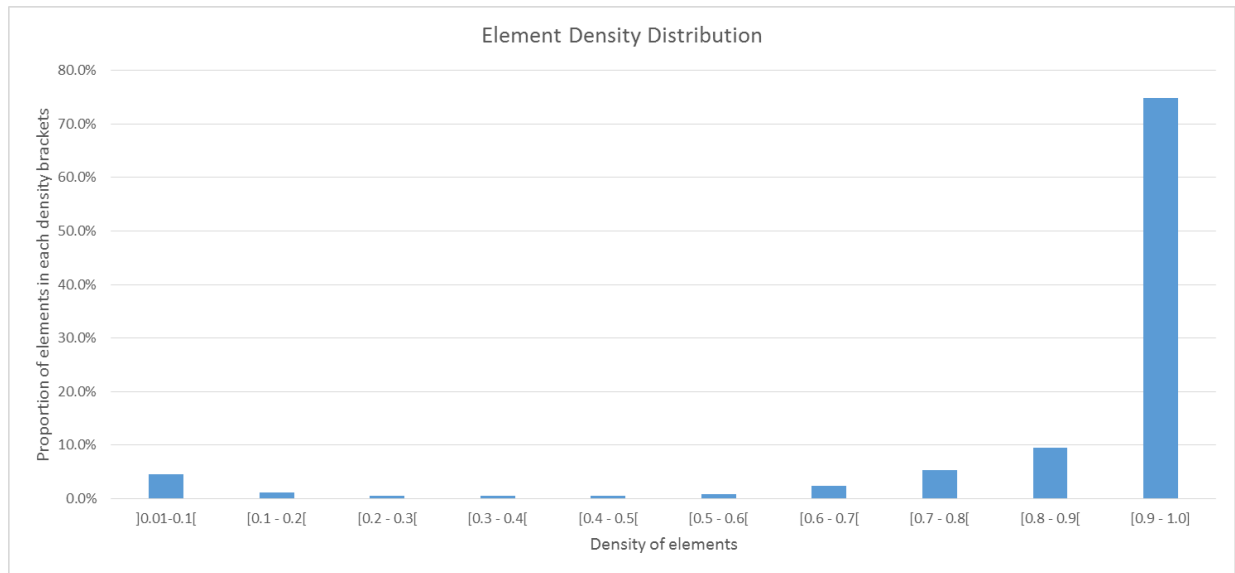


Figure 3.31 – Element density distribution of the flap track fitting topology optimization result

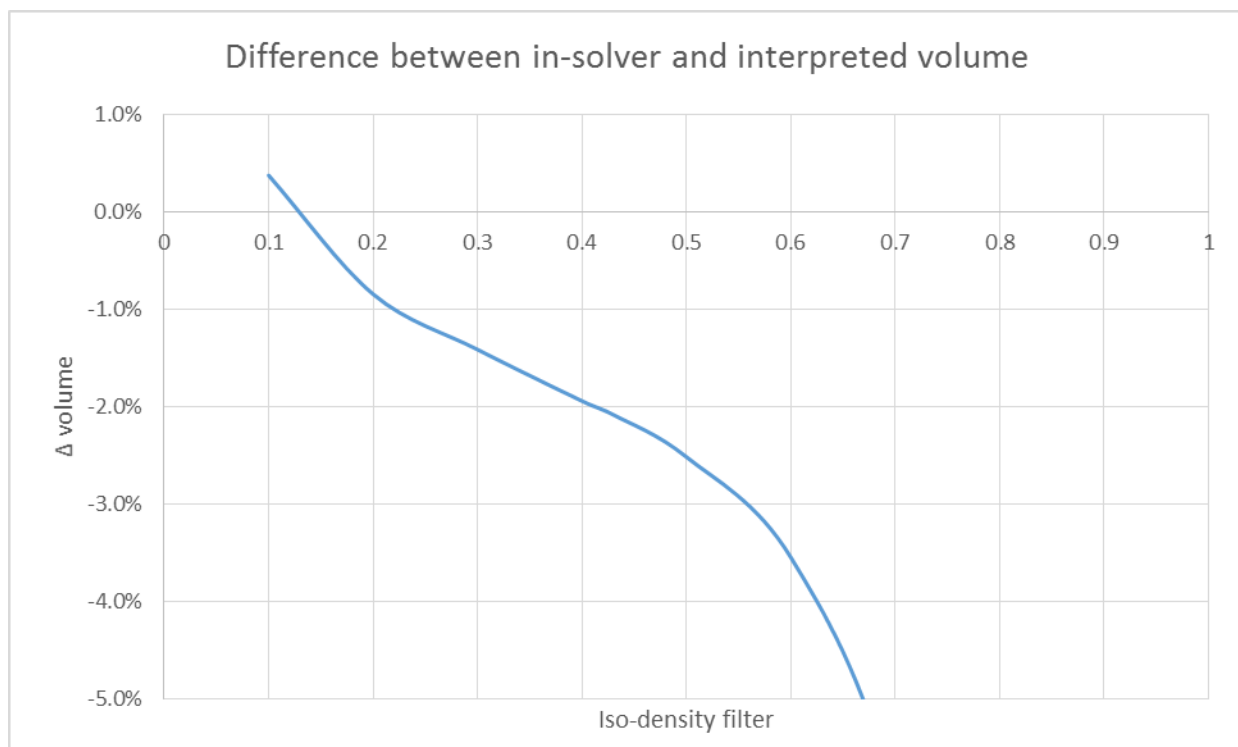
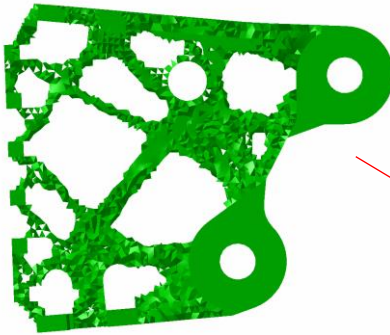
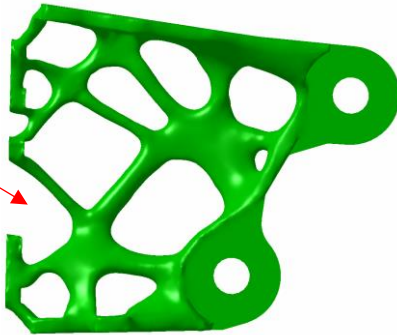



Figure 3.32 – Influence of final interpreted volume vs the chosen iso-density filter

As seen in Figure 3.30, the result geometry is rough and complex with several small elements. The interpretation was made both with mesh-based and feature-based tools and the produced geometries are presented in Table 3.5.

Table 3.5 – Comparison between geometry from optimization result, mesh-based modeling and feature-based modeling. Interpretation time is significantly shorter when interpreted with mesh-based software. The red arrow shows where one bolt has not been considered during partial interpretation with mesh-based software.

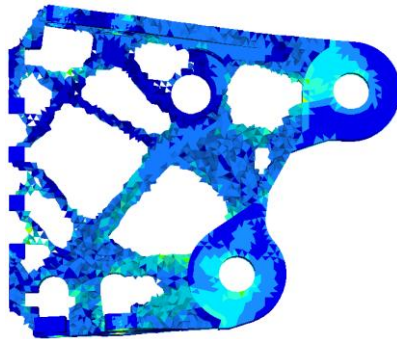
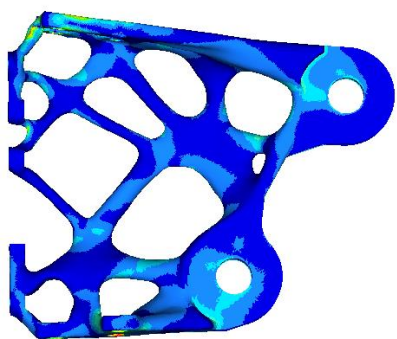
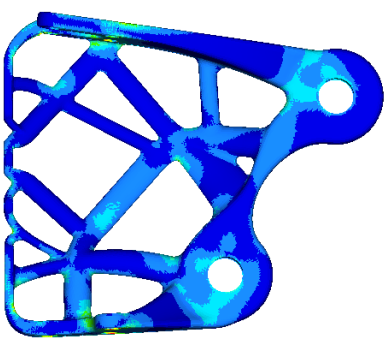
Optimization result		Mesh-based modeling	Feature-based modeling
			
Volume (in ³)	47.0	56.6 (+20.5%)	49.9 (+6.2%)
Modeling time (hours)	-	Less than 1	35-40

Extracting the optimization result and directly modify the mesh to smooth surfaces and correct small numerical artifact took around 1 hour. This gives the flexibility to follow exactly the topology. The conventional approach with feature-based modeling tool required over 35 hours of work.

One will notice small differences between the two interpretations, specifically one bolt attachment is missing in the mesh-based model. This is due to the fact that these models were done by 2 different engineers who interpreted the result differently.

The volume of the mesh-based model is higher than the other models because smoothing was done rather aggressively. In fact, with Blender, it is impossible to monitor the volume of the part being edited before it is completely closed. Thus it was not possible to prevent increasing the parts' volume above the target. Table 3.6 gathers the performance results from the three models.

Table 3.6 – Performance of optimization results and its interpretations

Optimization result		Mesh-based modeling	Feature-based modeling
			
Volume (in ³)	47.0	56.6 (+20.5%)	49.9 (+6.2%)
Max Stress (ksi)	70,670	62,880 (-11.0%)	64,720 (-8.4%)
Upper lug displacement	0.0403	0.0441 (9.4%)	0.0363 (-9.9%)
Lower lug displacement	0.0152	0.0200 (31.6%)	0.0149 (-2.0%)

The smoothed model obtained with mesh-based software shows larger displacement than the fully interpreted model. Finite element analysis shows that this comes from a larger compliance around the boundaries because an insufficient amount of material was added around the bolts. Modeling with the mesh-based tool is powerful but mastering it requires time and effort. In addition, Blender is not an aerospace tool and adding specific functions and requirements could improve the proposed design methodology.

The case study of the outboard fitting reveals that it is possible to interpret topology optimization results without having to fully remodel the part in a feature-based software. Manipulating the result as a mesh is possible and shortens the design life cycle. Although the results are slightly better when the part is fully remodeled with features, some incremental innovation in the software can open the door to advanced manipulations of optimization results such as features recognition.

3.3 Model validation

Once the geometry is interpreted, it is possible that some modifications still need to be done to reduce peak stresses. Size optimization helps in that matter as will be discussed in the following section.

Finally, in aerospace, many stress calculations are made in order to validate that the part and its assembly can bear the loads. Section 3.2.2 details how the certification calculations are usually done. Those topics will be addressed with help of the Global APU hinge example. Figure 3.33 shows the different steps used to optimize this part.



Figure 3.33 – Optimization of the Global APU door hinge from the design space to the interpretation

3.3.1 Size optimization and final analysis

As seen previously, topology optimization with SIMP method doesn't efficiently take into consideration stress concentrations. Therefore, it is common to have stress peaks above the material limit. Based on previous mechanical testing of PBFL Ti-6Al-4V, the maximum allowable stress at this design stage was set 100ksi. This would let a sufficient margin during the complete analysis detailed in the next section.

However, it was noted that stress level still exceeds this limit in tight angles and sharp corners of the parts. To locally modify the geometry, a free-shape optimization is ran. Figure 3.34 illustrates the process where a node area is selected (in red). During the free-shape optimization, the nodes on the surface are moved independently in order to minimize the objective, in this case the maximum stress level of the area. This allow to efficiently reduce the stress peak from 117ksi to 60ksi in this critical area near the attachments.

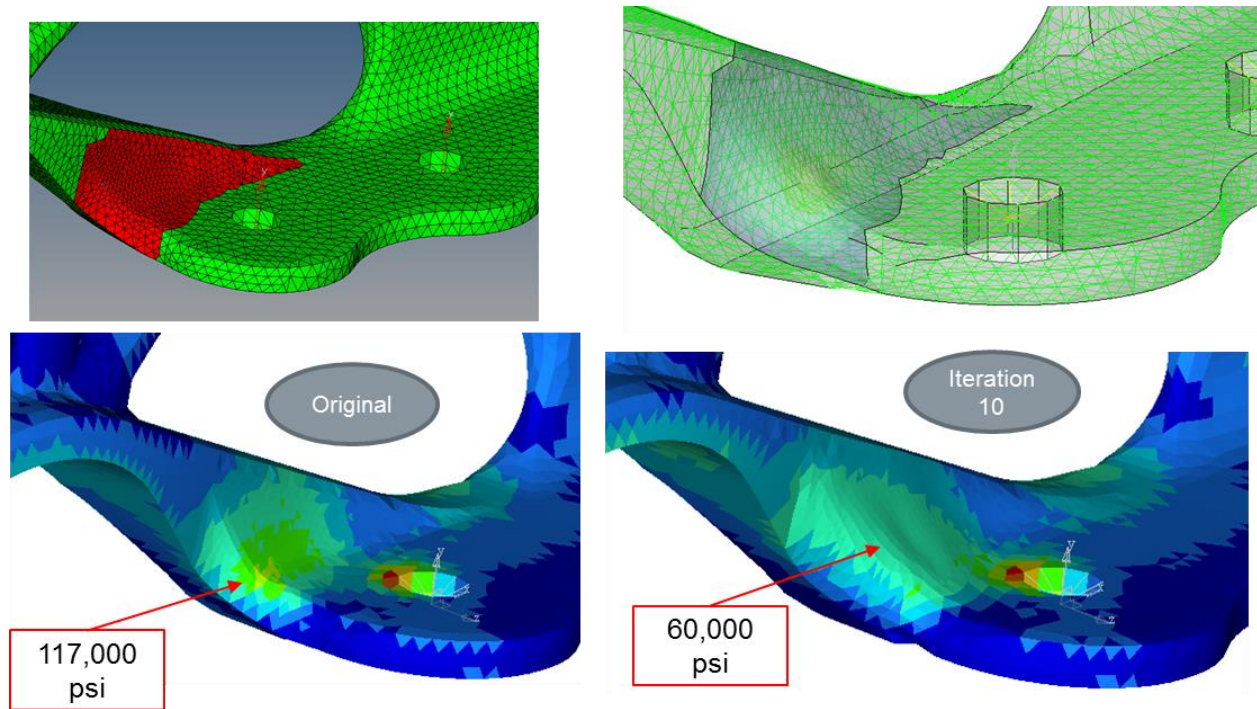


Figure 3.34 – Free-shape optimization of a section at the foot of the part. Nodes in the red (top left) area are moved to minimize the stress (top right).

Figure 3.35 shows another area where geometry has been optimized according to its sensitivity with the objective to lower the stress undergone by the part.

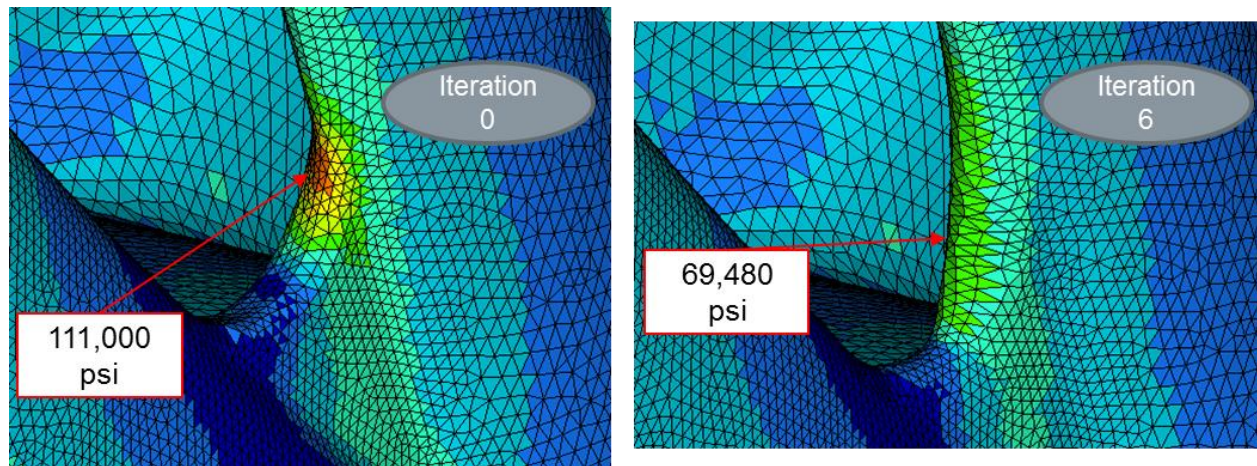


Figure 3.35 – Free-shape optimization of stress peak to lower the stress below the 100ksi limit

Free-shape optimization is comparable to a local level-set topology optimization since boundaries of the model are moved according to their sensitivities with the objective. However, because commercial topology optimization solutions using the SIMP method don't handle stress

concentrations, using free-shape after the topology optimization and interpretation is of great help. The following section details the final analyses of the interpreted parts.

3.3.2 Final design and analysis

Structural integrity of the parts has to be analyzed based on the loads and the allowable of the material. Since those material allowable for additive manufacturing are yet to be defined by the aerospace industry, the analyses were made based on the properties of wrought annealed AMS 4911, titanium Ti-6Al-4V.

At Bombardier Aerospace, loads are generally given by the “Loads and Dynamics” group whose job is to derive inertial and aerodynamic loads in the structure. The loads associated with the forward and aft APU door hinge are reported in Table 3.7 and Table 3.8. Coordinate system used to define loads orientation is illustrated in Figure 3.36.

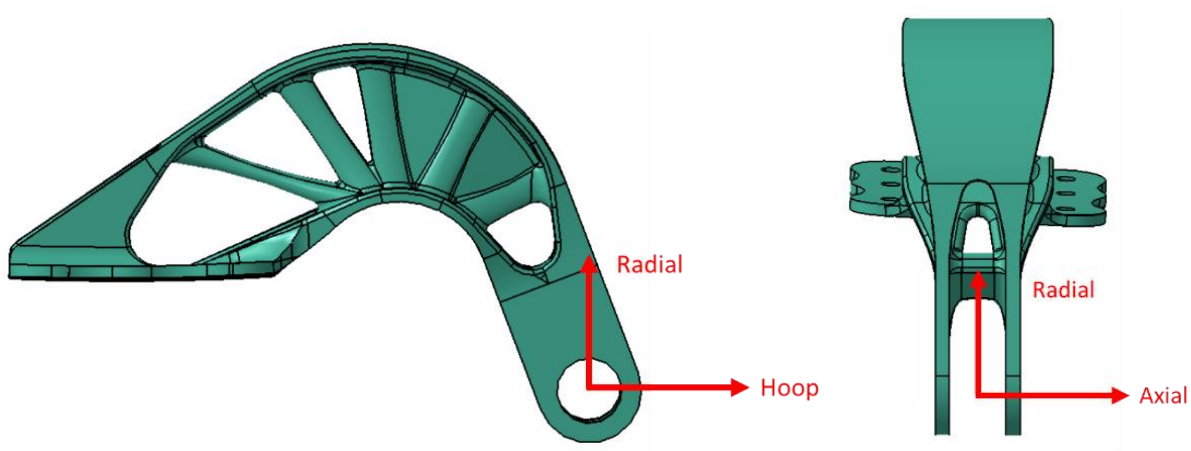


Figure 3.36 – Load coordinate system of forward hinge

Table 3.7 – Loads applied on forward hinge

Criticality	Loads	Description	Hoop (lbf)	Radial (lbf)	Axial (lbf)	Magnitude (lbf)
Ultimate	C15B'	Limit aerodynamic loading on aft fuselage with failure of other door attachments	-2849	223	0	2858
	C1B (ultimate)	1.5x limit aerodynamic loading on aft fuselage				2635
Limit	C1B	Limit aerodynamic loading on aft fuselage				1757
	C2	Limit aerodynamic loading on aft fuselage				1491

Table 3.8 – Loads applied on aft hinge

Criticality	Loads	Description	Hoop (lbf)	Radial (lbf)	Axial (lbf)	Magnitude (lbf)
Ultimate	C11B'	Limit aerodynamic loading C1B on aft fuselage with failure of other door attachments	-2006	221	156	2038
	C21	Limit aerodynamic loading C2 on aft fuselage with failure of other door attachments	1752	-163	24	1760
Limit	C1B	Limit aerodynamic loading on aft fuselage				1068
	C2	Limit aerodynamic loading on aft fuselage				946

Some of the loads are ultimate cases, which represent extreme situations that would occur statistically only once in the lifetime of the fleet of aircrafts. Therefore, in these situations yielding of the part is acceptable as long as failure doesn't occur. Thus, true elastic-plastic behavior of the material has to be modeled. Moreover, the parts being close to the auxiliary power unit (APU) operating at 200F, material properties had to be reduced to take into account the temperature knock-down. Figure 3.37 shows the true stress over true plastic strain if the Ti-6Al-4V at 200F. All calculations are detailed in Appendix – A.

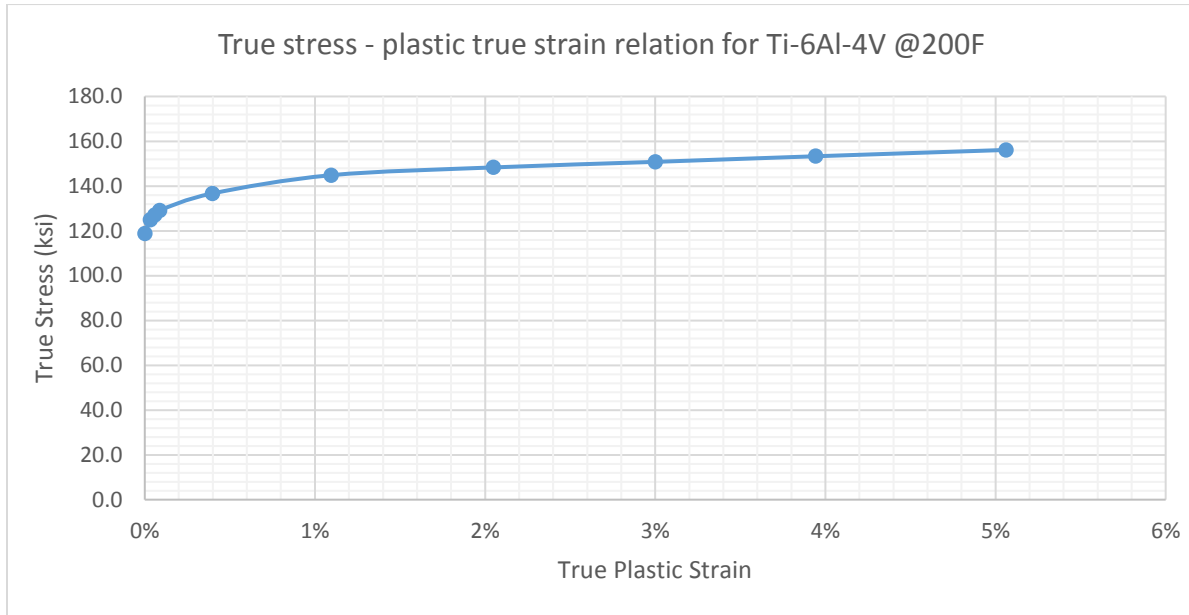


Figure 3.37 – True stress vs true plastic strain for Ti-6Al-4V at 200F

The limit and ultimate material properties used are listed in Table 3.9.

Table 3.9 – Material allowable at 200F for FE analyses

True yield stress strength (\tilde{F}_{ty})	113,600 <i>ksi</i>
True ultimate plastic strain ($\tilde{\epsilon}_{u,plastic}$)	0.05
True ultimate total stress strength (\tilde{F}_{tu})	140,500 <i>ksi</i>

Nonlinear models were built with complete material curves. Contact condition at the base plate was also considered to reproduce more accurately the configuration in the aircraft. Single point constraints were also modeled in order to simulate the actual stiffness of the structure under the hinges, as illustrated in Figure 3.38 and Figure 3.39.

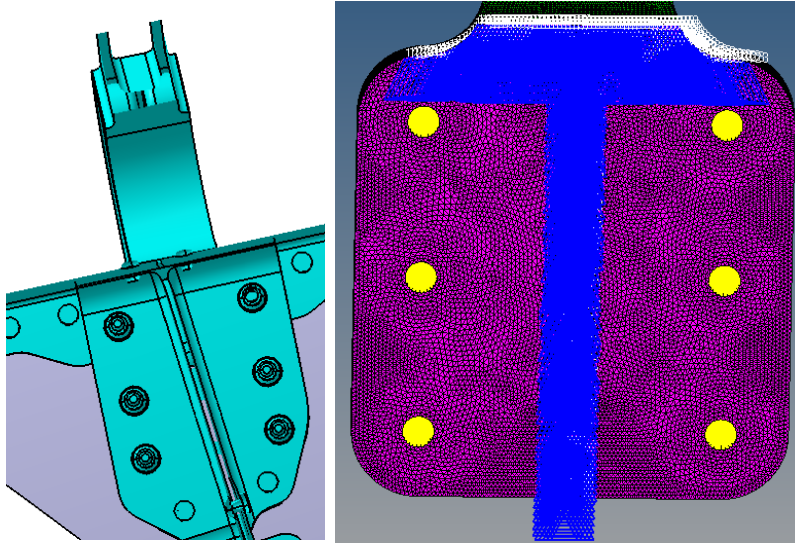


Figure 3.38 – Assembly of the hinge with stiffeners underneath (left) and FEA model with equivalent SPCs (right)

To analyze the integrity of the whole assembly, bolts with flexible elements (CBUSH) were also modeled with appropriate properties according to Huth calculations [33], see Appendix – A.

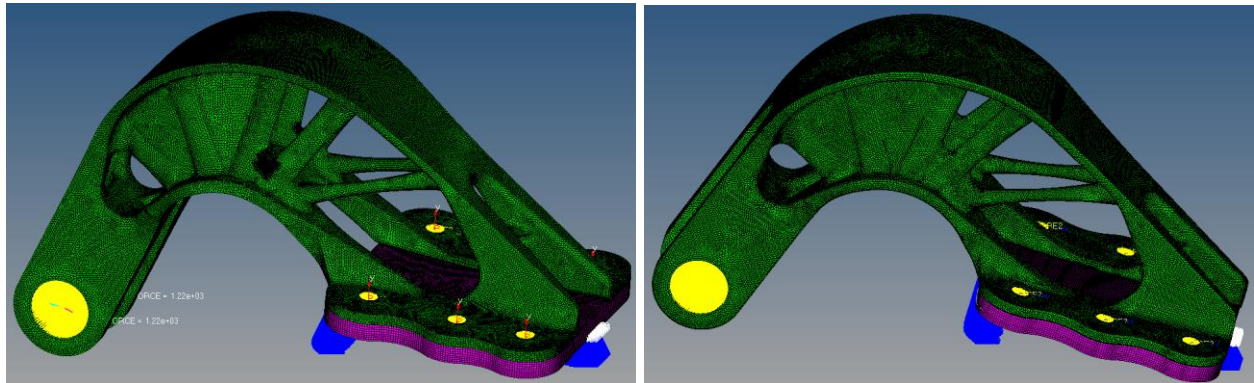


Figure 3.39 – Finite element models of the forward (left) and aft (right) optimized hinges

To determine if the parts have acceptable stress levels, the margins of safety in their bodies are computed. In fact, use of rigid body elements (RBE) at the bolts locations results in overestimated stress level at their vicinity. Therefore, stress around the bolts and around the lug is discarded from the analysis. The structural strength of the bolts and the lug are computed later in this section with analytical calculations.

Thus, the highest stress value not in direct contact with a boundary is taken as the reference. For the limit load cases:

$$Yield\ M.S. = \frac{\tilde{F}_{ty}}{1.15 * VM} - 1 \quad (18)$$

And for the ultimate load cases:

$$Failure\ M.S. = \frac{\tilde{F}_{tu}}{1.15 * VM_{eq}} - 1 \quad (19)$$

Where \tilde{F}_{tu} and \tilde{F}_{ty} are the true ultimate and yield stress strength, VM is the maximum Von Mises stress level monitored in the body of the parts and VM_{eq} is the equivalent Von Mises stress level in the plastic deformation stage of the material (see Figure 3.37). A fitting factor of 1.15 is added to the monitored stress to take into account manufacturing, handling and assembly uncertainties.

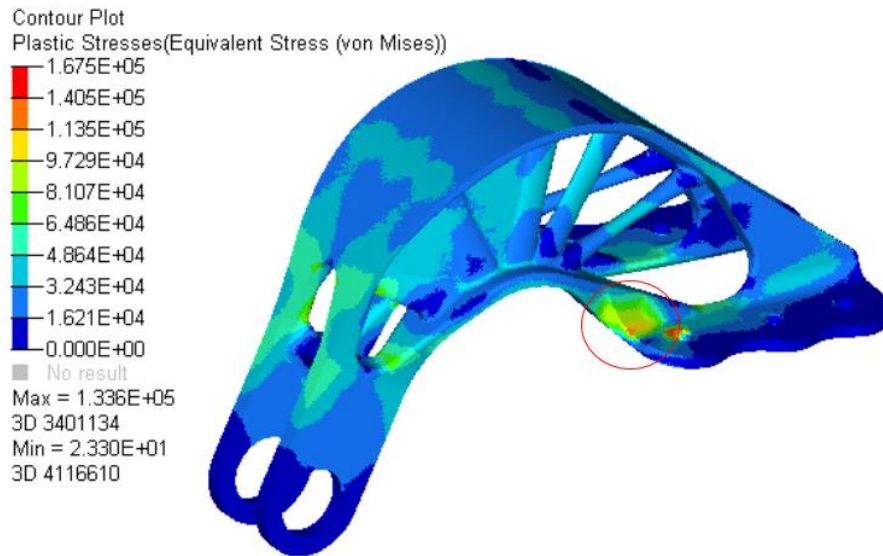


Figure 3.40 – C1B (ult.) maximum stress zone on forward hinge

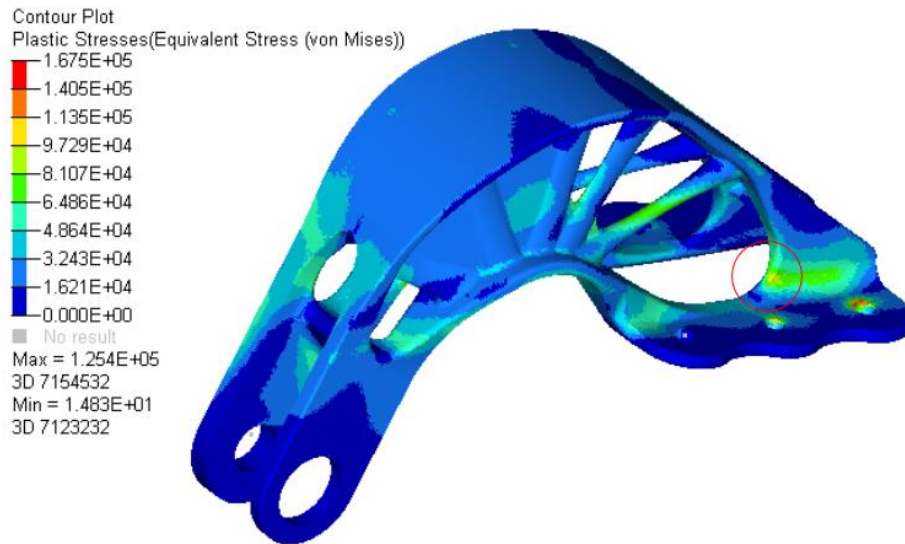


Figure 3.41 – C11B' Maximum stress zone on aft hinge

The maximum stress level is monitored in both parts, as pictured in Figure 3.40 and Figure 3.41 and the margins of safety are reported in Table 3.10 and Table 3.11..

Table 3.10 – Margins of safety of the forward hinge

		Von Mises stress (psi)	Margins of safety
Limit cases	C1B	63,732	55.1%
	C2	52,393	88.5%
Ultimate cases	C15B'	104,400	17.0%
	C1B (ult.)	117,100	4.3%

Table 3.11 – Margins of safety of the aft hinge

		Von Mises stress (psi)	Margins of safety
Limit cases	C1B	42,750	130.6%
	C2	64,190	53.7%
Ultimate cases	C11B'	103,000	18.6%
	C21	95,550	27.9%

After several free-shape optimizations in different areas of the parts, the strength of the parts is at an acceptable stress level with a minimum margin of safety of 4.3%.

As mentioned above, strength of the bolts and the lug cannot be validated with a FE analysis. Based on the semi-empirical methodologies developed by Bruhn [34] and Niu [35] and updated with internal data at Bombardier Aerospace, the margins of safety listed in Table 3.12 to Table 3.15 were computed for the strength of the lugs. All details are reported in Appendix – A.

Table 3.12 – Lug margins of safety of the forward hinge

Ultimate loads		Limit loads	
C15B'	C1B (ult.)	C1B	C2
54.1%	68.8%	129.5%	166.0%

Table 3.13 – Lug margins of safety of the aft hinge

Ultimate loads		Limit loads	
C11B'	C21	C1B	C2
323.0%	282.0	254.4%	301.1%

Loads applied on each bolts at every load cases are obtained with the FE analysis. Following the fasteners interaction equations presented in [35] and considering specifications given by the manufacturer of the bolts, the margins of safety for all load cases are computed.

Table 3.14 – Margins of safety of bolts on forward hinge

Bolt #	C15B'	C1B (ult.)	C1B	C2
1	274%	234%	512%	628%
2	248%	195%	462%	575%
3	425%	443%	776%	938%
4	395%	397%	712%	860%
5	262%	536%	1080%	1305%
6	227%	408%	822%	1015%

Table 3.15 – Margins of safety of bolts on aft hinge

Bolt #	C11B'	C21	C1B	C2
1	492%	167%	530%	1050%
2	317%	215%	625%	712%
3	644%	514%	1020%	1690%
4	501%	611%	1207%	1095%
5	505%	555%	1380%	1800%
6	276%	785%	1870%	717%

Since all margins of safety are positive, the designs are validated. However, numerical analyses is the first step toward qualification of the parts. In Chapter 4, physical testing of actual specimens and samples is explored.

3.4 Topology optimization with level set method

Topology optimization with the Level-Set Method (LSM) is a more recent technology (2001) than SIMP method (1989) and few functional software are available. Few works with 3D models exist and even fewer are commercial, most being prototypes from laboratories or universities. The only LSM topology optimization solver destined to commercial applications is ProTOp which was tested as reported in this section. Note that Optistruct has a LSM algorithm for topology optimization but its reliability is poor.

Optimizations were ran only with the CSeries hinge and the track support. The later didn't give any good results for reasons that will be discussed. However, detailed results of the CSeries hinge optimizations are reported at the end of this section. The benefits and limitations of using LSM compared to SIMP method are also presented.

The most important drawback with ProTOp is that it is a closed source software with very limited documentation. There are many editable parameters but how they influence the result and how they interact together is not known. For example, how the hole nucleation occurs during the optimization is unclear. This limits its use in a scientific work but it could still be of great commercial interest for the industry.

The second problem with ProTOp software is the lack of pre-processor and limited configuration capabilities. In fact, models have to be designed, configured with materials, loads, boundary conditions, etc. and meshed either in ABAQUS or PTC Creo. The later are however not the most common FEA tools in aerospace, which requires extra resources and time.

Moreover, ProTOp works only with simple models. Multipoint constraints elements such as RBE2 and RBE3 and spring elements such as CBUSH are not supported. This happened to be a problem on models with complicated attachments as the track support (see Figure 3.5 for details of its structure). Therefore, optimizations were run with single point constraints (SPC) applied at each bolt location which resulted in unrealistic stress distribution. Different SPC configurations were tried without success and are reported in Figure 3.42.

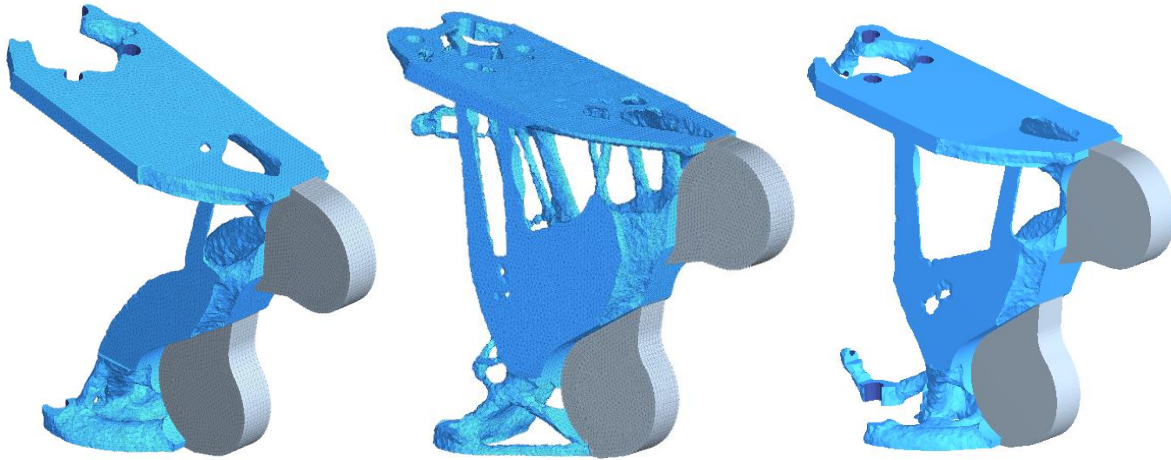


Figure 3.42 – Results of the track support optimizations with different single point constraints configurations giving unrealistic stress distributions

Finally, nonlinearities such as large displacement or plastic-strain materials are not taken into account. Although modeling contact is possible in ProTOp, if the model is pre-processed in PTC Creo, which was not available for our work.

Level-set method moves boundaries of the model instead of altering the designs space's elements' densities. Results from optimization with LSM contain only solid elements. In-solver performance validation is therefore much more reliable than models with intermediate densities elements. Unfortunately, ProTOp doesn't have enough in-solver processing capabilities to accurately evaluate results from an optimization.

Moreover, there is no need to arbitrarily segregate elements above and below a certain density level between 0 or 1 which often resulted in irrelevant features such as illustrated in Figure 3.43. LSM optimization always converges toward fully connected geometry and that makes it *de facto* more stable. This implies as well that larger design spaces can be used with accurate results.

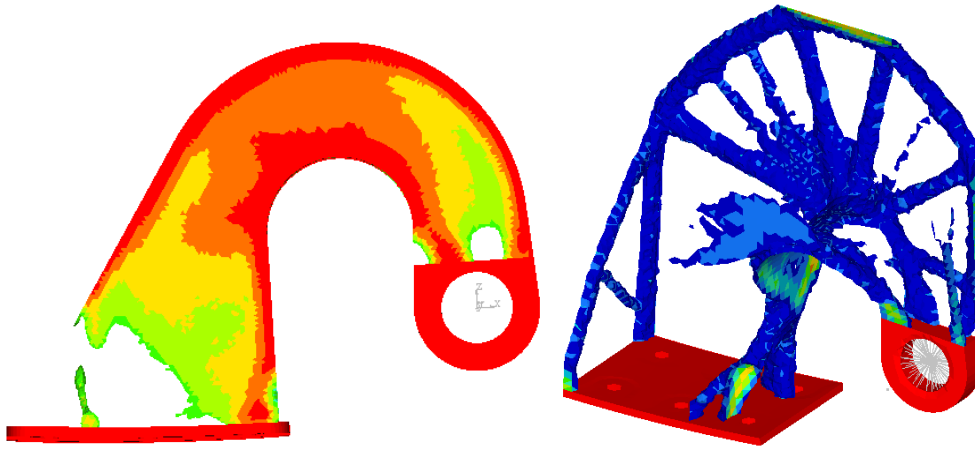


Figure 3.43 – Optimization results with SIMP method where iso-density filtering produces irrelevant features

Another benefit from dealing with boundary optimization algorithm is that the surfaces are automatically smoothed during optimization. This changes from the SIMP method where surface resolution was dependent on the element's size and type. Figure 3.44 illustrates two similar optimization results obtained from SIMP and LVM. Elements below 0.5 density in the SIMP model have been subtracted and we can see the roughness of all the features because the remaining elements are fixed in sizes. A coarser mesh would have given an even more “spiky” result whereas finer mesh would have flatten the surfaces. These spikes cause stress concentrations and corrupt the in-solver performance analysis.

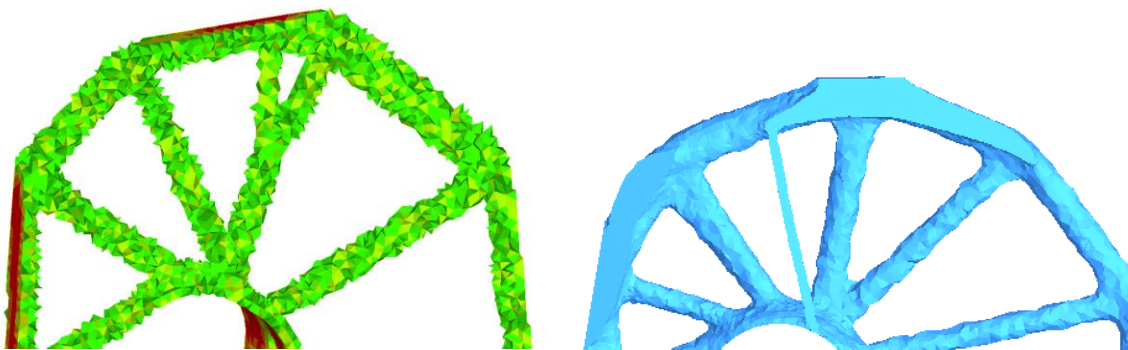


Figure 3.44 – Results from optimization with SIMP (left) and LSM (right).

Since LSM acts as a shape optimization and forces the mesh to produce smoothed features, spikes does not appear and uniform geometries are created. It is therefore easier to assess performance of

the results and, most of all, interpretation is much easier. Quality of the resulted geometries with LSM is so high, partial interpretation is often straightforward and only a remesh is necessary to run the FEA. A comparison of the interpretation methodology of optimization for both SIMP and LSM methods is depicted in Table 3.16.

Table 3.16 – Partial interpretation methodology with SIMP and LSM

Steps	SIMP	Level-Set Method
1	Result	Result
2	Iso-density filter	Remeshing
3	Mesh-based smoothing	FEA
4	Remeshing	
5	FEA	

A second interesting characteristic of topology optimization with LSM is that computation time is function of the surface complexity of the design space and not its volume. This allows the solver, in this case ProTop, to handle models with larger number of elements compared to SIMP solvers. Optimization with more elements generally gives more realistic stress distribution and thus, better results.

Table 3.17 – Comparison between two similar models optimized with SIMP (left) and LSM (right) on different computers

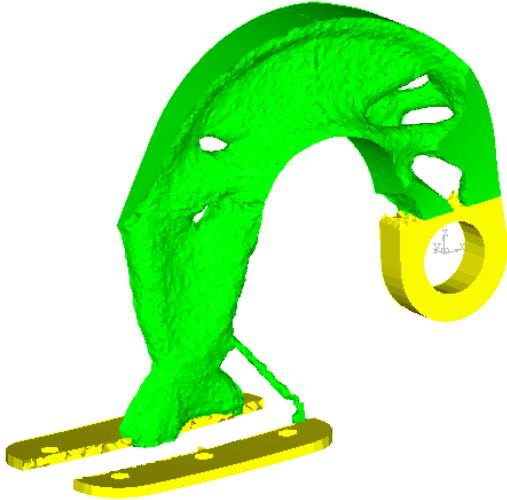
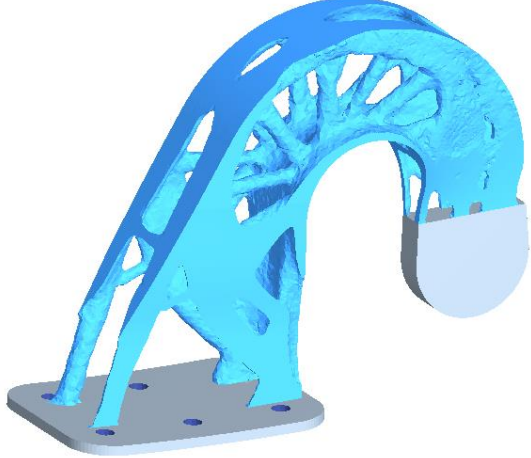
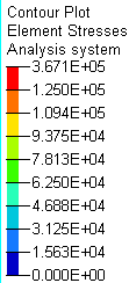
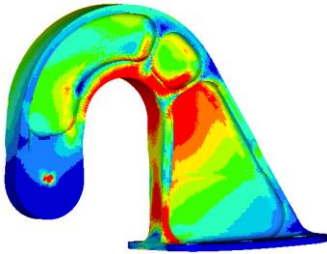
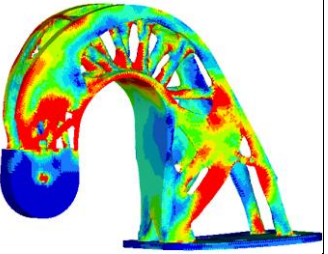
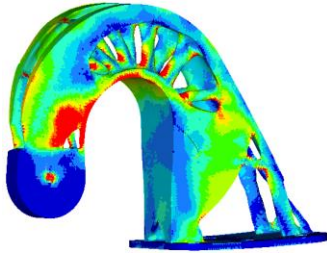
	SIMP	Level-Set Method
		
Elements	270,349	642,337
Cycles	48	80
Processor (GHz)	3.07	2.67
RAM (GBits)	12.00	3.80
Total time (h:min:sec)	1:18:15	0:46:54 (-41.0%)

Table 3.17 shows two identical optimizations ran with different solvers but with the same configuration: minimize compliance with volume target = 20%. Both models had similar design spaces but the model solved with LSM had a much finer mesh. Unfortunately, it was impossible to run both models on the same computer. However, from this simple comparison we notice that although the model solved with LSM had more elements, less computing power was required and while it converged after a greater number of iterations, it took significantly less time to do so.

Additionally, having more elements helps converging towards finer features which acts similarly to the free-shape optimization step. One will also notice the great difference between the resulted topologies of Table 3.17. Indeed, LSM result looks more rigid and suited to bear torsion loads.

The results from the LSM optimization in Table 3.17 are reported and compared with the original design of the CSeries hinge in Table 3.18. The optimizations were made to minimize compliance with a volume target and with a stress target. The average elements' size was at 0.04in for all three models and no interpretation was made on the models. This comparison highlights the properties of LSM optimization to increase the stiffness of the part and to reduce its stress level with little design effort.

Table 3.18 – Comparison between original design and LSM optimizations done with volume target and stress target

	Original design	Volume optimization	Stress optimization
			
Volume (in ³)	2.491	2.259 (-2.3%)	2.674 (+16.0%)
Peak stress (psi)	295,000	315,000 (+7%)	165,000 (-44%)
Max disp. (in.)	0.654	0.366 (-44.0%)	0.197 (-70%)



Topology optimization with level-set method is a promising structural analysis technology for additive manufacturing primarily since it only compute fully dense results, hence not requiring laborious intermediate interpretation. Furthermore, LSM produce near net shape results because it moves the model's boundaries and also deals more easily with models having large number of elements.

However, ProTOp software still has to be developed to replace advanced SIMP tools such as Optistruct. Indeed, the possible model configurations have to improve along with its in-solver analysis capabilities which are still limited. In parallel, documentation of the algorithms and parameter edition will help having better control over the results.

CHAPTER 4 CERTIFICATION OF ADDITIVE MANUFACTURING IN AEROSPACE

The APU door hinges of the Global aircraft as presented before was selected to be qualified for flight. The weight saving from the redesign was deemed significant enough for that (see Table 4.1). The initial stress analyses showed satisfactory results as well. Finally, the whole production cost from the supplier was shown to be equal or lower than the original machined parts.

Table 4.1 – Original (left) and optimized (right) demonstration models made in aluminum by additive manufacturing

	
4.621 in ³	3.021 in ³ (-34.6%)

However, as mentioned previously, the mechanical properties used during the analyses in Section 3.3.2 are based on limited test samples and relied on the properties of titanium produced with other processes. To qualify a part for airworthiness, the actual exact strength of the part has to be validated and the additive manufacturing process has to be proven statistically stable over the production of several builds. Qualification is the initial stage prior to certification as given by Transport Canada, the legal authority.

However, in our case, instead of qualifying the process, only the specific application of the APU door hinge on the Global aircraft would be qualified. The reason for this is that the technologies are still evolving and improvement is expected in the near future. The goal with this project was to put these low risk parts into production and at the same contribute to our understanding of this technology.

4.1 Qualification

Initially, 4 manufacturing lots have been produced with 88 coupons and 18 hinges made of Ti-6Al-4V. All those parts are being tested to validate or adjust the mechanical properties used in the analyses. They will be tested looking for to:

- 1) Set the initial stress allowable for Ti-6Al-4V made by laser powder-based fusion
- 2) Confirm the actual margin of safety of the hinges
- 3) Inspect void content of the process
- 4) Inspect dimensional tolerance of the process

A test matrix with all coupons details is provided in Appendix – B. All coupons are tested by Exova in Mississauga, Ontario.

4.1.1 Tensile coupons

Included in the 88 coupons, 47 are tensile coupons on which the following parameters will be compared and studied:

- Manufacturing lot: coupons are placed on 4 different lots to study variability
- Position in the build: borders vs center of the fusion chamber
- Orientation in the build: parallel (x/y) vs perpendicular (z) to the powder layers
- Heat treatment: one coupons series will be treated with hot-isostatic pressure at 1650F and 14,750 psi
- Temperature: 5 tensile coupons will be tested at 200F and 5 coupons tested at 400F
- Surface finish: 10 coupons are tested as-built without smoothing in the gauge length of the coupons
- Dimensions of the coupons: 2 sizes of tensile coupons are tested

Tensile specimens are crucial to determine yield (F_{ty}) and ultimate tensile strength (F_{tu}) as well as elongation.

4.1.2 Bearing, shear and compression coupons

To complement tensile tests, 10x bearing, 10x shear and 10x compression tests are done all in regular testing conditions. The later are used to determine the yield compression strength (F_{cy}), ultimate shear strength (F_{su}), yield (F_{by}) and ultimate bearing strength (F_{bu}).

4.1.3 Fatigue coupons

Moreover, even though the hinges are not usually solicited in fatigue during flights, 10 fatigue coupons will be tested in order to start accumulating data on that topic. The objective of the fatigue testing of this material is to be able to obtain its S-N curve. Such a curve for Ti-6Al-4V in AMS4928 condition is shown in Figure 4.1.

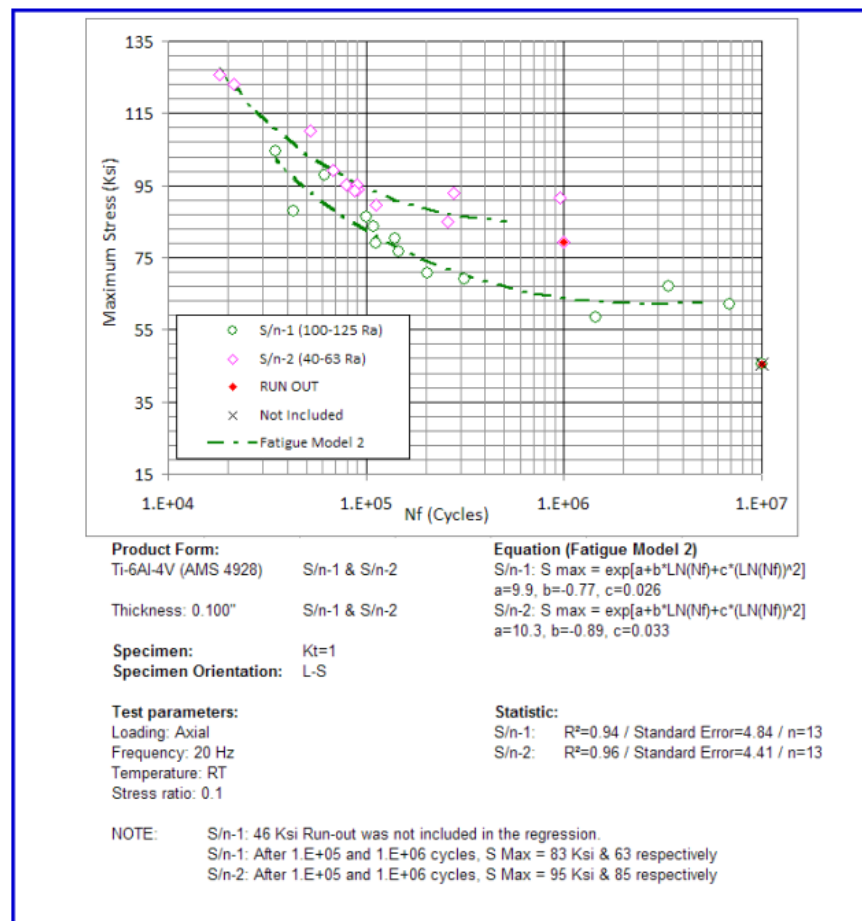


Figure 4.1 – S-N curve of AMS4928 titanium coupons with surface finish of 100-125 Ra and 40-63 Ra

Considering the limited amount of fatigue coupons tested, maximum stress level for failure at 10^5 cycles (P5) is targeted. Since there is a lot of variability in tensile fatigue results, test loading will be adjusted iteratively based on the previous result. The first coupon will be tested at 95ksi which corresponds to P5 for equivalent forging titanium on the figure above.

4.1.4 Non-destructive inspection of hinges

Prior to testing, the hinges will be inspected with X-ray micro-computerized tomography (CT-scan). Inspection at a resolution of $50\mu\text{m}$ to detect voids inside the parts and general inspection at $100\mu\text{m}$ to analyze the dimensional tolerance of the parts. The CT-scan will be performed by the National Research Council in Boucherville, Quebec.

4.1.5 Static hinge testing

In addition, 15 of the 18 hinges built with the coupons will be tested in static conditions as well. The goal is to validate the margins of safety calculated in Section 3.3.2 which is essential to certify the parts after qualification. Therefore, traction and compression tests on the parts will be done up to limit loads and then up to failure to know exactly how many pounds the hinge can sustain. Comparison with numerical analyses will be made to validate the model by monitoring real-time displacement of hinges and failure mode and location.

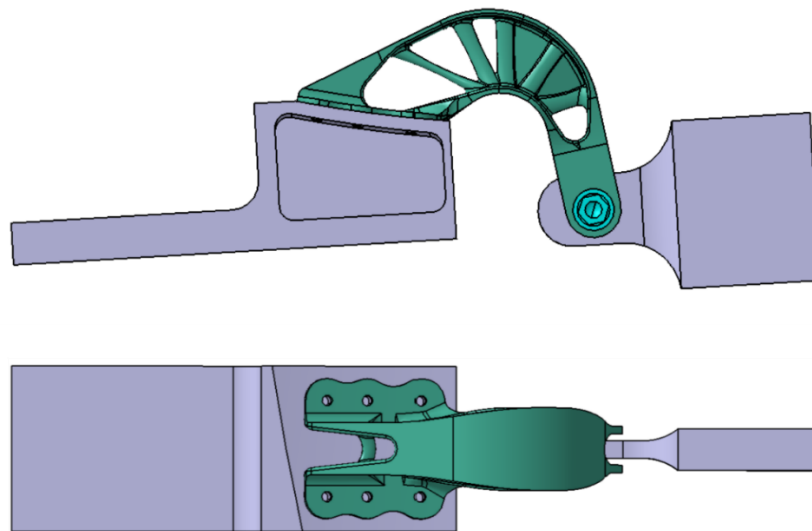


Figure 4.2 – Forward hinge with its fixture to ensure the test machine applies the loads in the desired orientation

Different fixtures were designed to reproduce accurately the load orientations. One of the 4 fixtures produced is illustrated as a 3D model in Figure 4.2. Those unique fixtures were difficult to manufacture because of the complex mating surface that follows the curvature of the fuselage on the aircraft. This virtual curvature is shown in Figure 4.3. In addition, all the holes have independent axis which requires 5-axis milling and because each fixture will be used between 2 to 7 times, the tolerances of the holes on the fixtures had to be wide enough to ensure assembly with the hinges.

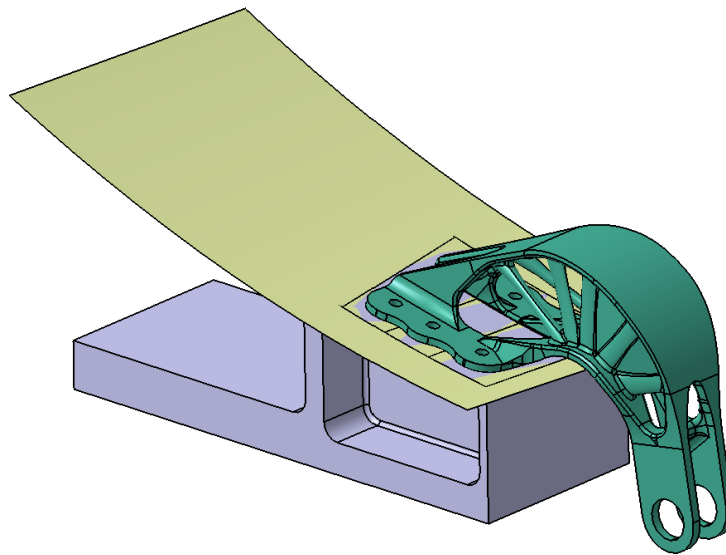


Figure 4.3 – Numerical render with a testing fixture (blue) with virtual mating surface (yellow) with the hinge (green)

The manufacturing challenges could have been overcome with a simpler design with a flat mating surface compensated by liquid shim. Manufacturing cost savings would then have allowed to produce 1 fixture per tested hinge and the 6 holes for fastening could have been drilled *in situ*, thus ensuring perfect fit of the fasteners.

4.1.6 Fatigue testing of hinges

Two of the 3 remaining hinges will then be tested in fatigue. As mentioned before, the APU door hinges on this aircraft should not be exposed to fatigue loading in normal using. However, to validate the fatigue data found with the coupons, the hinges will be tested at a given load to obtain a failure of the part around 100,000 cycles.

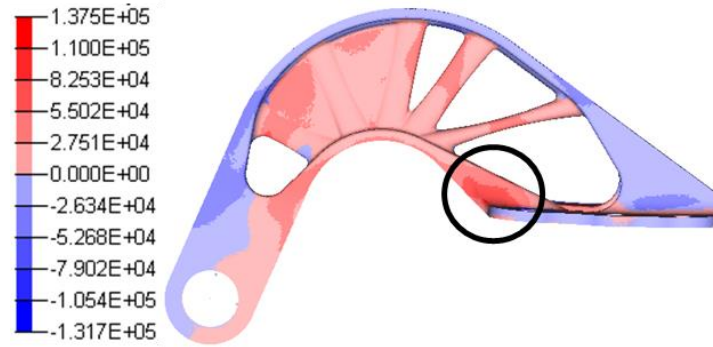


Figure 4.4 – Signed Von Mises stress of the hinge with a 1,952 lbf load magnitude

Both hinges will be tested with C1B load orientation. Magnitude of the load was calculated in order to obtain a 95ksi tensile stress point in a section of the parts. Thus, theoretically allowing 100,000 cycles before failure.

4.1.7 Chemical composition test

Finally, chemical composition of the material will be validated to determine content of: Carbon (C), Oxygen (O), Hydrogen (H), Nitrogen (N), Aluminum (Al), Iron (Fe) and Vanadium (V). The tolerances for Ti-6Al-4V with AMS4928 specifications are reported in

Table 4.2.

Table 4.2 – Ti-6Al-4V AMS4928 element content tolerance

Content	Tolerance
Titanium (Ti)	balance
Aluminum (Al)	5.50 - 6.75
Vanadium (V)	3.5 – 4.5
Iron (Fe)	0 - 0.3
Carbon (C)	0 – 0.08
Oxygen (O)	0 – 0.2

Table 4.2 – Ti-6Al-4V AMS4928 element content tolerance (continued)

Nitrogen (N)	0 – 0.5
Hydrogen (H)	0 - 0.0125

CHAPTER 5 CONCLUSION AND RECOMMENDATIONS

The motivation of this project is that a complete technology integration cycle was explored, from design to qualification of parts built using AM for the aerospace industry. The first objective of this thesis was to develop a design methodology specifically for additive manufacturing. Thus, through 3 case studies, the benefits and limitations of topology optimization were exposed. No detailed guidelines existed in the available literature on the configurations of an optimization and how to manage the output. As it is exposed in Table 5.1, in an industrial context, practical usage of this technology through case studies is really beneficial.

Table 5.1 – Summary of the results and their interests for the industrial partner and for professional development of the author

Results	Interest for industrial partner and for professional development
1. Topology optimization configuration improvement	<ul style="list-style-type: none"> • General guidelines based on case studies are useful for training purposes. • Unique competences useful as a professional aerospace product designer.
2. Results analysis method	<ul style="list-style-type: none"> • First systematic iso-density filter selection method for SIMP. • Comprehension of the influence of intermediate density elements on the reliability of the results.
3. Partial interpretation	<ul style="list-style-type: none"> • Helps going from 1 result validation loop per week to up to 10 loops per week. • Submission of a scientific paper contributes to the progress of science.

Table 5.1 – Summary of the results and their interests for the industrial partner and for professional development of the author (continued)

4. Industrial integration of AM	<ul style="list-style-type: none"> • Introduction of the optimized part reduces the weight of the aircraft of 1lbs. • Establishment of a material database. • Capacity to work in multidisciplinary environment.
---------------------------------	---

New solutions to accelerate design with topology optimizations were proposed. First, as seen previously, because of density homogenization of the elements, some optimizations results appear better in-solver than after interpretation. This interpretation step is time consuming so designers had to select and discard which result to interpret or not based on subjective parameters such as aesthetic of the result or similarity with already existing geometries. Here, an analytical method was proposed that help to mathematically predict if in-solver performance of an optimization result is reliable enough to be interpreted. This allows to favor interpretation of results with reliable performance.

Then, we addressed the problem of the time spent on interpretation. Since all actual design tools were feature-based, interpretation of topology optimization results implied building a new geometry based on the result. This is extremely long and it is sometimes hard to reproduce exactly the organic shapes of the result. Instead, an intermediate step was proposed called partial interpretation. At this step, the goal is only to smooth surfaces and get rid of numerical discrepancies. Therefore, a mesh-based software is used that modifies directly the 3D surfacing mesh of the optimization result. The example exposed in this study show that this step can reduce interpretation time from 30 hours to less than 1 hour. This can be improved in the future with software dedicated to finite element modifications with quality control of elements and volume monitoring to avoid growing the part unnecessarily.

Additionally, future opportunities enabled by the recent development of topology optimization with level-set method were documented in this work. With no variation of density, this method gives accurate and reliable performance that allows to save a lot of time. As well, since it is much faster than SIMP method, models with more elements can be used and therefore lead to finer results

easier to interpret. Commercial integration problems still exist that limit its usage in aerospace but it is promising.

Part selection was not studied in this article and it could consist in a complex project in itself. The 3 case studies presented here were selected based on few parameters such as size, material and weight. Potential benefits of a part to be made in additive manufacturing can be substantiated with more elaborated factors, e.g. number of functional surfaces, surface-to-volume ratio, part integration potential, etc.

A deeper analysis of the few manufacturing constraints of laser powder-based fusion technology could be beneficial for future work as well. Indeed, supporting material is a burden to take off the parts and this could come into consideration at a very early stage of the design lifecycle which was not considered here. In our case, we only relied on the supplier's feedback to change some geometries or to position the part differently in the build chamber.

The second objective of this work was to explore qualification and certification issues of additively manufactured parts for the aerospace industry. During the last 2 years, things evolved significantly in additive manufacturing and a clear path forward emerged. In order to qualify the technology of laser powder-based fusion, extensive testing is required and the whole industry would have to collaborate.

In the meantime, the approach taken in this work has been proven to be adequate. Qualifying a simple structural part such as the Global APU door hinge implies limited testing which is not sufficient for qualifying the process. However, because ongoing testing will be done once the part will be put into production, statistical data will be gathered slowly on the repeatability of the process. In the end, around 110,000\$CAD would have been necessary to qualify this new technology which is much lower than similar projects done in the past.

In this work, laser powder-based fusion is explored for production of metallic structural parts but there are many other applications for additive manufacturing in aerospace. Powder-based technologies are hardly scalable since the environment of the whole fusion chamber needs to be precisely controlled and handling powder is complex with limited recyclability. On the other hand, direct energy deposition with wire feed stock or powder projection has the potential of building much larger parts. For a structure integrator as Bombardier Aerospace which produces mostly large

components such as the fuselage, wings, cockpit, etc., this could be a disruptive innovation if it can reduce machining and assembly operations.

BIBLIOGRAPHY

- [1] Wikipédia, "Fabrication additive," 6 juin 2016. [Online]. Available: https://fr.wikipedia.org/wiki/Fabrication_additive. [Accessed 12 06 2016].
- [2] Wikipédia, "Optimisation topologique," 25 November 2015. [Online]. Available: https://fr.wikipedia.org/wiki/Optimisation_topologique. [Accessed 12 June 2016].
- [3] ASTM F2792-12, *Standard Terminology for Additive Manufacturing Technologies*, 2012.
- [4] Wikipédia, "Topology Optimization," 20 May 2016. [Online]. Available: https://en.wikipedia.org/wiki/Topology_optimization. [Accessed 12 June 2016].
- [5] A. S. o. D. f. R. a. E. (ASD(R&E)), "Technology Readiness Assessment (TRA) Guidance," Department of Defense, Washington, 2011.
- [6] Wohlers Associates, "Wohlers Report 2015," Wohlers Associate, Fort Collins, 2015.
- [7] GE Global Research , "3D Printing Creates New Parts for Aircraft Engines," [Online]. Available: <http://www.geglobalresearch.com/innovation/3d-printing-creates-new-parts-aircraft-engines>. [Accessed 12 June 2016].
- [8] Airbus Group, "Breakthrough for future Airbus A320," Janvier 2015. [Online]. Available: <http://www.airbusgroup.com/int/en/story-overview/Pioneering-bionic-3D-printing.html>. [Accessed 12 June 2016].
- [9] SpaceX, "Spaced launches 3D-printed part to space, created printed engine chamber," 14 July 2014. [Online]. Available: <http://www.spacex.com/news/2014/07/31/spacex-launches-3d-printed-part-space-creates-printed-engine-chamber-crewed>. [Accessed 12 June 2016].
- [10] Aerojet Rocketdyne, "Aerojet Rocketdyne Successfully Tests Complex 3-D Printed Injector in World's Most Reliable Upper Stage Rocket Engine," 7 March 2016. [Online]. Available:

<http://www.rocket.com/article/aerojet-rocketdyne-successfully-tests-complex-3-d-printed-injector-worlds-most-reliable>. [Accessed 12 June 2016].

- [11] ATW Online, "Additive Power," March 2016. [Online]. Available: http://www.atw-digital.com/airtransportworld/march_2016?sub_id=f4X5lNXI9HPa&pg=NaN#pgNaN. [Accessed 12 June 2016].
- [12] Metal Prices, "Aluminum 6063 Extrusion Billet," [Online]. Available: <https://www.metalprices.com/metal/aluminum/aluminum-6063-extrusion-billet-premium>. [Accessed 30 July 2016].
- [13] G. Rozvany, "Aims, scope, methods, history and unified terminology of computer-aided topology optimization in structural mechanics," *Structural Multidisciplinary Optimization*, vol. 21, no. 2, pp. 90-108, 2001.
- [14] M. Bendsoe and N. Kikuchi, "Generating optimal topologies in structural design using a homogenization method," *Computer methods in applied mechanics and engineering*, pp. 197-224, 1988.
- [15] M. Bendsoe, "Optimal shape design as a material distribution problem," *Structural Optimization*, vol. 1, pp. 193-202, 1989.
- [16] M. Bendsoe and O. Sigmund, *Topology Optimization : Theory, Methods and Applications*, Berlin: Springer, 2003.
- [17] O. Sigmund and K. Maute, "Topology Optimization approaches," *Structural and Multidisciplinary Optimization*, vol. 48, no. 6, pp. 1031-1055, 2013.
- [18] J. D. Deaton and R. V. Grandhi, "A survey of structural and multidisciplinary continuum topology optimization: post 2000," *Structural Multidisciplinary Optimization*, vol. 49, no. 1, pp. 1-38, 2014.

- [19] K. Svanberg, "The method of moving asymptotes - A new method for structural optimization," *International Journal for Numerical Methods in Engineering*, vol. 24, pp. 359-373, 1987.
- [20] C. Fleury, "CONLIN: an efficient dual optimizer based on convex approximation concepts," *Structural optimization*, pp. 81-89, 1989.
- [21] G. Vanderplaats, "A robust Feasible Directions algorithm for design synthesis," in *24th Structures, Structural Dynamics and Materials Conference*, Lake Tahoe, NV, 1983.
- [22] C. Le, J. Norato, T. Bruns, C. Ha and D. Tortorelli, "Stress-based topology optimization for continua," *Structural and multidisciplinary Optimization*, vol. 41, no. 4, pp. 605-620, 2010.
- [23] M. Werme, "Using the sequential linear integer programming method as a post-processor for stress-constrained topology optimization problems," *International Journal for Numerical Method in Engineering*, vol. 76, no. 10, pp. 1544-1567, 2008.
- [24] E. Holmberg, "Stress and fatigue constrained topology optimization," Linköping University, Department of Management and Engineering, Linköping, 2013.
- [25] S. Osher and J. Sethian, "Fronts propagation with curvature-dependent speed: Algorithm based on Hamilton-Jacobi formulations," *Journal of Computational Physics*, vol. 79, pp. 12-49, 1988.
- [26] M. Y. Wang, X. Wang and D. Guo, "A level set method for structural topology optimization," *Computer methods in applied mechanics engineering*, vol. 192, pp. 227-246, 2003.
- [27] G. Allaire, F. Jouve and M. Toader, "Structural optimization using sensitivity analysis and a level-set method," *Journal of Computational Physics*, vol. 194, no. 1, pp. 363-393, 2004.
- [28] N. van Dijk, K. Maute, M. Langelaar and F. van Keulen, "Level-set methods for structural topology optimization: a review," *Structural Multidisciplinary Optimization*, vol. 48, pp. 437-472, 2013.

- [29] H. Jia, H. Beom and Y. Wang, "Evolutionary level set method for structural topology optimization," *Computers and Structures*, vol. 89, pp. 445-454, 2011.
- [30] G. Allaire, F. de Gournay, F. Jouve and A. Toader, "Structural optimization using topological and shape sensitivity via a level set method," *Control Cybern*, vol. 34, no. 1, pp. 59-80, 2005.
- [31] M. Burger, B. Hackl and W. Ring, "Incorporating topological derivatives into level set methods," *Journal of Computational Physics*, vol. 194, no. 1, pp. 344-362, 2004.
- [32] M. Zhou, Y. Shyy and T. H.L., "Checkerboard and minimum member size control in topology optimization," *Structural and Multidisciplinary Optimization*, pp. 152-158, 2001.
- [33] F. Gunbring, Prediction and Modeling of Fastener Flexibility Using FE, Linköping: Press of Linköping University Institute of Technology, 2008.
- [34] E. Bruhn, Analysis and Design of Flight Vehicle Structures, Lafayette: Jacobs Publishing, Inc., 1973.
- [35] M. C.-Y. Niu, Airframe Structural Design, Los Angeles: Technical Book Company, 1988.
- [36] Batelle Memorial Institute, Metallic Material Properties Development and Standardization, Columbus, OH, 2008.
- [37] J. Ajaja, "Notes de cours - MTR4700 - Essai de traction," École Polytechnique Montréal, Montreal, 2014.
- [38] J.-P. Bailon and J.-M. Dorlot, Des Matériaux, Montréal: Presses Internationales Polytechnique, 2000.
- [39] Bombardier Aerospace, "Bombardier Manual - BM7024.01.03.02 - Strength of Metallica Structures - Joints and Fittings - Joints and Attachements," Bombardier Aerospace, Montreal, 2014.

- [40] R. Dehoff, C. Tallman, C. Duty, W. Peter, Y. Yamamoto, W. Chen and C. Blue, "Case Study: Additive Manufacturing of Aerospace Brackets," *Advanced Materials & Processes*, pp. 19-22, 2013.
- [41] M. Bendsoe and O. Sigmund, "Topology Optimization by distribution of isotropic material," in *Topology Optimization: Theory, Methods and Applications*, Berlin, Springer, 2003, pp. 1-68.
- [42] Government of Canada, "National Aircraft Certification," Transport Canada, 06 12 2012. [Online]. Available: <https://www.tc.gc.ca/eng/civilaviation/certification/menu.htm>. [Accessed 14 09 2015].
- [43] Loughborough University, "The 7 categories of Additive Manufacturing," [Online]. Available: <http://www.lboro.ac.uk/research/amrg/about/the7categoriesofadditivemanufacturing/>. [Accessed 30 October 2015].
- [44] D. Walker, D. Liu and A. Jennings, "Topology Optimization of an Aircraft Wing," in *56th AIAA/ASCE/AHS/ASC Structures, Structural Dynamics and Materials Conferences*, Kissimmee , Florida, 2015.
- [45] F. Gunbring, Predicting and Modeling of Fastener Flexibility Using Finite Element Method, Linkoping: Linkoping University, 2008.
- [46] Wikipédia, "3D Printing," 7 June 2016. [Online]. Available: https://en.wikipedia.org/wiki/3D_printing. [Accessed 12 June 2016].

APPENDIX A - GLOBAL APU HINGE ANALYSES CALCULATIONS

Material properties

Detailed calculations to obtain true stress / true strain curves are exposed in this section.

Table A.1 – Mechanical properties of wrought annealed Ti-6Al-4V titanium [36]

Properties	Room Temperature	% of room temperature property @ 200°F	Adjusted properties @200F
F _{tu} (ksi)	130	90%	117
F _{ty} (ksi)	120	88%	106
F _{su} (ksi)	79	90%	71
F _{cy} (ksi)	124	86%	107
F _{bru} (e/D=2) (ksi)	260	90%	234
F _{bry} (e/D=2) (ksi)	194	88%	171
E (Msi)	16.0	96%	15.4

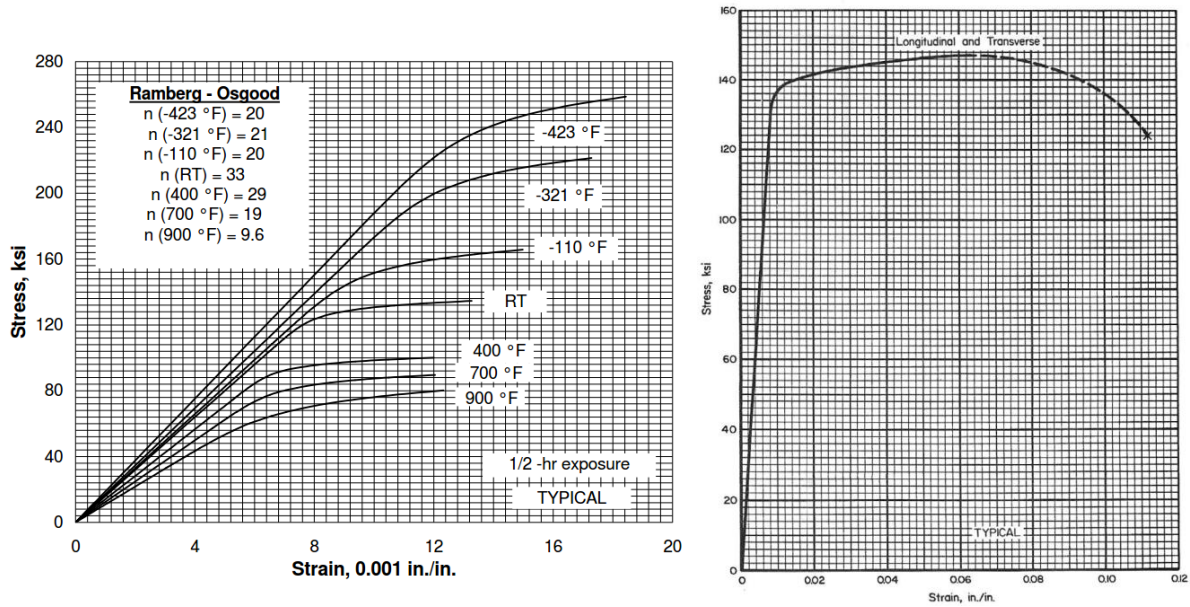


Figure A.1 – Ramberg-Osgood curve and complete engineering stress-strain curve of Ti-6Al-4V [36]

With help of the material engineering curves presented at Figure A.1, the true stress – true strain curve is derived. Following equations link the true strain $\tilde{\epsilon}$ and true stress $\tilde{\sigma}$ to the engineering stress σ and strain ϵ [37] [38]:

$$\tilde{\epsilon} = \ln(1 + \epsilon)$$

$$\tilde{\sigma} = \sigma(1 + \epsilon)$$

MMPDS - Ti-6Al-4V - AMS4911 - Annealed Plate 2in		Temperature knock-down factor	Corrected value @200F	Extracted true-stress / true-strain curve (@200F)		Extracted true-stress / true-strain curve (@RT)	
Eng Strain	Eng Stress	(@200F)	Eng Stress	True Strain	True Stress (ksi)	True Strain	True Stress (ksi)
0.0000	0	0.96	0	0.0000	0.0	0.0000	0.0
0.0073	118	0.96	112.7	0.0073	113.6	0.0073	118.9
0.0076	120	0.95	114.1	0.0076	115.0	0.0076	120.9
0.0080	124	0.95	117.3	0.0080	118.3	0.0080	125.0
0.0084	126	0.94	118.6	0.0084	119.6	0.0084	127.1
0.0088	128	0.94	119.9	0.0088	121.0	0.0088	129.1
0.0096	129	0.93	120.3	0.0096	121.4	0.0096	130.2
0.0108	132	0.93	122.5	0.0107	123.8	0.0107	133.4
0.0124	135	0.92	124.6	0.0123	126.2	0.0123	136.7
0.0200	142	0.92	130.4	0.0198	133.0	0.0198	144.8
0.0300	144	0.91	131.6	0.0296	135.5	0.0296	148.3
0.0400	145	0.91	131.8	0.0392	137.1	0.0392	150.8
0.0500	146	0.90	132.1	0.0488	138.7	0.0488	153.3
0.0620	147	0.90	132.3	0.0602	140.5	0.0602	156.1

Figure A.2 – Material data points at room temperature and at 200F

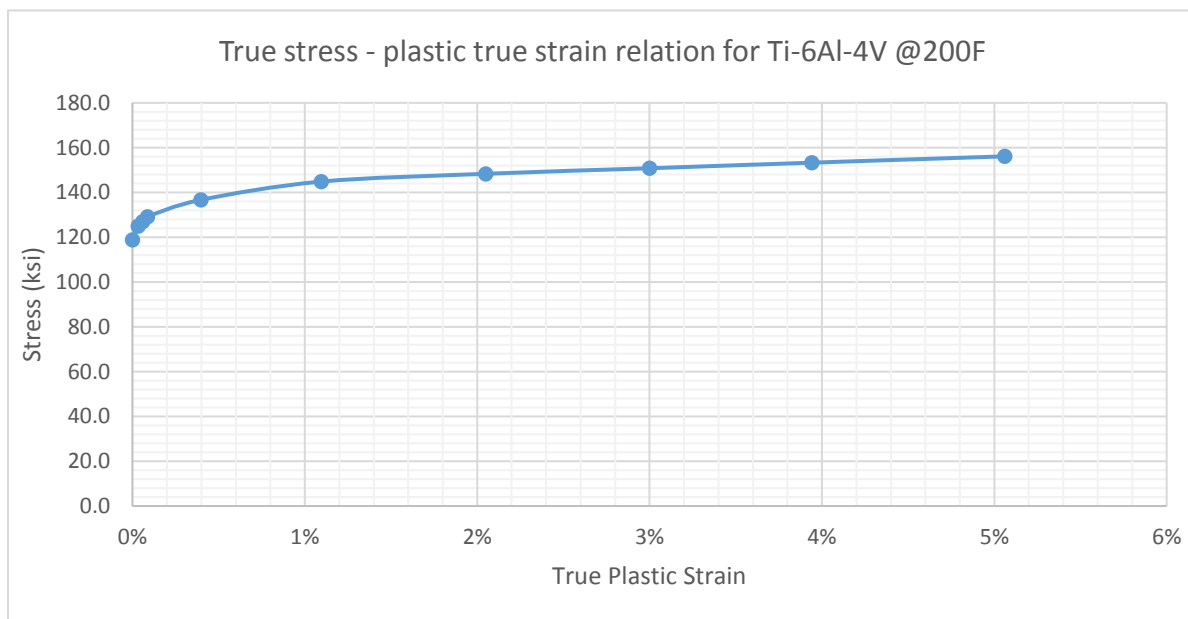


Figure A.3 – True stress vs true plastic strain for Ti-6Al-4V @200F

Lug calculations details

Details on margins of safety calculations are presented in this section.

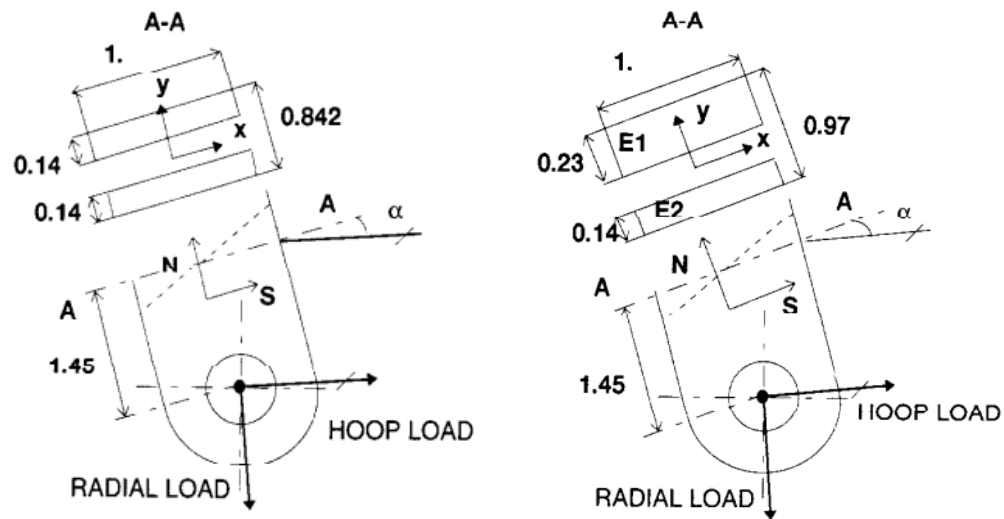


Figure A.4 – Dimensions of the forward (left) and aft (right) hinges

Outer and inner lugs of forward hinge have the same dimensions but dimensions of E1 and E2 of the aft hinge are different.

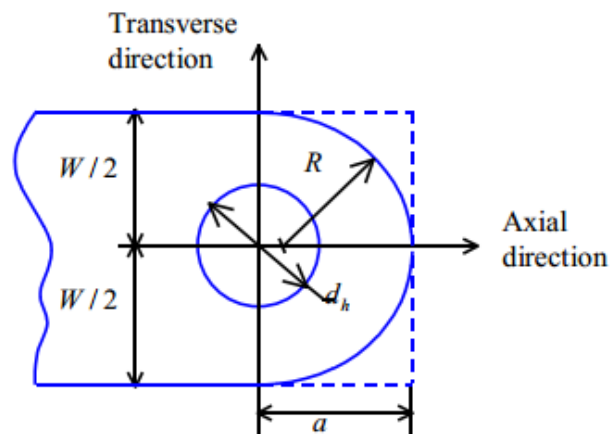


Figure A.5 – diagram of lug section

Table A.2 – Lugs parameters

Lugs	Forward	Aft	
		E1	E2
a (in.)	0.5	0.5	0.5
W (in.)	1	1	1

Table A.2 – Lugs parameters (continued)

d_h (in.)	0.63	0.44	0.63
t (in.)	0.14	0.23	0.14

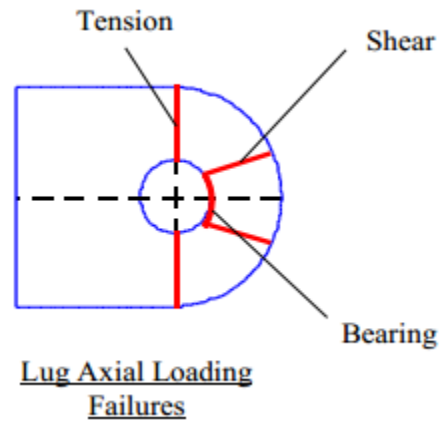


Figure A.6 – Lug axial loading failures

Allowable are calculated based on dimensions of the lugs and the material.

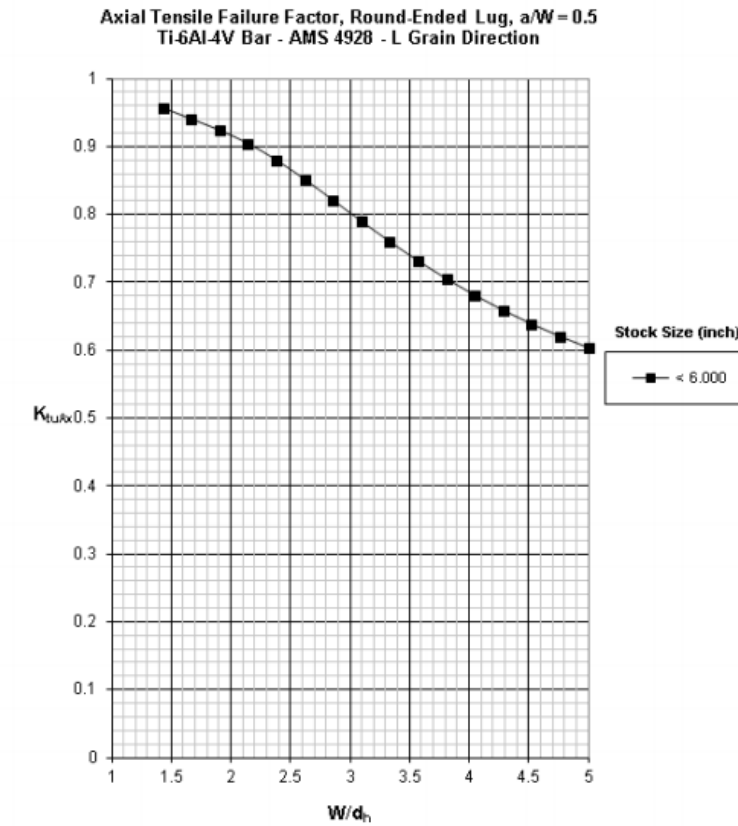


Figure A.7 – Axial tensile failure factor of Ti-6Al-4V

The allowable ultimate load for axial tension is:

$$P_{tuAx} = K_{tuAx} \times F_{tu} \times (W - d_h) \times t$$

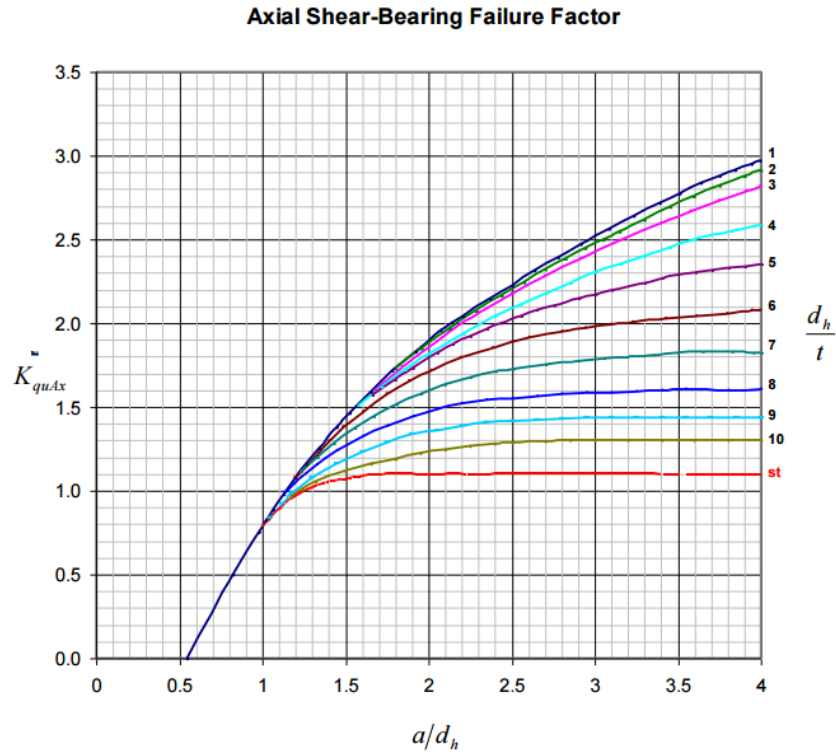


Figure A.8 – Axial shear-bearing failure factor

The allowable ultimate axial shear and bearing load is:

$$P_{quAx} = K_{quAx} \times F_{tu} \times d_h \times t$$

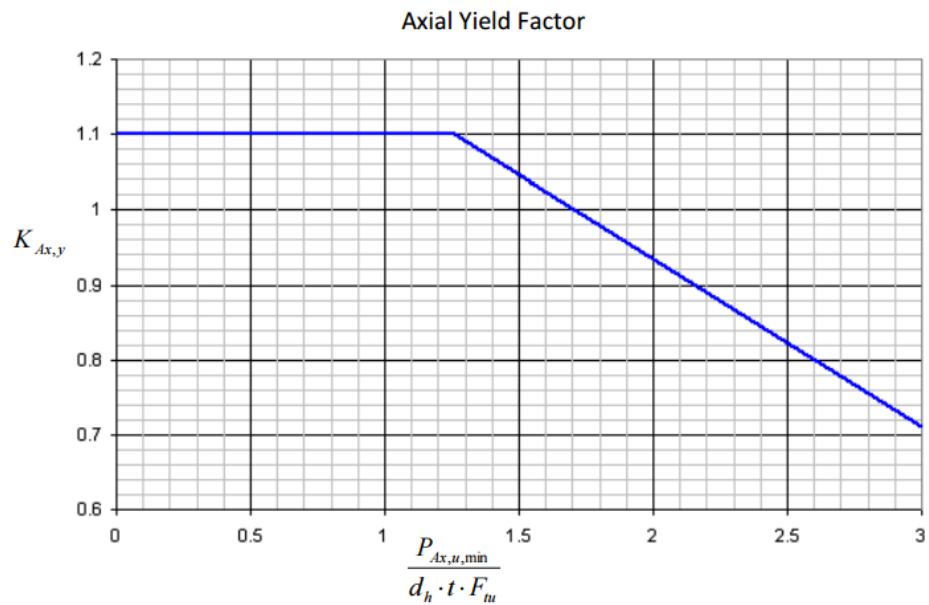


Figure A.9 – Axial yield factor

The allowable axial tension load for yield check is:

$$P_{tuAx} = K_{Ax,y} \times \frac{F_{ty}}{F_{tu}} \times \min(P_{tuAx}; P_{quAx})$$

When the axial component of the lug is directed toward the root of the lug, the axial failure mode is bearing. The ultimate compression allowable is:

$$P_{bru} = F_{bru} \times d_h \times t$$

The allowable bearing load for yield check is

$$P_{bry} = F_{br,y} \times d_h \times t$$

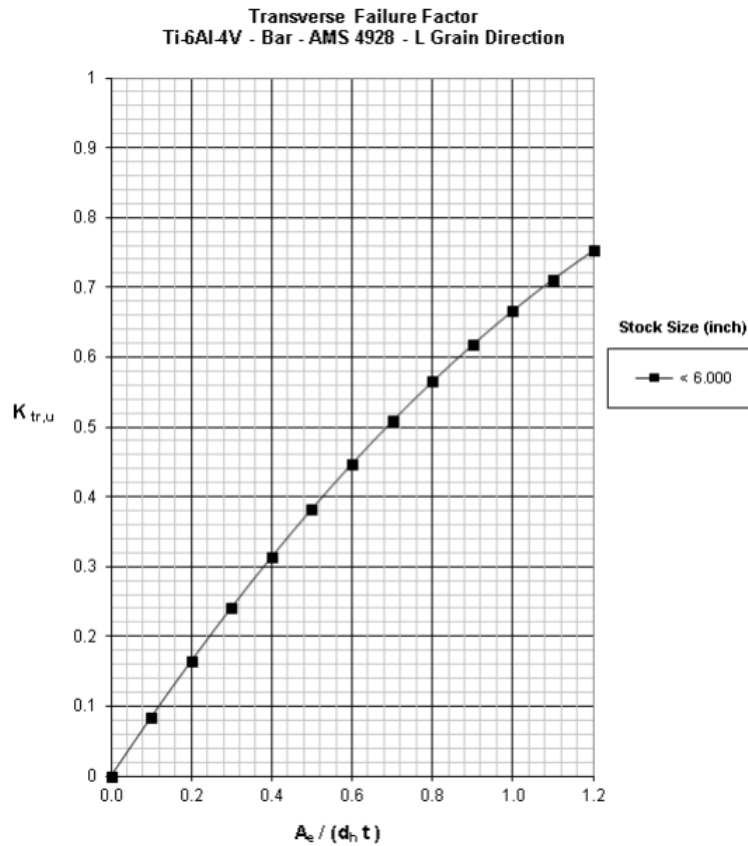


Figure A.10 – Transverse Failure Factor of Ti-6Al-4V

The ultimate transverse allowable load is defined by:

$$P_{tru} = K_{tru} \times F_{tu} \times d_h \times t$$

The allowable transverse load for yield check is:

$$P_{tr,y} = P_{tr,u} \times \frac{F_{ty}}{F_{tu}}$$

Factor K_{tru} is defined by the following equations and Figure A.10.

$$L_{e1} = a - \frac{d}{2 \times \sqrt{2}}$$

$$L_{e2} = L_{e3} = a - \frac{d}{2}$$

$$L_e = \frac{6}{\frac{4}{L_{e1}} + \frac{1}{L_{e2}} + \frac{1}{L_{e3}}}$$

$$A_e = L_e \times t$$

Table A.3 – allowable on each lug

	Ultimate			Limit		
	Forward	Aft – E1	Aft - E2	Forward	Aft – E1	Aft - E2
Axial tension (lbf)	5774	12878	5774	5101	11133	5101
Shear (lbf)	5119	11172	5119			
Axial compression (lbf)	20475	23519	20475	14962	17187	14963
Transverse (lbf)	3071	6115	2867	2783	5540	2597

According to the dimensions of the lug, applied loads are separated in axial (normal) and transverse (shear) components (see Figure A.4)

Table A.4 – Axial and transverse components of the forward hinge loads

	C15B'	C1B (ult.)	C1B	C2
Axial load (N) (lbf)	491	-377	-251	256
Transverse load (S) (lbf)	-2815	2608	1739	-1469

Table A.5 – Axial and transverse components of the aft hinge loads

	C21	C11B'	C1B	C2
Axial load (N) (lbf)	-356	375	-233	216
Transverse load (S) (lbf)	1723	-1983	1042	-901

Bushings are installed in the actual configuration and therefore, the overall load is shared between the outer and inner lug according to the following equations to make sure each lug can sustain at least 60% of the load:

$$\lambda_1 = \max\left(\frac{L_2}{L_1 + L_2}; 0.6\right) = 60\%$$

$$\lambda_2 = \max\left(\frac{L_1}{L_1 + L_2}; 0.6\right) = 60\%$$

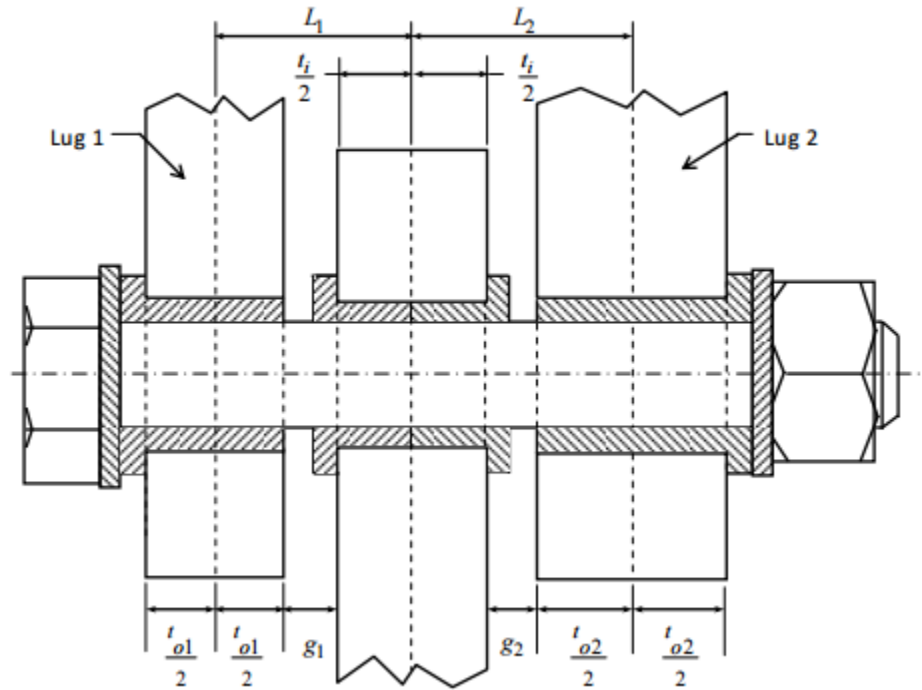


Figure A.11 – Load diagram of the loads in the elements of the lug assembly

Ultimate and yield margins of safety are evaluated with the following equations:

Compressive load cases

Axial load ratio is:

$$R_{Axu} = \frac{0.6 \times N}{P_{bru}} \text{ or } R_{Axy} = \frac{0.6 \times N}{P_{bry}}$$

The transverse load ratio is:

$$R_{tru} = \frac{0.6 \times S}{P_{tru}} \text{ or } R_{try} = \frac{0.6 \times S}{P_{try}}$$

The margin of safety is:

$$M.S. = \frac{1}{R_{Axu} + R_{tru}} - 1 \text{ or } M.S. = \frac{1}{R_{Axy} + R_{try}} - 1$$

Tension load cases

Axial load ratio is:

$$R_{Axu} = \frac{0.6 \times N}{P_{Axu}} \text{ or } R_{Axy} = \frac{0.6 \times N}{P_{Axy}}$$

The transverse load ratio is:

$$R_{tru} = \frac{0.6 \times S}{P_{tru}} \text{ or } R_{try} = \frac{0.6 \times S}{P_{try}}$$

The margin of safety is:

$$M.S. = \frac{1}{(R_{Axu}^{1.6} + R_{tru}^{1.6})^{0.625}} - 1 \text{ or } M.S. = \frac{1}{(R_{Axy}^{1.6} + R_{try}^{1.6})^{0.625}} - 1$$

Table A.6 – Margins of safety of the forward hinge

Ultimate loads		Limit loads	
C15B'	C1B (ult.)	C1B	C2
54.1%	68.8%	129.5%	166.0%

Table A.7 – Margins of safety of the aft hinge

Ultimate loads		Limit loads	
C11B'	C21	C1B	C2
323.0%	282.0	254.4%	301.1%

Fasteners calculations details

Fasteners properties of the model and margins of safety calculations details for each load case are presented here.

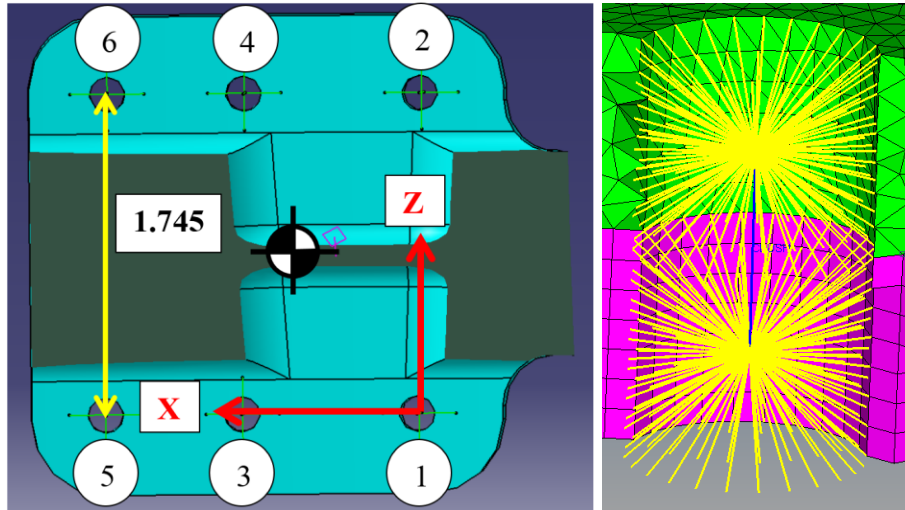


Figure A.12 – Fasteners between hinges and base plate are represented by RBE2 and CBUSH

Stiffness properties of CBUSH are calculated from Huth calculation [33] according to the materials used and each component's thickness and are given in the following table:

Table A.8 – CBUSH stiffness properties

dof	Stiffness (Psi)
k1	368,860
k2	1,796,648
k3	368,860
k4	1,769,090
k5	100
k6	1,769,090

From the loads extracted in the FE model, equivalent shear and tension loads on each bolts are:

$$P_{si} = \sqrt{F_{xi}^2 + F_{zi}^2}$$

$$P_{ti} = F_{yi}$$

Because load cases are ultimate loads, the tension in the bolt is assumed to be after separation of mating surfaces (see [39]).

To compute the margin of safety, the combine effect of tension and shear is taken into account with the load ratios:

$$R_s = \frac{P_{si}}{P_{su}}$$

$$R_t = \frac{P_{ti}}{P_{tu}}$$

The interaction envelope is:

$$(\lambda * R_s)^3 + (\lambda * R_t)^2 = 1$$

The reserve factor is λ . The margin of safety is calculated in the following tables.

Table A.9 – Bolts strength analyses from finite element model results

FWD Hinge – C15B'								
Bolt #	Fxi (lbf)	Fzi (lbf)	Fyi (lbf)	Psi (lbf)	Rsi	Rti	λ	MS
1	696.3	-80.04	61.01	700.89	0.27	0.01	3.74	274%
2	729.4	194.2	22.88	754.81	0.29	0.01	3.48	248%
3	-425.5	101.6	484.90	437.46	0.17	0.11	5.25	425%
4	-470.2	-83.3	458.20	477.52	0.18	0.10	4.95	395%
5	-280.0	-378.2	1040.00	470.57	0.18	0.24	3.62	262%
6	-301.7	522.9	1021.00	603.69	0.23	0.23	3.27	227%
FWD Hinge – C1B (ult.)								
Bolt #	Fxi (lbf)	Fzi (lbf)	Fyi (lbf)	Psi (lbf)	Rsi	Rti	λ	MS
1	-701.6	353.4	-1570.0	785.58	0.30	0.00	3.34	234%
2	-732.5	-505.0	-1602.0	889.71	0.34	0.00	2.95	195%
3	363.6	-309.3	141.6	477.36	0.18	0.03	5.43	443%

Table A.9 – Bolts strength analyses from finite element model results (continued)

4	411.4	323.6	138.5	523.42	0.20	0.03	4.97	397%
5	242.2	333.1	-56.6	411.85	0.16	0.00	6.36	536%
6	269.1	-440.0	6.4	515.77	0.20	0.00	5.08	408%
FWD Hinge – C1B								
Bolt #	Fxi (lbf)	Fzi (lbf)	Fyi (lbf)	Psi (lbf)	Rsi	Rti	λ	MS
1	-421.3	75.04	-46.93	427	0.16	0.00	6.12	512%
2	-442.9	-145.2	-25.66	466	0.18	0.00	5.62	462%
3	251.2	-162.3	-12.33	299	0.11	0.00	8.76	776%
4	281.3	159	-45.20	323	0.12	0.00	8.12	712%
5	170.5	143	-50.92	222	0.08	0.00	11.80	1080%
6	187.8	-213.6	-25.70	284	0.11	0.00	9.22	822%
FWD Hinge – C2								
Bolt #	Fxi (lbf)	Fzi (lbf)	Fyi (lbf)	Psi (lbf)	Rsi	Rti	λ	MS
1	355.6	-56.7	39.2	360.10	0.14	0.01	7.28	628%
2	372.6	111.6	22.5	388.95	0.15	0.01	6.75	575%
3	-214.7	133.2	10.9	252.66	0.10	0.00	10.38	938%
4	-239.4	-130.4	38.0	272.61	0.10	0.01	9.60	860%
5	-147.2	-112.9	43.2	185.51	0.07	0.01	14.05	1305%

Table A.9 – Bolts strength analyses from finite element model results (continued)

Bolt #	Fxi (lbf)	Fzi (lbf)	Fyi (lbf)	Psi (lbf)	Rsi	Rti	λ	MS
1	269	-134	555	301	0.11	0.13	6.30	530%
2	228	96	505	247	0.09	0.11	7.25	625%
3	192	-129	80	231	0.09	0.02	11.20	1020%
4	153	126	65	198	0.08	0.01	13.07	1207%
5	125	125	-8	177	0.07	0.00	14.80	1380%
6	97	-92	-5	133	0.05	0.00	19.70	1870%
AFT Hinge – C2								
Bolt #	Fxi (lbf)	Fzi (lbf)	Fyi (lbf)	Psi (lbf)	Rsi	Rti	λ	MS
1	-153	-169	-31	228	0.09	0.00	11.50	1050%
2	-272	-174	-86	323	0.12	0.00	8.12	712%
3	-138	43	45	145	0.06	0.01	17.90	1690%
4	-192	-55	181	200	0.08	0.04	11.95	1095%
5	-106	-33	161	111	0.04	0.04	19.00	1800%
6	-110	209	419	236	0.09	0.09	8.17	717%

APPENDIX B - TEST MATRIX OF QUALIFICATIONS COUPONS

	Tensile X/Y	Tensile Z	Tensile X/Y	Tensile Z	Tens. x/y 200F	Tens. Z 200F	Tens. x/y 400F	Tens. Z 400F	Bearing X/Y	Bearing Z	Shear X/Y	Shear Z	Compression X/Y	Compression Z	Axial fatigue X/Y	Axial fatigue Z	Chemical Composition
	ASTM E8		ASTM E8 (smaller)		ASTM E21				ASTM E238		ASTM B769		ASTM E9		ASTM E466		AMS4911N
Drawing	BLS - 9301 - R3		BLS - 9301 - R5 Long		BLS - 9301 - R3				Exova Bearing		Exova shear		Exova Compression		BLS - 9370		
Build 1	A1	B1	C1	D1	E1	F1	G1	H1	I1	J1	K1	L1	M1	N1	O1	P1	Q1
	A2	B2	C2	D2	E2	F2	G2	H2	I2	J2	K2	L2	M2	N2	O2	P2	
		B3		D3		F3		H3	I3	J3	K3	L3	M3	N3			
									I4	J4	K4	L4	M4	N4			
Build 2	A3	B4							I5	J5	K5	L5	M5	N5			
	A4	B5													O3	P3	
	A5	B6															
		B7															
		B8															
Build 3		B9															
	A6	B10													O4	P4	
	A7	B11															
	A8	B12															
		B13															
Build 4		B14															
		B15															
	A9	B16													O5	P5	
	A10	B17															
	A11	B18															
		B19															
	B20																
	B21																
	As manufactured																
	Hot Isostatic Pressure (HIP)																

APPENDIX C – ARTICLE 1: PAPER OF PARTIAL INTERPRETATION SUBMITTED TO THE CANADIAN AERONAUTIC AND SPACE JOURNAL

Submitted may 10th 2016

Topology optimization of the flap track fitting of a business aircraft for additive manufacturing

**J.-P. Carmona (a), J. Chaussée (b), L. Birglen (a), Martin Deshaies (b), Franck Dervault (b),
Sylvain Turenne (a)**

(a) Polytechnique Montréal, Montréal QC,

(b) Bombardier Aerospace Inc., Montréal QC

Abstract

This paper is the case study of a flap track fitting of a business aircraft. The goal was to reduce weight of the part by redesigning it whilst considering the part will be produced by additive manufacturing. A new design process workflow is proposed that integrates topology optimization at the beginning of the process. Opportunities and limitations of design for additive manufacturing with topology optimization were encircled. An innovative method for optimization results interpretation is also presented. This method uses tools for mesh-based model from video game open-source software Blender. Conventional feature-based model has also been produce to compare the two methods. The present case study suggests that the new design for additive manufacturing process allows reducing weight of the parts and shorten the design life cycle.

Introduction

Additive manufacturing technologies have improved significantly in the recent years. Selective laser melting and electron beam melting of metals, for instance, offer great possibilities for aerospace part design [40]. With much less manufacturing constraints, design methodology needs to be addressed to capture those possibilities. Numerical tools like topology optimization can help put functionalities of a part at the forefront of the design process. This paper studies the redesign of an aircraft component for additive manufacturing with help of topology optimization. The part studied is the support of the flap track of a business aircraft. This part is selected because of its complex loading and its compact environment. Thus, it is really hard for engineers and designers to predict the ideal topology at a preliminary step of the design.

Several topology optimization algorithms exist in commercial software. The solver used in the study is Optistruct by Altair®. It uses the SIMP (Solid Isotropic Material Penalization) method that varies the density of a finite element model to study the optimal material distribution of a part in a design space [41]. In this study, the objective and the constraints are varied and their influence is exposed on the results.

In addition, the traditional design methodology with topology optimization implies an interpretation of the results at the end by remodeling the part in a feature-based software. In this paper, an innovative method for interpretation is explored with a mesh-based software that allows to manipulate directly the STL model of the optimization results. This can significantly reduce the design life cycle of a part for additive manufacturing as well as increasing the fidelity of the interpretation to the optimization results.

Assumptions and methodology

The fittings are two mirrored parts nested in the flap track assembly. For simplicity only the outboard fitting will be redesigned. Material properties are going to be considered equal to those of PH13-8Mo from an annealed plate. The flap track fitting is subject to repeated load cycles. However, no fatigue analysis will be conducted on the part for simplification purposes. Thus, only static strength is calculated. Fitting factor used for static margin of safety calculation is 1.15. Boundary conditions (size and positions of fasteners and lugs) are kept unchanged during the study to limit the impact on the rest of the assembly.

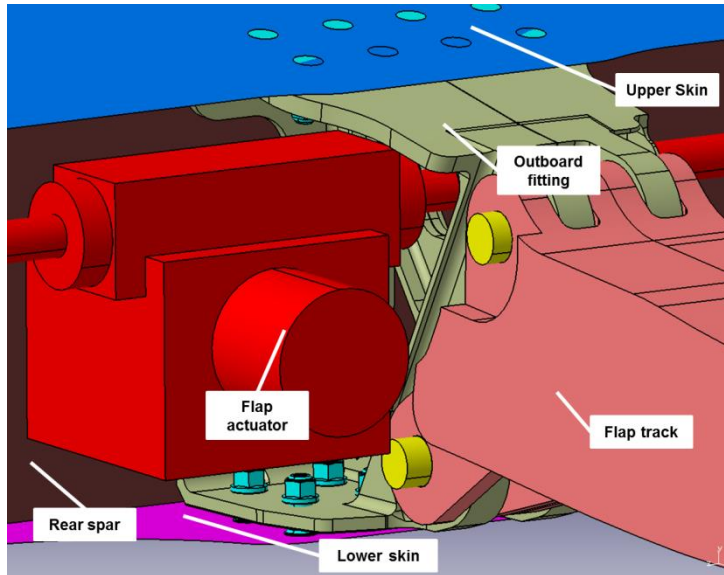


Figure C.1 – Model view of flap assembly

for additive manufacturing starts by analyzing the performance of the initial part in terms of the criteria aforementioned. When the benchmark is set, the topology optimization study begins by producing the design space. The optimization is then launched with several different set of parameters in order to reveal different results. Those results are analyzed and compared and a final topology is chosen for interpretation.

In this paper, the interpretation is made twice with two different methods. The first is a rework of the optimization results directly with mesh-based tools and the second is a traditional complete re-interpretation of the results with NURBS and solid parametric tools. Finally, the two models are analyzed with finite elements to compare their performance with the original part.

Finite element modeling

Two finite element models are built to analyze the outboard fitting. The first model includes several components from the track assembly: skins and spar of the wing and the fasteners. It is used as a benchmark to evaluate the performance of the original and final optimized part but is too complex to perform the topology optimizations. Therefore, a second model is built with less components and simpler boundary conditions. The simplified model acts as a benchmark to compare results from topology optimization because their configuration is the same.

The criteria of success of the redesign are:

- Reducing the weight of the part compared to original fitting.
- Respect the stress allowable in the fitting. The Von Mises stress away from the boundary conditions compared to yield tensile strength of material should give a positive margin of safety.
- Stiffness of the fittings is crucial to ensure proper deployment of the flap. Therefore, displacements of lugs (upper and lower) could not exceed the original values by more than 15%.

Thus, the redesign of the outboard fitting

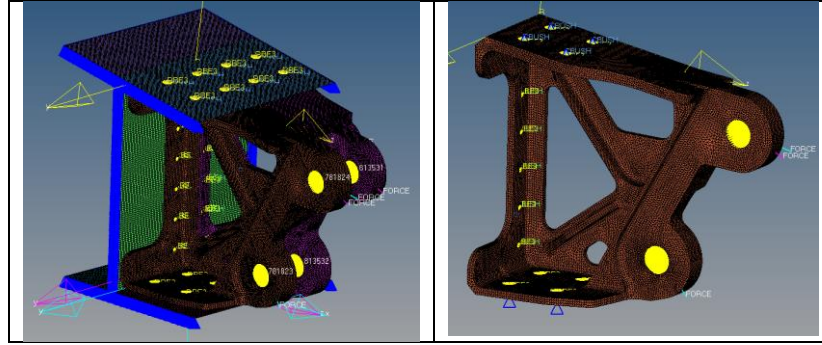


Figure C.2 – complete (right) finite element model will be used to validate the final designs only and the simplified (left) model will be used to perform the topology optimization study.

Design space analysis

The input model of a topology optimization is a 3D envelope called the design space. It represents the maximum allowable space one part can be comprised in. Due to its exiguous environment, the maximum design space of the track support is easily definable.

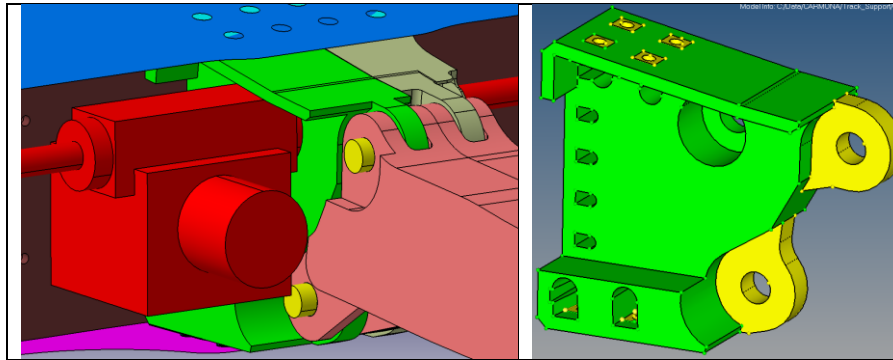


Figure C.3 – Design space of the outboard fitting in the flap assembly (left) and isolated view (right). areas (represented in yellow on the Figure C.3).

It is important that a clearance exists around each bolt to ensure installation. The lugs and the sections around each bolt are non-design spaces, meaning that material cannot be taken off these areas (represented in yellow on the Figure C.3).

Optimization parameters

Topology optimization with SIMP method converges towards a local optimum of its function. By changing the responses, the constraints and the objective of the optimization, different results (local optimums) are obtained. Thus, to analyze different optimums, it is important to launch various optimizations with different parameters. According to Altair® documentation, the most robust optimization parameters are reported in Table C.1.

Table C.1 – Optimization parameters matrix

setup	Mesh	Objective	Constraints	Range/value	Min. Dim.
1	Coarse	Min. compliance	Vol. fraction	10%	12x
2	Coarse	Min. compliance	Vol. fraction	15%	12x
3	Coarse	Min. volume fraction	Nodes disp.	Below original disp.	12x
4	Coarse	Max. weighted frequency (3 first modes)	Vol. fraction	10%	12x
5	Coarse	Max. weighted frequency (3 first modes)	Vol. fraction	15%	12x
6	Fine	Min. compliance	Vol. fraction	15%	18x
7	Coarse	Min. compliance	Vol. fraction	15%	5x
8	Coarse	Max. weighted frequency (3 first modes)	Vol. fraction	15%	5x

It is widely accepted that the use of minimum member size constraint (Min. Dim.) really helps convergence of results [32] [41]. Minimum member size constraint is used to limit the size of the smallest feature of the topology. It is often necessary to avoid checkerboard pattern. The influence of this parameter will be briefly exposed by comparing optimization results with a high and a low value of minimum member size constraint. Optimization setups 7 and 8 are similar to setups 2 and 5 respectively except that minimum member size was reduced from 12 to 5 times the average element size.

Results

Results from the analysis of the original part are reported in *Figure C.4*.

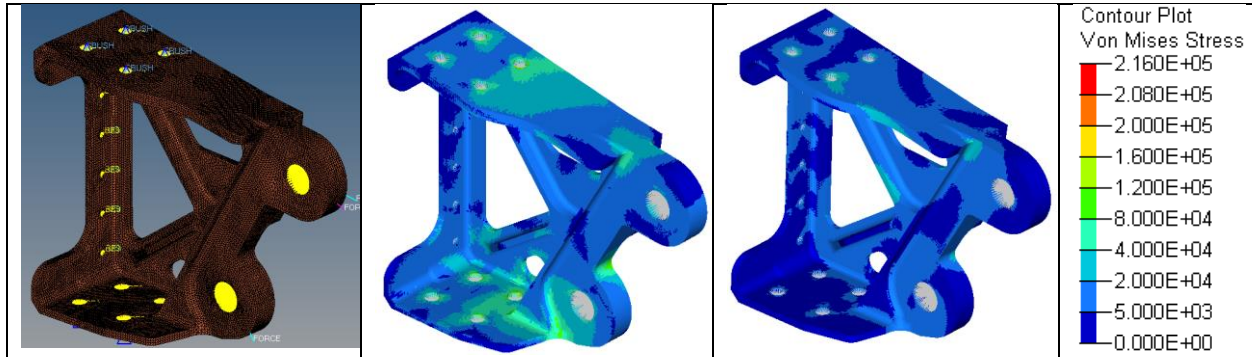


Figure C.4 – Finite element model (first on the left) and Von Mises stress contour of load case 1 (second) and load case 2 (third) of the outboard fitting. The part was first analyzed with the simplified model.

Margin of safety for the two static load cases evaluated on the original part are calculated with the following equation:

$$MS = \frac{F_{ty}}{VM_{max} \times FF} - 1$$

With the yield tensile strength ($F_{ty}=200,000\text{psi}$) of the material, the maximum Von Mises stress (VM_{max}) in the part and the fitting factor ($FF=1.15$).

Table C.2 – Margin of safety of original part

Load case 1	0.83
Load case 2	3.35

Table C.3 gathers the results of the optimizations. Lugs displacements, absolute maximum principal stress and volume of parts are the metrics used to compare the optimization results with the simplified model of the original part. However, monitoring compliance helps to understand how a model responds to a given load case. Maximum principal stress is monitored away from boundary conditions to avoid capturing unrealistic stress peaks. Due to high stress level, results 3 and 4 are discarded. Result from setup 1 shows relatively high lugs displacements, thus it is discarded as well.

Table C.3 – Optimization results are compared to simplified model of the original part (see Figure C.2).

Setup	Upper lug disp (inches)		Lower lug disp (inches)		Max Mises (ksi)	Von Stress	Compliance		Volume (in ³)	Δ volume
	LC1	LC2	LC1	LC2	LC1	LC2	LC1	LC2		
Original	0.0488	0.0222	0.0279	0.0130	95	40	694	102	77	-
1	0.0558	0.0442	0.0226	0.0229	137	97	194	700	37	-52%
2	0.0403	0.0314	0.0152	0.0132	95	58	131	524	47	-39%
3	0.0487	0.0222	0.0278	0.0130	350	53	126	1329	36	-52%
4	0.0863	0.0451	0.0316	0.0347	382	150	309	1795	37	-52%
5	No convergence of the solver due to conditioning problem of minimum member size constraint									
6	No convergence of the solver due to conditioning problem of minimum member size constraint									
7	0.0392	0.0308	0.0160	0.0098	77	50	117	500	47	-39%
8	0.0524	0.0275	0.0187	0.0153	240	111	154	1076	47	-39%

Models 7 and 8 are completely different from their counterparts with higher minimum member size and present better results in general. The problem with these topologies resides in the interpretation of small and thin features resulting from the lower minimum member size constraints. There are wide 1-element-thick surfaces that can lead to buckling which is not taken into consideration in our optimizations (see Figure C.5). On top of it, several checkerboard patterns are present which don't have any physical sense [32]. Therefore, optimizations 7 and 8 are discarded as well.

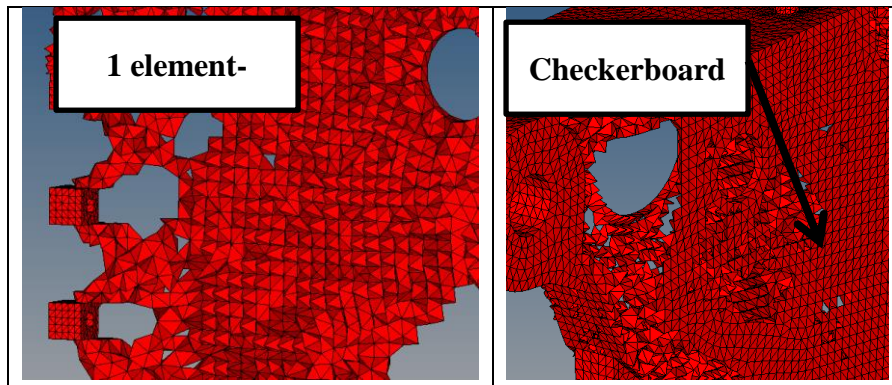


Figure C.5 – Results from optimization 7 and 8 with thin features and checkerboard effect

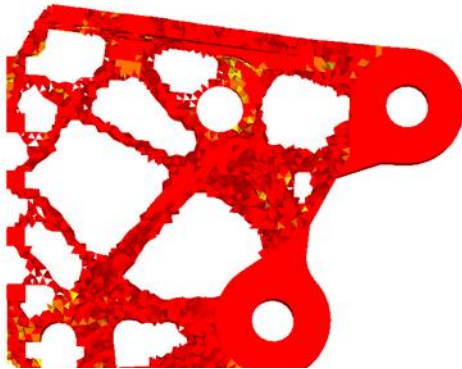


Figure C.6 – Optimization 2 gave the most satisfactory results and is used for interpretation

Setup 5 takes the same optimization function than setup 4 but with a volume fraction constraint of 15% instead of 10%. Similarly, setup 6 has the exact same configuration than setup 2 but with a finer meshing. However, setups 5 and 6 did not converge correctly. In fact, the solver is more stable when minimum member size constraint is between 3 and 12 time the average element size.

Therefore, with minimum member size at 18 times the average element size, setup 6 runs unstably. Even though setup 5 has a minimum member size constraint within the prescribed range, it is assumed that it did not converge correctly because it is too close to the limit of 12 times the average element size. This result suggests that the allowable range should be decreased to 10 times the average element size.

Finally, although the upper lug displacement is significantly higher than original, setup 2 presents valid results in general and is used in the final interpretation.

Interpretation

Elements from optimization results with density above 0.9 can be extracted as iso-density meshes in STL format. Although it can give good guidelines to a designer for interpretation, the iso-density mesh raw from optimization is really rough and some tools can help in that sense. Conventional aerospace CAD software like CATIA®, are made to manipulate NURBS and perform Boolean operations. To freely manipulate a mesh, video game software like Blender comes in handy. In addition, it is free and open source.

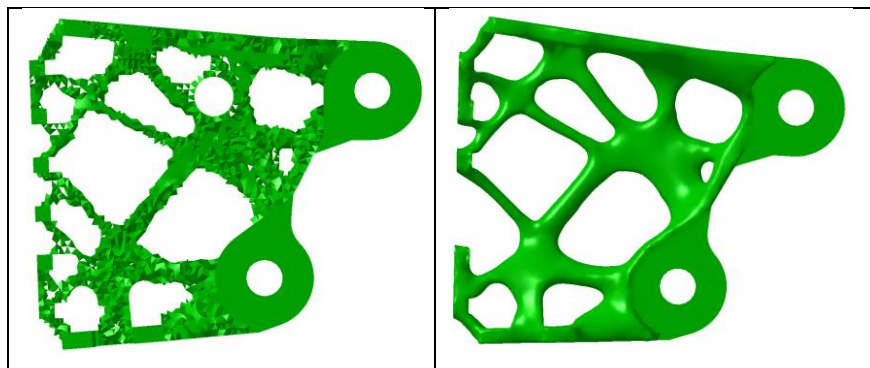


Figure C.7 – Comparison between results out of the optimization solver (left) and after smoothing in Blender (right)

The key features used in Blender are in the sculpting environment. This allows directly to smooth, inflate/deflate, drag, flatten, etc. the mesh. Sculpting tools in Blender dynamically change density of the mesh to ensure proper smoothing.

However, Blender has its limitations when it comes to straight edges and planes.

Figure 8 shows an example of

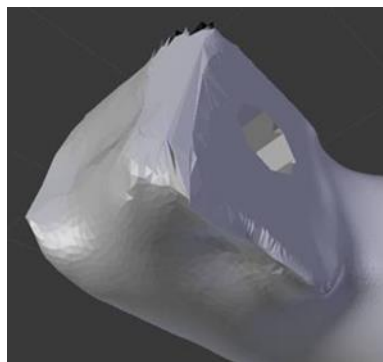


Figure C.8 – Damaged elements around bolts due to sculpting in Blender

damaged surfaces around a bolt after sculpting the surrounding. Although it is possible to protect elements (like non-design spaces) from sculpting, it is fastidious and further development needs to be pursued in this area. This problem is minor when considering that final design is made with actual datum in CAD environment.

A feature-based parametric CAD model has also been done in order to see how it could be integrated in the design process. *Figure C.9* illustrates the part in its CAD environment. Modeling such a part is really complex and time extensive. Even considering the effort, the geometry still deviates from the topology results. On the long term, avoid modeling in feature-based model would significantly improve efficiency and lead time of the design process.



Validation

The smoothed and CAD models are analyzed in the complete assembly to evaluate their stress distribution, displacement and weight (see *Figure C.2*). The results show that CAD interpretation is, regarding almost all criteria of success, better than smoothed model. Moreover, both interpretations have positive stress margins of safety.

Figure C.9 – Interpretation of optimization setup 2 in Catia V5

Stress level is significantly higher in both optimized models than in the original part. This is understandable since stress level has never been a constraint during optimizations. Actually, optimizations were formulated to reduce general compliance thus, limiting displacement of the load application points. For this reason, lugs displacements are really similar for the 3 models and optimized parts are lower than 15% above the original displacements (see *Table C.4*).

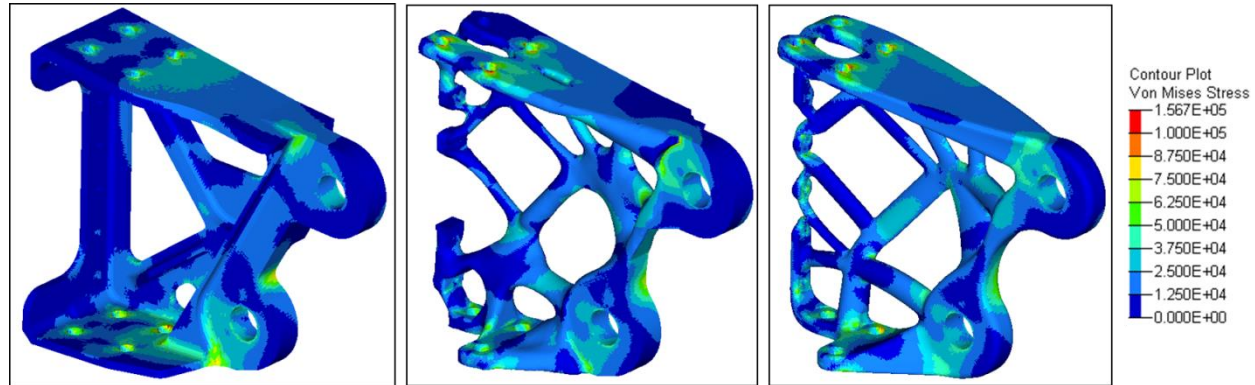


Figure C.10 – Von Mises stress distribution from finite element analyses of the original and the optimized models for load case 1, the most severe. Ultimate tensile strength of Ph13-8Mo steel is 208,000psi.

The mesh automatically generated by Blender during smoothing does not recognize features (like plane surface, diameter, etc.) and is not quality optimized. Stress distribution and peaks might be a little bit inaccurate in the smoothing interpretation due to mesh condition.

Finally, as shown in *Table C.4*, there are big discrepancies between displacements results from Setup 2 and the final optimized models (smoothing and CAD models). This is mostly explained by the fact that the optimization setups are modeled with simplified boundary conditions and the final parts are modeled within complete flap assembly (see *Figure C.2*), thus leading to much different stiffnesses and lugs' displacements. Moreover, we see that the stress in Setup 2 is higher because it has rigid boundary conditions.

*Table C.4 – Results of static finite element analysis on original part, smoothing interpretation, CAD interpretation and results from setup 2. Original model results are from the complete model (see *Figure 2*).*

Model	Upper lug disp. (inches)		Lower lug disp. (inches)		Abs max P1 stress (ksi)		Margin of safety		Volume (in ³)	Δ weight
	LC1	LC2	LC1	LC2	LC1	LC2	LC1	LC2		
Original (complete)	0.0494	0.0255	0.0325	0.0071	88	33	0.98	4.27	77	-
Smoothing interpretation	0.0538	0.0289	0.0346	0.0071	82	46	1.12	2.78	56.2	27%
CAD interpretation	0.0508	0.0288	0.0333	0.0071	96	33	0.81	4.27	49.9	35%
Setup 2	0.0403	0.0314	0.0152	0.0132	95	58	0.83	2.00	47	39%

Conclusion

The case study of the outboard fitting reveals that it is possible to interpret topology optimization results without having to fully remodel the part in a feature-based software. Manipulating the result as a mesh is possible and shortens the design life cycle. Although the results are slightly better when the part is fully

remodeled with features, some incremental innovation in the software will open the door to advanced manipulations of optimization results like features recognition.

The final parts show acceptable static stress level. However, it is important to mention that no fatigue analysis was conducted on the models and doing so could significantly influence the allowable stress level in the parts. Modifications to the parts would be necessary and therefore, the weight saving could decrease.

For numerical resources limitation purposes, it was mandatory to build one simplified model to perform the optimizations and one complete model to validate the final and original parts. This separation has been proven to be misleading when monitoring stiffnesses of the components. Therefore, special care should be taken to respect the compliance of the original structure when simplifying the model.

It has also been shown that during the optimization, when the minimum member size constraint is above 12 times the average element size, convergence of the algorithm can be compromised. Consequently, mesh size and minimum member size constraint of the model should be carefully chosen to obtain the desired minimum feature size in the final topology. In a future case study, it could be interesting to investigate different element types in order to have larger elements thus increasing minimum member size constraint.

Works Cited

- [1] Wikipédia, "Fabrication additive," 6 juin 2016. [Online]. Available: https://fr.wikipedia.org/wiki/Fabrication_additive. [Accessed 12 06 2016].
- [2] Wikipédia, "Optimisation topologique," 25 November 2015. [Online]. Available: https://fr.wikipedia.org/wiki/Optimisation_topologique. [Accessed 12 June 2016].
- [3] ASTM F2792-12, *Standard Terminology for Additive Manufacturing Technologies*, 2012.
- [4] Wikipédia, "Topology Optimization," 20 May 2016. [Online]. Available: https://en.wikipedia.org/wiki/Topology_optimization. [Accessed 12 June 2016].
- [5] A. S. o. D. f. R. a. E. (ASD(R&E)), "Technology Readiness Assessment (TRA) Guidance," Department of Defense, Washington, 2011.
- [6] Wohlers Associates, "Wohlers Report 2015," Wohlers Associate, Fort Collins, 2015.
- [7] GE Global Research , "3D Printing Creates New Parts for Aircraft Engines," [Online]. Available: <http://www.geglobalresearch.com/innovation/3d-printing-creates-new-parts-aircraft-engines>. [Accessed 12 June 2016].

- [8] Airbus Group, "Breakthrough for future Airbus A320," Janvier 2015. [Online]. Available: <http://www.airbusgroup.com/int/en/story-overview/Pioneering-bionic-3D-printing.html>. [Accessed 12 June 2016].
- [9] SpaceX, "Spaced launches 3D-printed part to space, created printed engine chamber," 14 July 2014. [Online]. Available: <http://www.spacex.com/news/2014/07/31/spacex-launches-3d-printed-part-space-creates-printed-engine-chamber-crewed>. [Accessed 12 June 2016].
- [10] Aerojet Rocketdyne, "Aerojet Rocketdyne Successfully Tests Complex 3-D Printed Injector in World's Most Reliable Upper Stage Rocket Engine," 7 March 2016. [Online]. Available: <http://www.rocket.com/article/aerojet-rocketdyne-successfully-tests-complex-3-d-printed-injector-worlds-most-reliable>. [Accessed 12 June 2016].
- [11] ATW Online, "Additive Power," March 2016. [Online]. Available: http://www.atw-digital.com/airtransportworld/march_2016?sub_id=f4X5lNXI9HPa&pg=NaN#pgNaN. [Accessed 12 June 2016].
- [12] Metal Prices, "Aluminum 6063 Extrusion Billet," [Online]. Available: <https://www.metalprices.com/metal/aluminum/aluminum-6063-extrusion-billet-premium>. [Accessed 30 July 2016].
- [13] G. Rozvany, "Aims, scope, methods, history and unified terminology of computer-aided topology optimization in structural mechanics," *Structural Multidisciplinary Optimization*, vol. 21, no. 2, pp. 90-108, 2001.
- [14] M. Bendsoe and N. Kikuchi, "Generating optimal topologies in structural design using a homogenization method," *Computer methods in applied mechanics and engineering*, pp. 197-224, 1988.
- [15] M. Bendsoe, "Optimal shape design as a material distribution problem," *Structural Optimization*, vol. 1, pp. 193-202, 1989.

- [16] M. Bendsoe and O. Sigmund, *Topology Optimization : Theory, Methods and Applications*, Berlin: Springer, 2003.
- [17] O. Sigmund and K. Maute, "Topology Optimization approaches," *Structural and Multidisciplinary Optimization*, vol. 48, no. 6, pp. 1031-1055, 2013.
- [18] J. D. Deaton and R. V. Grandhi, "A survey of structural and multidisciplinary continuum topology optimization: post 2000," *Structural Multidisciplinary Optimization*, vol. 49, no. 1, pp. 1-38, 2014.
- [19] K. Svanberg, "The method of moving asymptotes - A new method for structural optimization," *International Journal for Numerical Methods in Engineering*, vol. 24, pp. 359-373, 1987.
- [20] C. Fleury, "CONLIN: an efficient dual optimizer based on convex approximation concepts," *Structural optimization*, pp. 81-89, 1989.
- [21] G. Vanderplaats, "A robust Feasible Directions algorithm for design synthesis," in *24th Structures, Structural Dynamics and Materials Conference*, Lake Tahoe, NV, 1983.
- [22] C. Le, J. Norato, T. Bruns, C. Ha and D. Tortorelli, "Stress-based topology optimization for continua," *Structural and multidisciplinary Optimization*, vol. 41, no. 4, pp. 605-620, 2010.
- [23] M. Werme, "Using the sequential linear integer programming method as a post-processor for stress-constrained topology optimization problems," *International Journal for Numerical Method in Engineering*, vol. 76, no. 10, pp. 1544-1567, 2008.
- [24] E. Holmberg, "Stress and fatigue constrained topology optimization," Linköping University, Department of Management and Engineering, Linköping, 2013.
- [25] S. Osher and J. Sethian, "Fronts propagation with curvature-dependent speed: Algorithm based on Hamilton-Jacobi formulations," *Journal of Computational Physics*, vol. 79, pp. 12-49, 1988.

- [26] M. Y. Wang, X. Wang and D. Guo, "A level set method for structural topology optimization," *Computer methods in applied mechanics engineering*, vol. 192, pp. 227-246, 2003.
- [27] G. Allaire, F. Jouve and M. Toader, "Structural optimization using sensitivity analysis and a level-set method," *Journal of Computational Physics*, vol. 194, no. 1, pp. 363-393, 2004.
- [28] N. van Dijk, K. Maute, M. Langelaar and F. van Keulen, "Level-set methods for structural topology optimization: a review," *Structural Multidisciplinary Optimization*, vol. 48, pp. 437-472, 2013.
- [29] H. Jia, H. Beom and Y. Wang, "Evolutionary level set method for structural topology optimization," *Computers and Structures*, vol. 89, pp. 445-454, 2011.
- [30] G. Allaire, F. de Gournay, F. Jouve and A. Toader, "Structural optimization using topological and shape sensitivity via a level set method," *Control Cybern*, vol. 34, no. 1, pp. 59-80, 2005.
- [31] M. Burger, B. Hackl and W. Ring, "Incorporating topological derivatives into level set methods," *Journal of Computational Physics*, vol. 194, no. 1, pp. 344-362, 2004.
- [32] M. Zhou, Y. Shyy and T. H.L., "Checkerboard and minimum member size control in topology optimization," *Structural and Multidisciplinary Optimization*, pp. 152-158, 2001.
- [33] F. Gunbring, Prediction and Modeling of Fastener Flexibility Using FE, Linköping: Press of Linköping University Institute of Technology, 2008.
- [34] E. Bruhn, Analysis and Design of Flight Vehicle Structures, Lafayette: Jacobs Publishing, Inc., 1973.
- [35] M. C.-Y. Niu, Airframe Structural Design, Los Angeles: Technical Book Company, 1988.
- [36] Batelle Memorial Institute, Metallic Material Properties Development and Standardization, Columbus, OH, 2008.

- [37] J. Ajaja, "Notes de cours - MTR4700 - Essai de traction," École Polytechnique Montréal, Montreal, 2014.
- [38] J.-P. Bailon and J.-M. Dorlot, *Des Matériaux*, Montréal: Presses Internationales Polytechnique, 2000.
- [39] Bombardier Aerospace, "Bombardier Manual - BM7024.01.03.02 - Strength of Metallica Structures - Joints and Fittings - Joints and Attachements," Bombardier Aerospace, Montreal, 2014.
- [40] R. Dehoff, C. Tallman, C. Duty, W. Peter, Y. Yamamoto, W. Chen and C. Blue, "Case Study: Additive Manufacturing of Aerospace Brackets," *Advanced Materials & Processes*, pp. 19-22, 2013.
- [41] M. Bendsoe and O. Sigmund, "Topology Optimization by distribution of isotropic material," in *Topology Optimization: Theory, Methods and Applications*, Berlin, Springer, 2003, pp. 1-68.
- [42] Government of Canada, "National Aircraft Certification," Transport Canada, 06 12 2012. [Online]. Available: <https://www.tc.gc.ca/eng/civilaviation/certification/menu.htm>. [Accessed 14 09 2015].
- [43] Loughborough University, "The 7 categories of Additive Manufacturing," [Online]. Available: <http://www.lboro.ac.uk/research/amrg/about/the7categoriesofadditivemanufacturing/>. [Accessed 30 October 2015].
- [44] D. Walker, D. Liu and A. Jennings, "Topology Optimization of an Aircraft Wing," in *56th AIAA/ASCE/AHS/ASC Structures, Structural Dynamics and Materials Conferences*, Kissimmee , Florida, 2015.

- [45] F. Gunbring, Predicting and Modeling of Fastener Flexibility Using Finite Element Method, Linköping: Linköping University, 2008.
- [46] Wikipédia, "3D Printing," 7 June 2016. [Online]. Available: https://en.wikipedia.org/wiki/3D_printing. [Accessed 12 June 2016].